ELECTRICALLY DRIVEN ION SEPARATIONS USING MEMBRANES COATED WITH POLYELECTROLYTE MULTILAYERS OR CONDUCTIVE FILMS

By

Yan Zhu

A DISSERTATION

Submitted to
Michigan State University
in partial fulfillment of requirements
for the degree of

Chemistry – Doctor of Philosophy

2016

ABSTRACT

ELECTRICALLY DRIVEN ION SEPARATIONS USING MEMBRANES COATED WITH POLYELECTROLYTE MULTILAYERS OR CONDUCTIVE FILMS

By

Yan Zhu

Ion-exchange membranes are attractive for salt recovery and brackish water desalination because they provide high selectivities between cations and anions. Nevertheless, typical ion-exchange membranes show only modest selectivities among cations or anions, and such selectivities are important in applications including water softening, acid recovery, and salt purification. This dissertation explores coating of membranes with polyelectrolyte multilayers (PEMs) or conductive films to enhance selectivity in electrically driven ion transport.

Adsorption of PEMs on Nafion membranes gives rise to high monovalent/divalent cation selectivities in electrodialysis (ED), but the high cost of Nafion may preclude its use in many ED applications. This work demonstrates that relatively inexpensive Fujifilm cation-exchange membranes modified with protonated poly(allylamine) (PAH)/poly (4-styrenesulfonate) (PSS) films have extremely high K^+/Mg^{2+} cation selectivities >1000 in ED. The high exclusion of Mg^{2+} suggests a complete and dense PEM, presumably because the smooth Fujifilm surface allows formation of a continuous coating. The PEM formed on the anode side of the membrane is essential for the high selectivity, whereas the cathode-side coating contributes only a small amount to resistance of the membrane system and little selectivity. Current density-voltage curves and transference numbers suggest that water splitting occurs at overlimiting currents. Overall, these highly selective membranes may be attractive for salt purification and salt recovery using ED.

Although PEM-modified cation-exchange membranes show high cation-selectivity during ED, the current efficiency is only ~0.5, which implies that unwanted ions carry 50% of current. Adsorption of $(PDADMAC/PSS)_n$ films on Nafion membranes leads to high monovalent /divalent cation selectivity in ED, and moreover, the monovalent cation current efficiency is as high as 0.8. $(PDADMAC/PSS)_3$PDADMAC films give the highest current efficiency in both K^+/Mg^{2+} and Li^+/Co^{2+} separations. The high current efficiency presumably results from the high aqueous swelling of $(PDADMAC/PSS)_n$ films to increase the monovalent cation permeance. However, $(PDADMAC/PSS)_n$ films are not stable in solutions with high salt concentrations, so future work should aim to increase the film stability.

The high selectivity of PEMs partly stems from the high surface charge of the thin film. Thus, instead of introducing membrane surface charge through adsorption of polyelectrolytes, this work also aimed to develop conductive membranes to create surface charge using an electrical potential applied between the conducting membrane and a reference electrode in the source phase. The potential-dependent surface charge should alter cation and anion partitioning into the membrane. Electroless deposition of gold followed by electrosynthesis of poly(3,4-ethylenedioxythiophene) gives highly conductive membrane with sheet resistances <100 Ω/□. Unfortunately, the ion fluxes do not significantly change with applied potential.

Finally, this dissertation investigates the possible mechanism of high salt rejection in nanofiltration through PEM-coated NF270. The surface charge may create regions of nonelectroneutrality in the membrane, and the low concentration of the excluded ion in this region should control the resistance to salt transport.

To my Mother Rong Ye and Father Xiao-Qing Zhu

ACKNOWLEDGEMENTS

At the end of my journey at MSU, I would like to thank many people. Without their love and support, I could not finish the dissertation.

Firstly, I need to express my deepest gratitude to my advisor, Dr. Merlin Bruening, for his guidance, support, understanding, and patient. Conducting research is a process to gain new knowledge that people have not understood, so research may not always work and could be very frustrating. While, I am very impressed by his passion and attitude in research and I also appreciate his suggestions and encouragement during the hard times.

I would like to thank my second reader Dr. Gary Blanchard for the kindly discussions and help during my study. I also need to thank my committee members, Dr. Dana Spence and Dr. Vlad Tarabara, for their instructions inside and outside classrooms which are invaluable to build a solid background for my research. Besides, I would like to thank Dr. Greg Swain for many years solid training in electrochemistry.

In addition to faulty members, I am fortune to work in Bruening group with nice group members. I would like to thank Dr. Chao Cheng, Dr. Jason Armstrong, Dr. Nick White for their discussions and suggestions in my research. I also appreciate the current and former group members for the great time that we work together in the lab. Besides, I am grateful to many good friends in graduate school, Xingyi Yang, Chen Qiu, Zhe Jia, Yuling Xie and Chen Zhang. I appreciate your company and lots of fun time that we spent together.

Finally, I should give many thanks to my family. I left my parents for six and half years, and only went back once during my graduate school. I appreciate their endless love and support, and thank for their understanding and encouragement for me to pursuit my education and career in USA.

Michigan State University is a very important stop in the journey of my life, where I learned how to face to myself, accept imperfections, overcome obstacles, be a better person, and also make a better world for others. This is the end of my graduate school study at MSU, but also a beginning of my next journey. Keep going.

TABLE OF CONTENTS

LIST OF TABLES

LIST OF FIGURES

KEY TO ABBREVIATIONS

AEM	Anion-exchange membrane
CE	Counter electrode
CEM	Cation-exchange membrane
CNTs	Carbon nanotubes
CVD	Chemical vapor deposition
DD	Diffusion dialysis
DMF	Dimethylformamide
DMSO	Dimethyl sulfoxide
ED	Electrodialysis
EDOT	Ethylenedioxythiophene
EDR	Electrodialysis reversal
EG	Ethylene glycol
FO	Forward osmosis
HA	Hyaluronic acid
ICP-OES	Inductively coupled plasma-optical emission spectroscopy
LbL	Layer-by-layer assembly
MPA	3-mercaptopropionic acid
NF	Nanofiltration
NPs	Nanoparticles
PAA	Poly(acrylic acid)
PAH	Poly(allylamine hydrochloride)
PAN	Polyaniline

PDADMAC	Poly(diallyl dimethyl ammonium chloride)
PDMAEMA	Poly[2-(dimethylamino) ethyl methacrylate]
PEDOT	Poly(3.4-ethylenedioxythiophene)
PEI	Poly(ethyleneimine hydrochloride)
PEMs	Polyelectrolyte multilayers
PPy	Polypyrrole
PSS	Poly(styrene sulfonate)
PVDF	Polyvinylidene fluoride
RE	Reference electrode
RO	Reverse osmosis
SEM	Scanning electron microscopy
WE	Working electrode

Chapter 1 Introduction and Background

This dissertation investigates selective ion transport through cation-exchange membranes modified with polyelectrolyte multilayers (PEMs), nanofiltration membranes, and membranes with thin conductive skins. Coating Fujifilm cation-exchange membranes with PEMs through layer-by-layer assembly (LbL) leads to remarkable electrodialysis selectivities > 1000 in the transport of monovalent over divalent cations. LbL polyelectrolyte adsorption generates a dense film that excludes the passage of multivalent cations. Moreover, adsorption of PEMs that swell strongly in water leads not only to high electrodialysis selectivities, but also to electrically efficient ion transport. The highly charged PEM surface contributes significantly to selectivity, so this work additionally aimed to increase the charge on the membrane surface through application of an external potential. Such studies included coating of membranes with conducting films.

To provide background for my research, this chapter first reviews membrane-based ion-separation techniques, including nanofiltration, diffusion dialysis and electrodialysis. I emphasize ion-exchange membranes, concentration polarization and energy efficiency in electrodialysis. The second section of this chapter discusses LbL polyelectrolyte adsorption, deposition factors that affect PEMs properties, and the swelling of PEMs. Subsequently, I introduce the development of conductive membranes, their potential applications and an outline of this dissertation.

1.1 Membrane-based ion separations

This research aims to develop highly selective ion-exchange membranes to enhance ion separations for applications such as water softening,[1-2] salt recovery[3-4] and acid recovery.[5] Traditionally, precipitation and ion exchange are the most common techniques for separating ions.[6] However, precipitation often requires the addition of corrosive reagents such as strong bases, and sulfide precipitation produces toxic H_2S fumes.[7] Ion exchange enables the interchange of ions between two electrolytes, and ion-exchange chromatography separates ions based on ion-exchange between a stationary phase and a mobile phase, particularly for analyzing ions and separating proteins.[8] Unfortunately, preparative ion-exchange separations generate large amounts of eluent waste during the resin regeneration.[9]

Membranes provide a barrier for selective ion permeation, and the rate of permeation depends on pore size, surface charge, and ion solubility in the membrane matrix. Membrane-based separations are potentially attractive for their high energy efficiency, minimal use of chemical additives, and scalable application.[10] Using a variety of membranes and operation conditions, membrane-based ion-separation techniques include nanofiltration (NF), reverse osmosis (RO), diffusion dialysis (DD), electrodialysis (ED), forward osmosis (FO) and facilitated-transport dialysis. RO now holds the largest share of global water production through desalination.[11] The separation layer of RO membranes is so dense that these membranes reject ~99% of most ions.[10] Separations that target removal of specific ions often employ nanofiltration membranes, which have barrier layers with effective pore sizes around 1 nm. Due to a less dense membrane barrier layer (compared to RO membranes), NF can operate at lower pressures than RO and allow the passage of monovalent ions while rejecting divalent ions. Thus, NF is

attractive for water softening due to its high monovalent/divalent ion selectivity and low energy costs.[12]

In another membrane-based separation, FO extracts water from a feed solution into a receiving phase containing a high concentration of dissolved solute. Depending on the receiving-phase solute, subsequent water recovery can occur through methods such as evaporation of NH_4HCO_3.[13] FO is promising for wastewater pretreatment[14] and food processing.[15] Facilitated-transport dialysis demonstrates high selectivity, but still has technical challenges for widespread application.[16-17] In contrast, ED is a commercial process for brackish water desalination and concentration of salts in aqueous solutions,[18] and DD is the basis of hemodialysis. This section reviews DD, NF and ED, which are particularly relevant to my work.

1.1.1 Diffusion dialysis

Diffusion dialysis is a process in which substances permeate through a membrane due to a concentration gradient. In 1861, Graham first proposed separating small molecules from large ones by selective diffusion through a membrane.[19] As a more recent example, DD enables acid and alkali recovery using anion-exchange or cation-exchange membranes.[20] Figure 1.1 a) illustrates DD for recovery of HCl from a feed solution containing metal ions. An anion-exchange membrane separates the feed solution from the receiving phase and allows permeation of Cl^- under a concentration gradient. In contrast, the anion-exchange membrane prevents diffusion of metal ions, represented as M^+. To maintain electrical neutrality, H^+ passes through the anion-exchange membrane and transfers to the receiving phase. Although protons carry positive charge, they diffuse through the anion-exchange membrane due to their small size, low valence and high mobility. Figure 1.1 b) demonstrates the related NaOH recovery through DD.

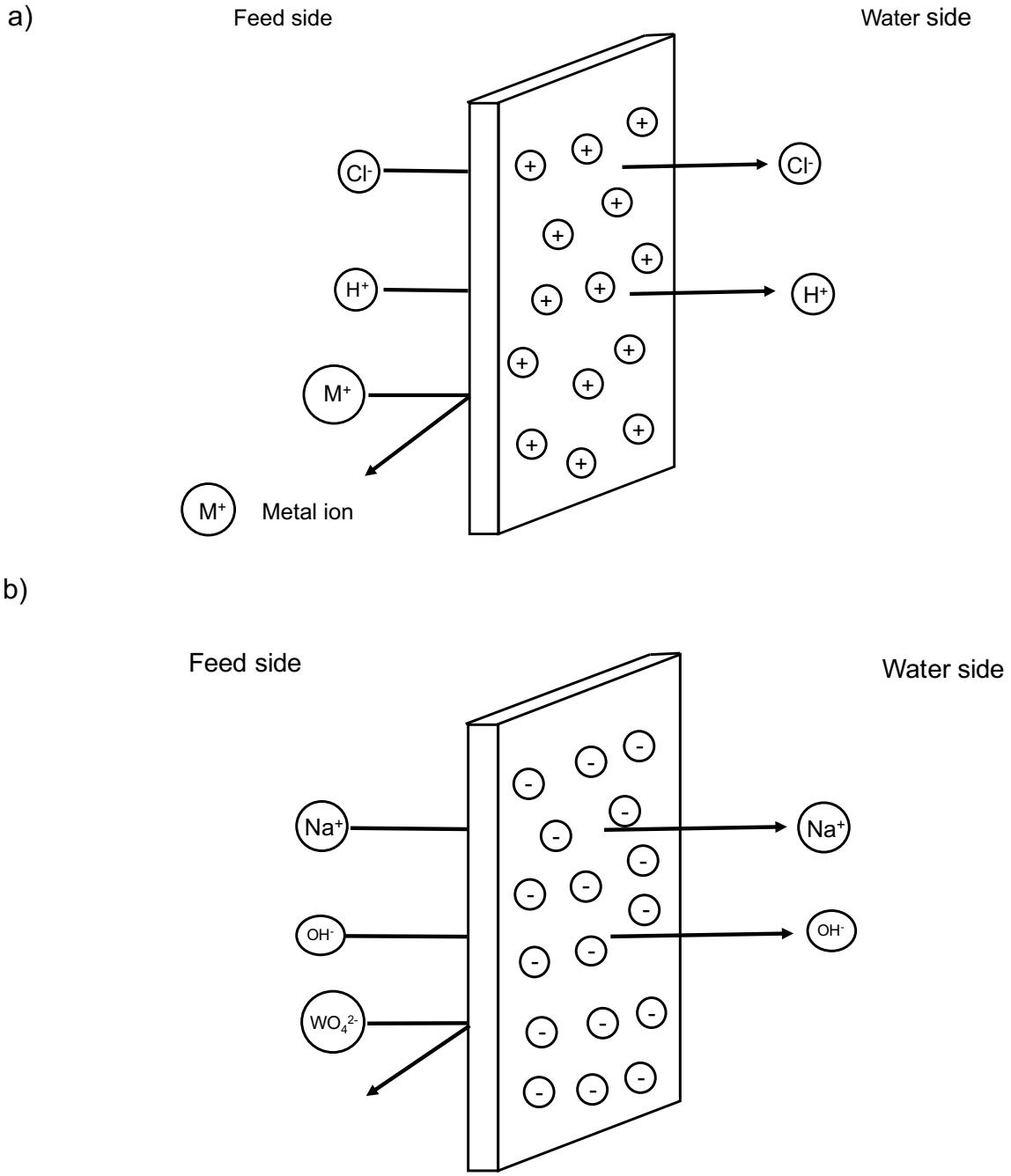

Figure 1.1 Scheme of diffusion dialysis to a) separation HCl from metal ions using an anion-exchange membane, and b) separate NaOH from a Na_2WO_4 solution. (Redrawn from J. Membr. Sci. 2011, 366, 1-16)

In ED, cation- and anion-exchange membranes should reject all anions and cations, respectively. In contrast in acid or base recovery through DD, anion-exchange membranes should allow H^+ passage and cation-exchange membranes should permit OH^- passage. Xu et al. fabricated anion-exchange membranes from poly(2,6-dimethyl-1,4-phenylene oxide) and used them to recover sulfuric acid from nickel sulfate with an acid recovery of 70% and nickel leakage less than 4%.[21] Kiyono et al achieved a $NaOH/Na_2SO_4$ diffusive selectivity of 102 through mixed matrix hollow fiber cation-exchange membranes.[22]

Diffusion dialysis can also enrich radioactive species. Wallace employed 0.01 M $UO_2(NO_3)_2$ as the feed solution and 2 M HNO_3 as the receiving phase to move UO^{2+} through a cation-exchange membrane. In this type of dialysis, often known as Donnan dialysis, protons diffuse to the feed and UO^{2+} diffuse to the receiving solution to maintain electrical neutrality. Wallace achieved a 28-fold UO^{2+} enrichment in the receiving solution.[23]

Ion-exchange membranes are not the only materials that show high selectivity in diffusion dialysis. Cheng et al deposited polyelectrolyte multilayers on porous alumina to create membranes that exhibit a K^+/Mg^{2+} selectivity >350 in DD.[24] This selectivity stems from electrostatic exclusion of divalent ions in highly charged PEMs as well selective size exclusion of the larger hydrated ion. Chapter 4 describes my efforts to introduce electric charge on conductive membrane surfaces to influence the ion permeance and selectivity during DD.

1.1.2 Nanofiltration

Nanofiltration is a pressure-driven process similar to RO, but NF employs more permeable membranes with an effective pore size of ~1 nm. Thus, the properties of NF membranes lie between those of ultrafiltration and RO membranes, i.e. NF membranes reject

molecules with molecular weights >300-500 Da, but they allow permeation of small, monovalent ions.[25] Additionally, compared to RO the high permeability of NF membranes makes them attractive for low-pressure water softening and organic pollutant removal.[12]

Models of ion transport in NF include both solution-diffusion processes and convective transport through nanopores. However, the latter mechanism seems inconsistent with the low permeability of ultrathin barrier layers, and Freger recently showed that the diffusion coefficients of small molecules are inconsistent with pore diameters determined from hydraulic permeability data.[26] Thus, the solution-diffusion model may better explain the high selectivity of NF membranes in many applications.[27-29] In this model, Equation 1.1 describes the salt flux J_i through a membrane barrier layer, where $C_{i,f}$ and $C_{i,p}$ are the concentrations of ion i in feed and permeate solutions, respectively, and B is the salt permeability constant.

$$J_i = B\ (C_{i,f} - C_{i,p}) \tag{1.1}$$

The volumetric flux J_V depends on the pressure drop across the membrane Δp, the osmotic pressure $\Delta\pi$ and the permeability constant A according to equation 1.2.

$$J_v = A(\Delta p - \Delta\pi) \tag{1.2}$$

Equation 1.3 describes the rejection of ion i, R_i, which is one of the primary measures of membrane performance.

$$R_i = \left(1 - \frac{C_{i,f}}{C_{i,p}}\right) \times 100\% \tag{1.3}$$

In another important measure of a separation, equation (1.4) shows the selectivity (α) for solute A over solute B. After substitution of equation 1.3, one can also express α in terms of rejections.

$$\alpha = \frac{C_{A,p}/C_{A,f}}{C_{B,p}/C_{B,f}} = \frac{100-R_A}{100-R_B} \tag{1.4}$$

NF ion fluxes depend on the size and charge of the ion. Both increased size and electrostatic exclusion will decrease *B* in equation (1.1) and give rise to lower ion fluxes and higher rejections. For charged and uncharged species, increases in size can decrease both partitioning into the barrier layer and diffusion coefficients.[30] In charged NF membranes, ion rejections also rely on electrostatic exclusion. Kosutic et al. showed that the rejection of organic molecules exploits size exclusion,[31] and Chellam et al. demonstrated that molecular diffusion also affects the rejection.[32] For ionic components, Schaep et al. reported that the rejections of Na_2SO_4, $MgCl_2$ and NaCl are similar on negatively charged (NF 40) and positively charged (UTC 20) membranes that possess small pore radii near 0.4 nm.[33] However, with NTR 7540 membranes with a larger pore size of 0.8 nm, ion rejection depends primarily on electrostatic exclusion.[34] The results suggest that with very small pore sizes, size exclusion controls ion rejections, but at larger pore sizes, electrostatic exclusion may dominate.

Although NF membranes are highly effective in commercial water softening, challenges including membrane fouling, low chemical resistance and modest selectivities still limit NF in some cases.[25] Membrane modification shows promise for potentially alleviating some of these challenges. For example, Li et al. fabricated NF membranes from polyhexamethylene guanidine hydrochloride through interfacial polymerization to create materials that inhibit growth of bacteria.[35] Nanofiltration membranes coated with polyanionic brushes resist fouling by oil emulsions.[36] By increasing membrane surface charge through layer-by-layer assembly, Ouyang et al. achieved a Na^+/Mg^{2+} selectivity of 22 with a solution flux of 0.85 $m^3/(m^2$ day) at 5 bar. Specifically, they coated alumina membranes with five poly(styrene sulfonate) (PSS)/ protonated poly (allylamine hydrochloride) (PAH) bilayers.[1] Additionally, the Cl^-/SO_4^{2-} selectivity was 35 for $(PSS/PAH)_4PSS$-coated coated alumina and 27 with PSS/poly(diallyl dimethyl ammonium

chloride) (PDADMAC) films deposited on ultrafiltration membranes.[37-38] Moreover, Cheng et al. suggest that even the very small passage of Mg^{2+} through $(PSS/PAH)_4$-coated alumina membranes is due to membrane imperfections.[24] In addition to increasing selectivity, dual-layer polybenzimidazole/polyethersulfone NF hollow fiber membranes remove heavy metals from wastewater, and PBI resists chemical degradation.[39]

NF applications include the treatment of ground water,[40-41] wastewater reclamation,[42-43] water softening[44-46] and recovery of monovalent ions.[47] In addition, NF applications are expanding in pharmaceutical manufacturing and biotechnology. Several studies developed membrane-based purification of active pharmaceutical ingredients from genotoxic impurities.[48-50] In chapter 5 of this dissertation, we examine NF salt rejections and find that charged surfaces may create regions of nonelectroneutrality in the membrane. These regions likely control the resistance to salt transport.

1.1.3 Electrodialysis

Electrodialysis is an electric field-driven separation technique in which ions migrate across ion-selective membranes from a feed stream to a receiving stream. Commercial ED configurations include a series of alternating cation-exchange and anion-exchange membranes between two electrodes (Figure 1.2). As a dilute salt solutions flow between cation- and anion-exchange membranes, cations migrate toward the cathode through the cation-exchange membrane, and the anion-exchange membrane in the neighboring receiving compartment ensures these cations remain in the receiving solution. Similarly, anions migrate from the dilute compartment toward the anode through an anion-exchange membrane, and the neighboring cation-exchange membrane in the receiving compartment retains these ions in the concentrate

solution. Thus, this configuration removes ions from the electrolyte solutions flowing through the dilute compartments to deionize the solution and potentially concentrate the ions in neighboring receiving compartments. Each stack contains two electrodes and several dilute/concentrate chambers.

Meyer et al. first proposed an ED cell with a stack of membranes between two electrodes.[51] However, at the time the high electrical resistance and low stability of ion-exchange membranes in harsh conditions limited commercial applications. With the development of high quality ion-exchange membranes, commercial ED for demineralizing brackish water began in the 1950's. ED industrial processes for demineralizing and concentrating electrolyte solutions rapidly appeared thereafter. In the 1960s, the Asahi company first produced salt from seawater through electrodialysis,[52] and during the 1970s electrodialysis reversal (EDR) was developed to reduce the scale formation in long-term ED.[53] Simultaneously, the development of bipolar membranes, which contain both cation-exchange and anion-exchange layers in one membrane, expanded ED into applications such as acid production[54-58] and demineralizing whey and soy proteins in the food industry.[59] This section discusses ion-exchange membranes for ED, concentration polarization during ED, energy and capital costs of ED separations, and lastly, applications of this technology.

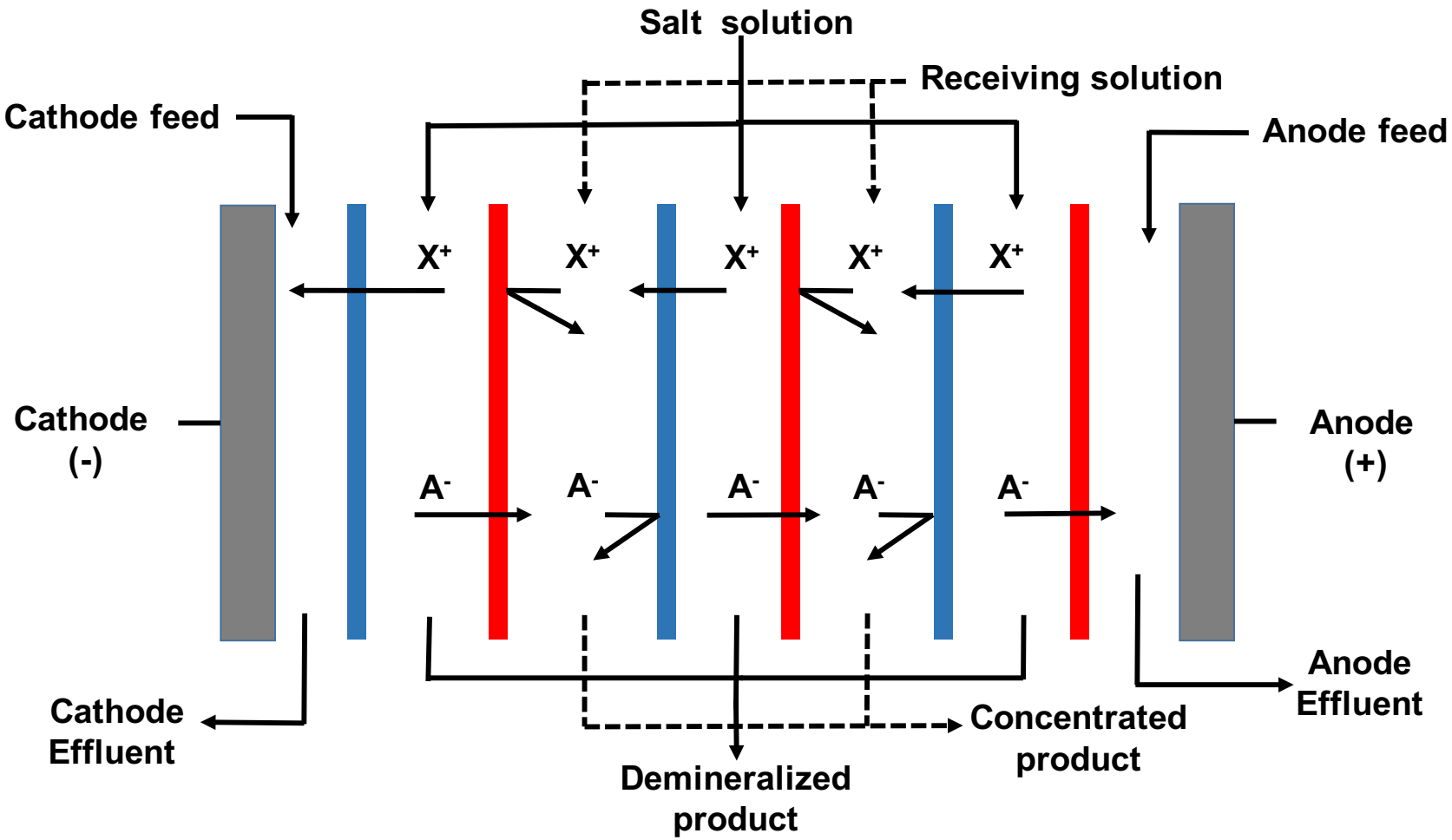

Figure 1.2 Scheme of an electrodialysis stack for desalination. Anion- (red) and cation- (blue) exchange membranes allow selective passage of anions and cations, respectively. (Redrawn from Desalination 2007, 205, 38-46)

1.1.3.1 Ion-exchange membranes

Ion-exchange membranes form the core of electrodialysis cells. In cation-exchange membranes (CEM) fixed negative charges from functional groups such as $-SO_3^-$, $-COO^-$, and $-C_6H_4O^-$ limit the passage of anions to enable selective cation transport. On the other hand, anion-exchange membranes (AEM) include positively charged groups such as $-NH_3^+$, $-NRH_2^+$, and $-SR_2^+$ to restrict cation transport.[61] Because the ionic groups absorb water, membranes must contain a high degree of crosslinking or insoluble phases to limit swelling.[62-63]

1.1.3.1.1 Homogeneous and heterogeneous ion-exchange membranes

Ion-exchange membranes can contain either homogeneous or heterogeneous distributions of charged sites. Heterogeneous membranes consist of fine cation- or anion-exchange powders dispersed in binder polymers.[64] Figure 1.3a schematically shows the structure of a heterogeneous membrane and the counter-ion transport pathway. (The term counter-ion refer to ions with a charge opposite in sign to that of the ion-exchange membrane fixed charge.) Because the binder polymer provides mechanical strength, ion-exchange resin materials need not satisfy strict mechanical requirements. Thus, heterogeneous ion-exchange membranes can exploit many ion-exchange materials.[64] However, the electrochemical properties of heterogeneous membranes are relatively poor because the heterogeneity may lower the membrane conductivity and limit economical current densities.[65] Moreover, counter-ions pass through the ion-exchange phase, not the non-conducting binder polymer region, which may cause local concentration polarization.[66] Thus, homogeneous ion-exchange membranes are more common than heterogeneous materials in commercial applications.

a)

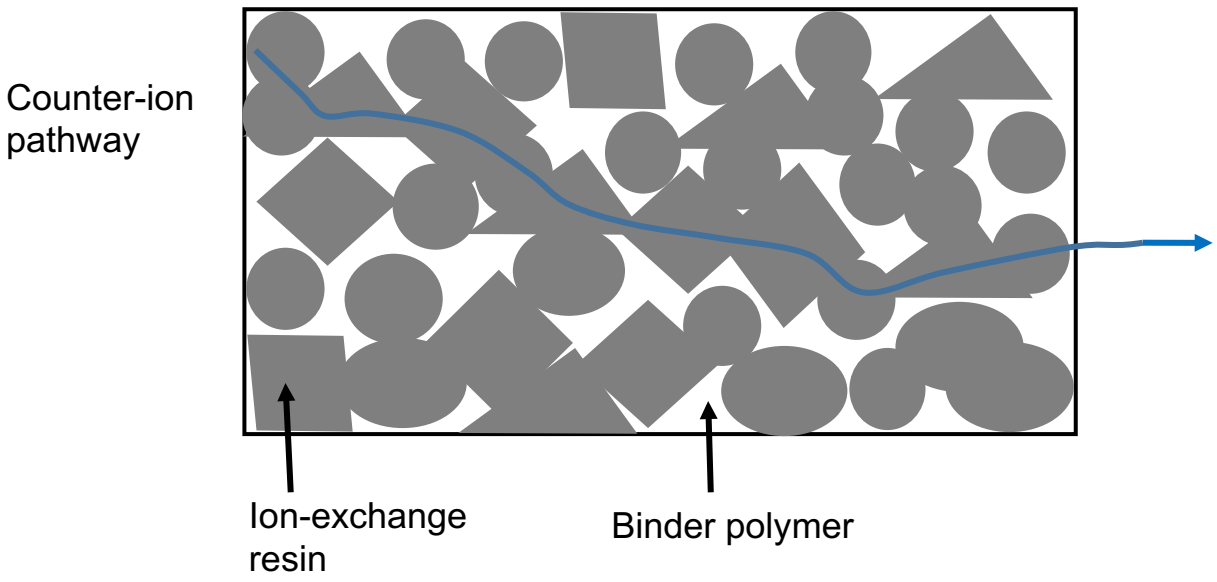

b)

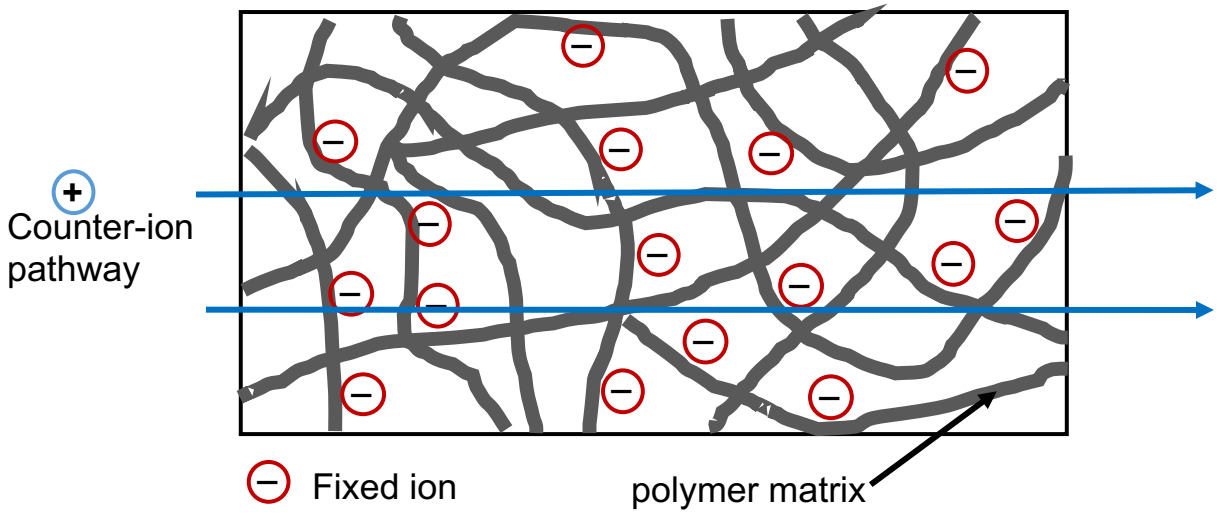

Figure 1.3 Schematic illustrations of a) an ion-exchange membrane with a heterogeneous structure consisting of resin powder and binder polymer and b) a cation-exchange membrane with a homogeneous structure. (Redrawn from Desalination 2010, 264, 268-288)

Homogeneous ion-exchange membranes consist of a single-phase, so the polymer matrix must fulfill two functions: mechanical support and ion exchange. Figure 1.3b shows the schematic membrane structure. The three general approaches to prepare homogenous ion-exchange membranes include polymerization of monomers containing cationic or anionic groups, introduction of charged moieties onto solid polymer films, and introduction of anionic or cationic moieties into a polymer followed by dissolution and casting into a film.[52] Homogeneous membranes prepared by polymerization of monomer and subsequent formaldehyde crosslinking show good electrochemical properties, but poor mechanical strength.[67-68] In the 1960s, Walther Grot from DuPont synthesized the fluorocarbon based ion-exchange membrane with the tradename Nafion.[69] This polymer is attractive because of its high conductivity and stability in harsh conditions.

1.1.3.1.2 Cost-effective cation-exchange membranes

The rapid development of ion-exchange membranes expanded their applications from labs to industry.[70] However, some applications require high temperature and oxidizing conditions in which many membranes are not stable.[71] Currently, the cation-exchange membranes developed for those conditions, such as Nafion, Aciplex, and Flemion, consist of perfluorinated, polymers.[72] The polytetrafluoroethylene backbone provides stability in harsh environments, and sulfonic acid groups on side chains give a high proton conductivity (Figure 1.4a). Many studies exploited such membranes in direct methanol and proton-exchange membrane fuel cells.[73] Nevertheless, production of perfluorinated membranes is expensive due to safety concerns when working with fluorinated monomers and the cost/availability of the perfluoroether comonomers.[68] Nafion membranes cost more than 1000 US$/m^2 (based on the Ion Power price list, Oct. 2016), and this high price will limit most large-scale applications.

Thus, many studies aimed to create alternatives to fluorinated ion-exchange membranes. Fan et al. developed cation-exchange fuel cell membranes based on sulfonated and phoshphonated polystyrene (Figure 1.4b). They claim that the tertiary hydrogen atom at position Y is the primary reason for the instability of current polystyrene membranes, so replacing the hydrogen with other covalently boned groups should enhance the membrane stability.[74] Hibino et al. used poly(arylene ether sulfones) to prepare solid electrolyte membranes to prevent fuel crossover at high ion-exchange capacity (Figure 1.4c). Polybenzimidazoles doped with high acid concentrations provide high ionic conductivity comparable with Nafion at low cost (Figure 1.4d).[70] However, these alternative cation-exchange membranes are still far from large-scale applications.

a)

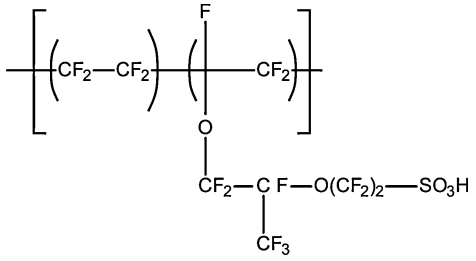

b)

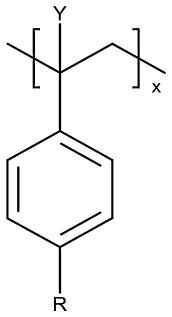

c)

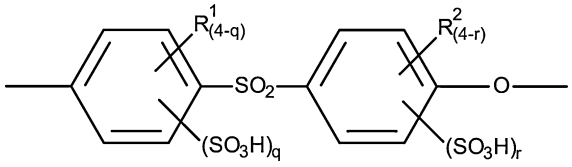

d)

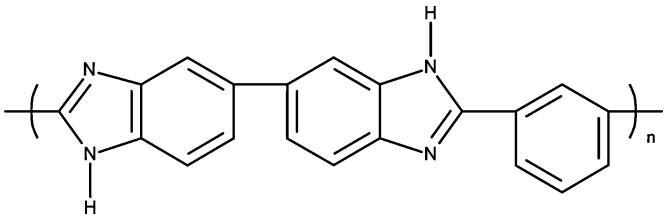

Figure 1.4 Basic structure of common cation-exchange materials for electrodialysis and fuel cell membranes. (a) Nafion, (b) polystyrenes, (c) poly(arylene ether sulfones) and (d) acid-doped polybenzimidazole membrane. (Reprinted with permission from Chemical Engineering Research and Design 2012, 90, 950-959)[72]

1.1.3.2 Concentration polarization and limiting current

Concentration polarization, which occurs at the interface between a well-stirred solution and the ion-exchange membrane, significantly limits the rate and energy-efficiency of ED. Specific to ED, concentration polarization results from differences in the ion transport number (sometimes called the transference number) in an ion-exchange membrane and in the bulk solution. The ion transport number is simply the fraction of the total current that a given ion carries. Figure 1.5 demonstrates an example of concentration polarization in a cation-exchange membrane. In a perfectly selective CEM, only cations carry current. In contrast both anions and cations carry current in the solution, where cations migrate toward the CEM and anions migrate in the opposite direction. Thus, the cations become depleted at the solution/membrane interface because the number of cations electrically migrating from the bulk solution to this interface is less than the number cations electrically migrating within the CEM. This depletion gives rise to a concentration gradient that results in diffusion of cations to the CEM. Steady-state occurs when the cation concentration gradient at the membrane surface is large enough that the sum of diffusive and electromigration cation fluxes to the membrane surface are equal to the electrical migration of the cation within the CEM. (Diffusion in the CEM is negligible due to the large membrane thickness and the relatively low ion diffusion coefficients in the membrane.) Note that anion depletion also occurs at the membrane/solution interface in Figure 1.5 because anions move into the solution from this interface, but they do not enter the interface from a perfectly selective CEM.

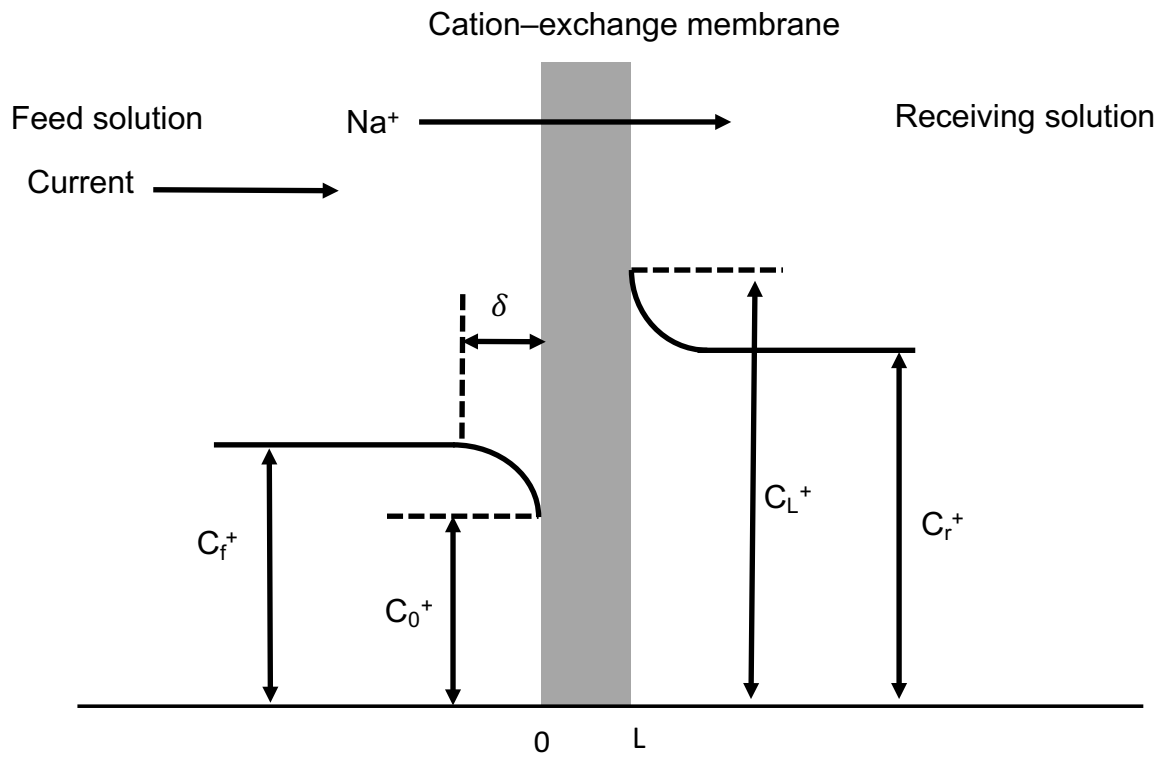

Figure 1.5 Schematic drawing of the sodium ion concentration near a cation-exchange membrane during electrodialysis from a solution containing a Na^+ salt. The vertical axis is the concentration, and the cation concentration is C_f^+ in feed phase, C_0^+ at the membrane surface (feed side), C_L^+ at the membrane surface (receiving side), and C_r^+ in the receiving phase. L is the membrane thickness. (Redrawn from Membrane Technology and Applications, 2nd ed.: J. Wiley: Chichester; New York, 2004)

As the applied current increases, the steady-state ion concentration at the membrane surface decreases and eventually approaches zero. The applied current density when the surface concentration approaches zero is termed the limiting current density, which is the maximum current that one can apply in energy-efficient electrodialysis. Above the limiting current, the system can no longer supply sufficient cations (or anions for an anion-exchange membrane) to

the membrane, and other species must carry current. These species may include OH^- and H^+ formed due to water splitting near the membrane/solution interface, where high potential gradients occur due to ion depletion. Both high resistances in the depleted region and significant side reactions such as water splitting consume much of the applied energy.

Based on equating the cation flux in the solution and in the membrane when the surface cation concentration is zero,[75-77] equation 1.5 describes the limiting current density, I_{lim}, where D^+ is the diffusion

$$I_{lim} = \frac{D^+ F C^+}{\delta(1-t^+)} \qquad 1.5$$

coefficient of the cation in water, F is Faraday's constant, C^+ is the bulk concentration of the cation, δ is the depletion layer thickness and t^+ is the cation transport number.

Experimental estimations of the limiting current often employ a plot of applied current density vs transmembrane potential (I-V curve, e.g. Figure 1.6). Initially, the current density increases linearly with the transmembrane potential according to Ohm's law (Ohmic region). As the current approaches and exceed the limiting value, the current density does not increase significantly with transmembrane potential ("plateau region") because the diffusive flux of cation from the feed solution reaches a maximum and cannot supply additional cation flux for increased migration into the CEM. However, as the current density exceeds an overlimiting value, the current again increases with transmembrane potential due to water splitting or electroconvection.[78-79] One can estimate the limiting current density from the intersection of the Ohmic and "plateau" regions in the I-V curve.

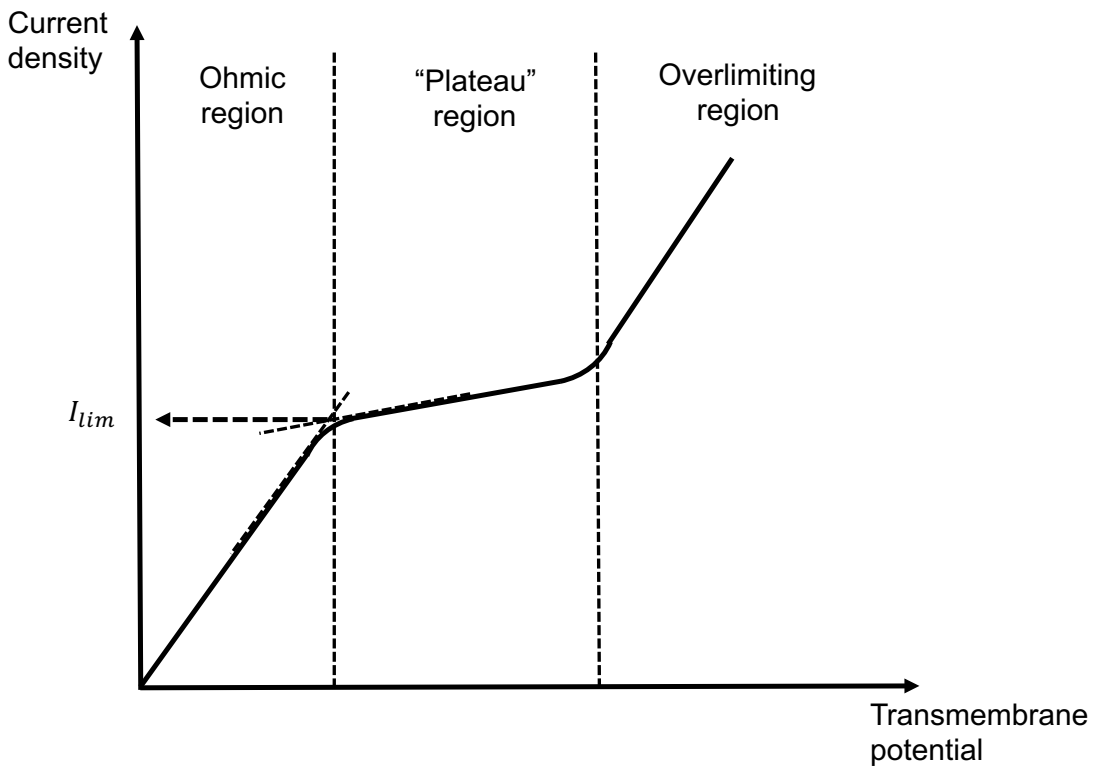

Figure 1.6 Schematic drawing of current density vs transmembrane potential during electrodialysis through an ion-exchange membrane. The intersection of the lines describing the Ohmic and plateau regions gives a value for the limiting current. (Redrawn from Desalination 2010, *264*, 268-288)[18]

1.1.3.3 ED costs

The total cost of electrodialysis for desalination includes the purchase of electricity to separate ions across a stack of membranes, capital investments, and plant maintenance and labor costs. Equation 1.6 describes the power consumed (*P*) to drive a separation

$$P = i^2 R \tag{1.6}$$

where i is the current through the membrane and *R* is the system resistance. When the transport number of the desired ions is unity, the current is proportional to the charge migrating across the membranes according to equation 1.7

$$i = zQF(C_f - C_r) \tag{1.7}$$

where z is the charge of the desired ion, Q is the volume flow, and C_f and C_r are ion concentrations in the feed at the ED compartment inlet and outlet, respectively. Introducing equation 1.7 into equation 1.6 gives the minimum energy cost for the separation

$$E = R\left(zQF\left(C_f - C_r\right)\right)^2 \tag{1.8}$$

The investment cost, including membrane and cell fabrication, as well as plant maintenance and labor costs are proportional to the size of the plant. The required membrane area for a given separation rate fixes the plant size. Thus, the higher the current density, the smaller the plant size needed to produce a certain amount of deionized or concentrated solution. The total cost in electrodialysis is primarily the sum of energy and investment costs (Figure 1.7). At a certain current density, the total cost reaches the minimum value. However, limiting currents are also important because operation at overlimiting currents will reduce the current efficiency so equation 1.7 will require an efficiency correction. For low-concentration feed solutions, the limiting current is often much lower than the current density for minimum total cost.[18]

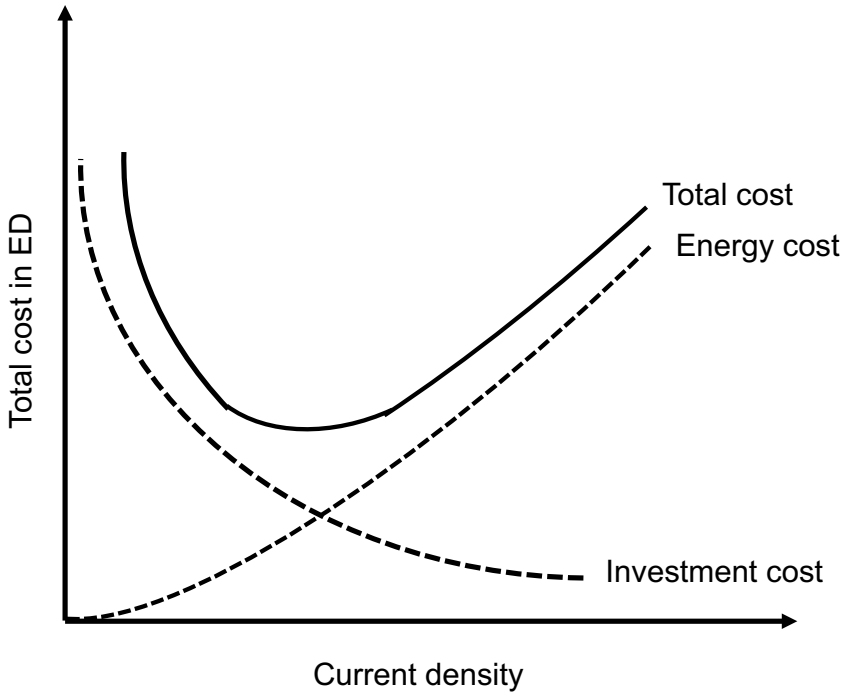

Figure 1.7 Schematic diagram illustrating the various costs in electrodialysis as a function of the applied current density. (Redrawn from Desalination 2010, 264, 268-288)

1.1.3.4 Application of ED

The largest ED application is probably the production of potable water from brackish water.[80] Electrodialysis is competitive for desalting feed solutions with salt concentrations in the 500-2000 ppm range, whereas reverse osmosis has the economic advantage for feed salt concentrations above 2000 ppm.[80] The advantages of ED for desalination of brackish water include high water recovery rates, long membrane lifetimes, and low membrane fouling due to the reversal process. However, ED cannot remove neutral components such as suspended solids, bacteria and viruses, so a full purification process requires pre- or post-treatment.[81] Moreover, electrodes are expensive, and as mentioned ED is only cost-effective in a certain range of feed concentration and product water quality.

In some cases, ED is also effective in water demineralization and wastewater treatment. Industrial wastewater treatment includes demineralization of boiler feed water and desalination of contaminated water. Due to the increasing cost of fresh water and environmental concerns, recycling of wastewater is a necessity. Electrodialysis is particularly attractive for such processes because it can achieve water recoveries up to 95%. In other practical applications, ED can concentrate and recovery nickel from rinse water or recover acids such as HCl, HNO_3 and HF from spent pickling solutions.[82] ED applications in the food industry and biotechnology include deionization of whey as well as other protein and sugar solutions, and removal of organic acids from fermentation broths.[83] Moreover, ED can serve as a pre-concentration process prior to evaporation for salt recovery from sea water.[18]

1.2 Functional thin films

Thin polymer films provide a wide range of coatings that help to prevent corrosion of metals,[84-86] resist fogging of glass,[87-90] and decrease surface fouling.[91] Additionally, polymer films can serve as active interfaces for chemical sensors[92-95] or affinity coatings that capture specific substrates.[96] Ultrathin films with thicknesses on the nm scale are attractive as barrier layers for membrane filtration because such films have a relatively small resistance to water flux and can dramatically improve selectivity or fouling resistance. This dissertation explores coating of membranes with thin polymer films to achieve high ion-transport selectivities. Specifically, we frequently coat membranes with polyelectrolyte multilayers. Thus, this section discusses layer-by-layer adsorption of functional thin films, the layer-by-layer coating mechanism, and factors that affect film properties.

1.2.1 Layer-by-layer assembly of polyelectrolyte multilayers

Layer-by-layer (LbL) assembly of thin films is now a widespread technique because of its precise control over film thickness, roughness, and surface charge using a wide variety of coating materials and substrates. Generally, LbL assembly of polyelectrolytes is a repeating process that includes adsorption of a charged polymer on a substrate, rinsing to remove weakly adhered material, adsorption of an oppositely charged polyelectrolyte on the same substrate, and a second rinsing step. Repetition of this sequence yields the desired number of bilayers on a surface (Figure 1.8),[97] and variation of the number of bilayers affords thickness control at the nm scale.

The assembly of polyelectrolyte multilayers usually, though not always, relies on charge overcompensation after adsorption of each polyelectrolyte. The initial layer adsorbs on the substrate through electrostatic or other attractions to create a highly charged surface. In subsequent steps the polyelectrolytes adsorb to the oppositely charged surface and overcompensate the surface charge to change its sign.[98-100] Schlenoff et al. explained polyelectrolyte multilayer formation as an entropy driven assembly because the adsorption of a single polyelectrolyte molecule releases numerous counterions into solution.[101] In addition to charge compensation and release of counterions, covalent binding, hydrogen-bonding, and host-guest interactions can also promote LbL assembly with a wide range of deposition materials including proteins, lipids, nanoparticles and nucleic acids.[102-105] Moreover, LbL assembly applies not only to planar substrates, but also to a range of substrates including porous membranes, colloids, nanoparticles and nanorods.[106-107] Figure 1.9 demonstrates the various substrates and coating materials for LbL assembly.

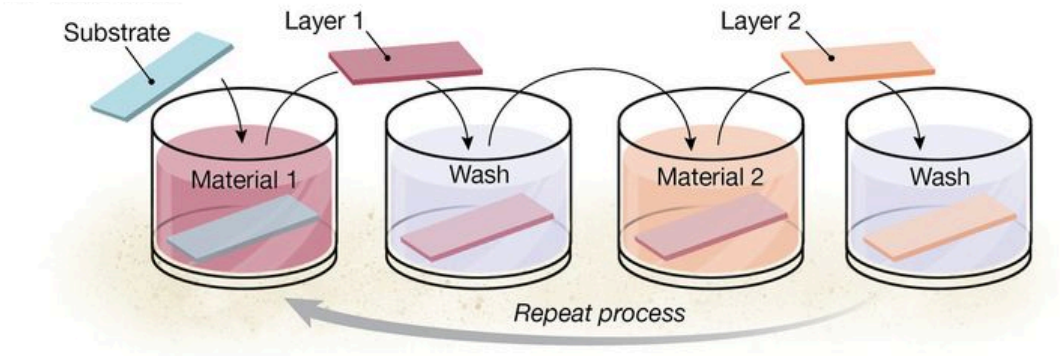

Figure 1.8 Schematic diagram of layer-by-layer adsorption (Reprinted with permission from Science 2010, 348, 2491)

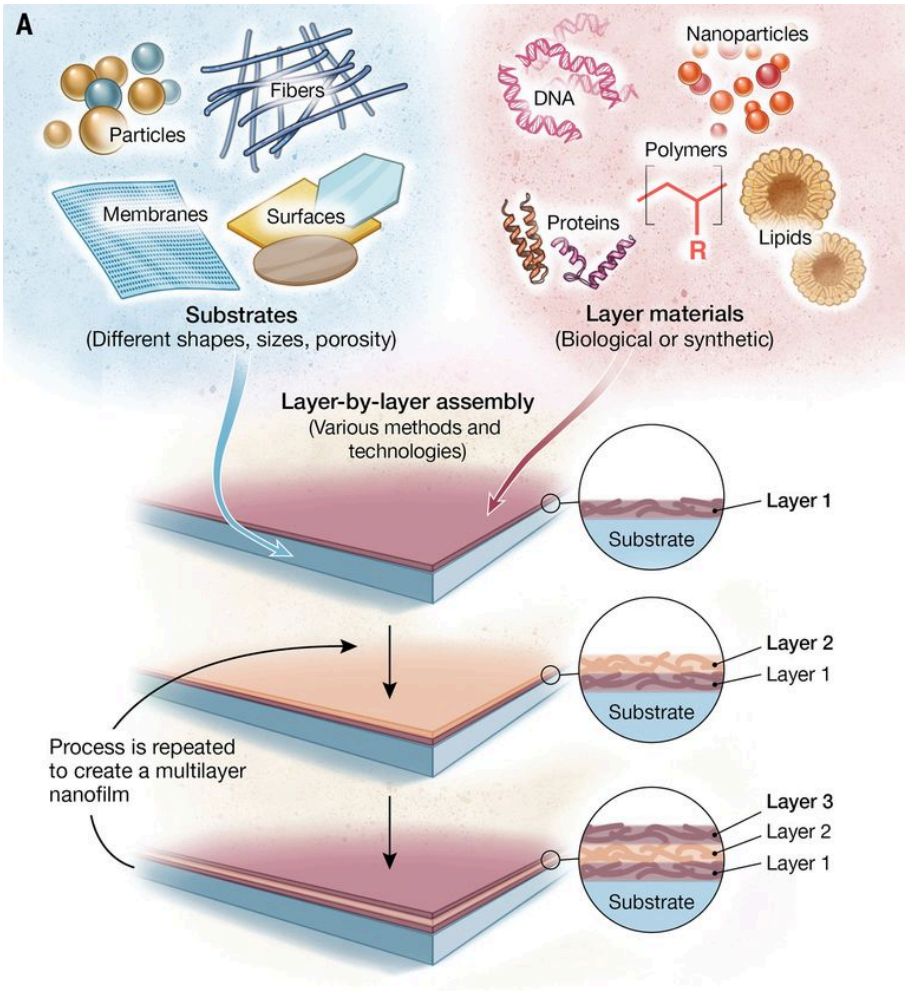

Figure 1.9 Schematic overview of LbL assembly with various substrates and coating materials (Reprinted with permission from Science 2010, *348*, 2491)[108]

Techniques for LbL assembly fall into several categories including immersive,[109-111] spin,[112-113] spray,[114-115] electromagnetic[116] and fluidic assembly.[117-118] Immersive assembly, also known as dip assembly, is the most common method for LbL thin film deposition because it is simple and tends to gives homogeneous films.[119] However, the immersive assembly process is time consuming, requires significant amounts of coating materials especially for large substrates and generates waste solutions. These drawbacks are major problems in industrial applications. Thus researchers developed spin and spray assembly to increase the rate of polyelectrolyte adsorption or reduce the amount of waste solution. Electromagnetic assembly on electrodes or magnetic substrates employs electric or magnetic fields to enhance polyelectrolyte adsorption. Fluidic assembly coats a substrate in the channel of a flowing stream.

This dissertation focuses on LbL films prepared from through immersive assembly. The common polyanions include ionized forms of poly(acrylic acid) (PAA),[120] PSS,[38] poly(vinylsulfonic acid),[121] and hyaluronic acid (HA),[122] whereas the widely used polycations include PAH, poly(diallyl dimethyl ammonium chloride) (PDADMAC), and poly(ethyleneimine hydrochloride) (PEI). Figure 1.10 shows structures of some of these polyelectrolytes.

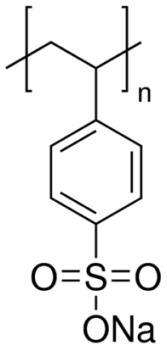

poly(4-sodium styrene sulfonate)

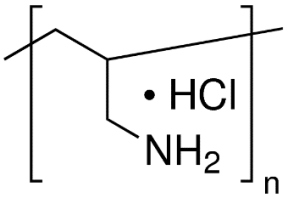

poly(allylamine hydrochloride)

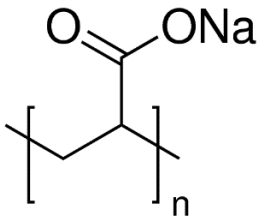

poly(acrylic acid) sodium salt

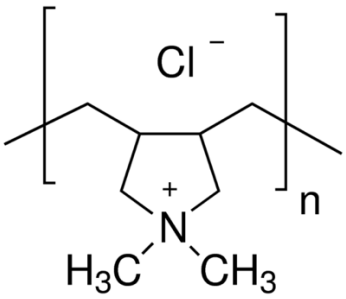

poly(diallyl dimethyl ammonium chloride)

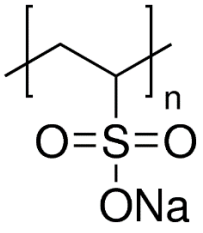

poly(vinylsulfonic acid) sodium salt

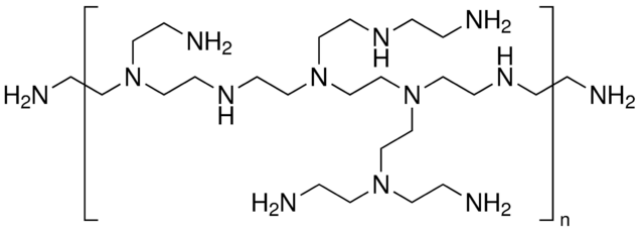

poly(ethyleneimine hydrochloride), branched

Figure 1.10 Structures of common polyelectrolytes used in LbL adsorption.

1.2.2 Factors affecting film growth in layer-by-layer assembly

The thickness, charge and structure of polyelectrolyte multilayers formed through LbL assembly depend on the constituent polyelectrolytes, deposition pH, supporting electrolyte concentration, and assembly methods. The density of charge on the polyelectrolyte affects film thickness, which can increase linearly or exponentially with the number of bilayers, depending on the polyelectrolyte system. For example, $(PSS/PAH)_n$ film thicknesses increases linearly with the number of bilayers,[123] whereas $(PDADMAC/PSS)_n$ or $(HA/chitosan)_n$ films sometimes show an exponential growth mechanism.[124-125] Under the same adsorption conditions, the thickness per bilayer for PSS/PDADMAC is 7 times higher than for PSS/PAH.[109, 124] Choi et al. reported that the thicknesses of star-shaped PAA/poly[2-(dimethylamino) ethyl methacrylate](PDMAEMA) films are two or three times higher than the thicknesses of linear PAA/PDMAEMA with the same number of bilayers.[126]

In addition to polyelectrolyte type, the supporting electrolyte composition and concentration in deposition solutions also affect PEM growth. The supporting salt screens the charge on the polymer chain to reduce the charge repulsion between the repeating units. As a consequence, polymers trend to coil and form thicker films in the presence of supporting electrolyte. In contrast, without the supporting salt, polymer chains extend to minimize charge repulsion, and adsorption under such conditions yields relatively thin films.[127] The coil conformation (films deposited in the presence of salt) also leads to higher surface charge than the extended structure (films deposited without salt).[109, 128] The thicknesses of $(PDADMAC/PSS)_{10}$ films increase from around 10 nm for films adsorbed from solutions containing 0.1 M NaCl to 300 nm for films adsorbed from 2 M NaCl,[109] and the surface roughness also dramatically

increases.[129] The higher roughness leads to adsorption of more polymer because of increased surface area.

In addition to supporting electrolyte concentrations, several studies show that salt composition affects the film thickness. Dubas et al. reported the thicknesses of 10-bilayer PDADMAC/PSS films deposited from different solutions containing a series of cations with a constant anion (chloride). The less hydrated cations lead to thicker films due to a stronger interaction with polyanions.[109] Similarly, the anion of the supporting electrolytes also influences film thickness. Salomaki et al. studied the growth of PSS/PDADMAC films with a series of anions ranging from cosmotropic to chaotropic (F^-, $HCOO^-$, BrO_3^-, Cl^-, ClO_3^-, Br^-, NO_3^-, ClO_4^-). The chaotropic anions strongly interact with polycations, screening the polyelectrolyte charges, therefore resulting in coil structures and thicker films.[130-131] The 10-bilayer film thickness increases from around 20 nm in NaF to 90 nm in NaBr, and the anion composition had a stronger influence on film thickness than the cation composition. Moreover, Dressick and coworkers reported that divalent anions in the deposition solutions lead to thicker films than monovalent anions.[130]

The pH of the deposition solution dramatically affects the film thickness when depositing weak polyelectrolytes. The ionization of some functional groups such as amines and carboxylic acids depends on pH, and more extensive ionization creates a higher charge density on the polymer, which gives rise to thinner PEMs. For example, at pH 2.5, 70% of the carboxylate groups on PAA are in the carboxylic acid form, whereas, at pH 4.5, 70% of the acid groups are ionized to carboxylates. The less charged PAA at pH 2.5 gives a thicker $(PAH/PAA)_{30}$ film than the lower charged PAA at pH 4.5.[132] However, if the charge density is too low, films are not stable.[133]

1.2.3 Swelling of polyelectrolyte multilayers

Controlling the swelling of PEMs is important for selective ion transport and release of small molecules. Schlenoff et al. introduced the concept of extrinsic and intrinsic charge compensation to help explain the swelling of PEMs.[134] Intrinsic compensation refers to attainment of charge neutrality through pairing of charges from polycation and polyanion segments. Conversely, extrinsic compensation achieves charge neutrality by pairing charges on the polyelectrolytes with counter ions from salt (Figure 1.11). The fraction of extrinsic and intrinsic charge compensation in PEMs influences the film swelling, partly because intrinsic compensation cross-links polymer chains. In contrast, extrinsic compensation creates ion-exchange sites to make film more hydrophilic, less cross-linked and more prone to swelling in water. The supporting electrolyte concentration surrounding a PEM can also affect the charge compensation. High salt concentrations tends to break ionic cross-links, thereby increasing the fraction of extrinsic compensation.[133]

a)

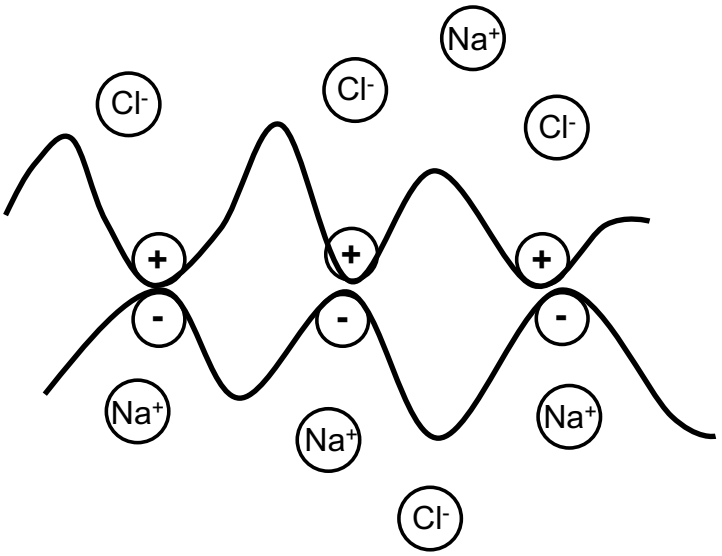

b)

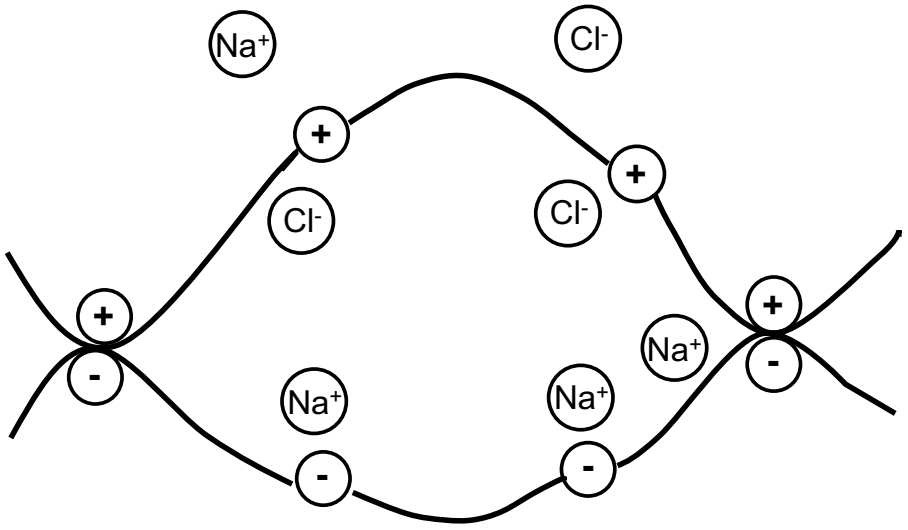

Figure 1.11 Schematic structure of (a) intrinsic compensation and (b) extrinsic compensation of polyelectrolyte chains. (Redrawn from Current Opinion in Colloid & Interface Science 2014, *19*, 25-31)[135]

In chapters 2 and 3, I utilize $(PAH/PSS)_n$ or $(PDADMAC/PSS)_n$ films to enhance the selectivity among cations during ED through cation-exchange membranes. Steitz and coworkers found that PAH/PSS multilayers are relatively insensitive to supporting salt concentration.[136] However, $(PDADMAC/PSS)_n$ films show greater swelling in aqueous solutions with high salt concentrations.[128] Dubas et al. reported that the volume swelling coefficient of $(PSS/PDADMAC)_n$ films is 20 times higher than for $(PSS/PAH)_n$ films of similar thickness.[137] Moreover, the terminal layers influence film swelling. In 0.5 M NaCl, PSS/PDADMAC multilayer films with PDADMAC termination swell 4 times more than the corresponding films terminated with PSS, presumably because PDADMAC penetrates the entire film and disrupts cross-linking of polymer chains.[138] For PSS/PAH multilayers, PAH-terminated films swell 25% less than PSS-terminated films.[139]

Several groups reported that the swelling of PEMs influences their permeability. PDADMAC/PSS films are 2 times more permeable to perchlorate ions than PAH/PSS.[140] Stair and coworkers reported that cross-linking of PEMs dramatic decreases the permeation of multivalent anions.[141] Extrinsic compensation may provide ion exchange sites that accelerate diffusion with a strongly nonlinear relation between diffusion and the concentration of ion-exchange sites.[137]

1.3 Development of electrically conductive membranes

The most common driving forces for transmembrane transport include pressure, concentration, and electrical potential differences across the membrane. With the rapid development of conductive materials, electrically conductive membranes have attracted attention for controlling transport. In the 1980s, Wagner and Aizawa suggested a membrane separation

method based on an electrochemical reaction of membrane materials under an electrical potential.[142] In the1990s, several groups investigated whether electrostatic interactions between analytes and conducting membranes could influence the transport of charged analytes.[143]

Separations with electrically conductive membranes differ from conventional ED due to the nature of the separation mechanism. With a conductive membrane, the electrical potential between the membrane and solution may change the ion partitioning into the membrane, or the potential could change the oxidation state of the membrane material and consequently change its permeability and swelling. In conventional ED, a transmembrane electrical potential drives the ion movement, but the separation relies on the relative ionic affinities of the ion-exchange membrane and the ion mobilities in the membrane.

Conductive membranes have many potential applications including protein rejection and adsorption,[144] removal of organic contaminants,[145] removal bacteria and viruses,[146] and resisting membrane fouling.[147] Chapter 4 describes my effort to develop ion-separation membranes with conducting surfaces.

1.3.1 Fabrication of electrically conductive membranes

1.3.1.1 Conductive polymers

Various electrically conducting materials including conductive polymers, carbon and metals can serve as conductive membrane coatings or free standing membranes. There are several well-studied conductive polymer systems including polyaniline (PAN), polypyrrole (PPy), polyacetylene, polythiophene and their derivatives and copolymers.[148] The conductivity stems from conjugated backbones in which a series of π-bonds overlap to allow electron delocalization. Importantly, addition of dopants into the polymer structure enhances the

conductivity.[149] The dopants increase the number of charge carriers by removing or adding electrons to the polymer chains. Both electrons in unoccupied energy states (n-type) or mobile holes in filled energy states (p-type) can serve as charge carriers, but most conductive polymers, such as PAN, poly(3.4-ethylenedioxythiophene) (PEDOT), PPy, and polythiophene are p-type.

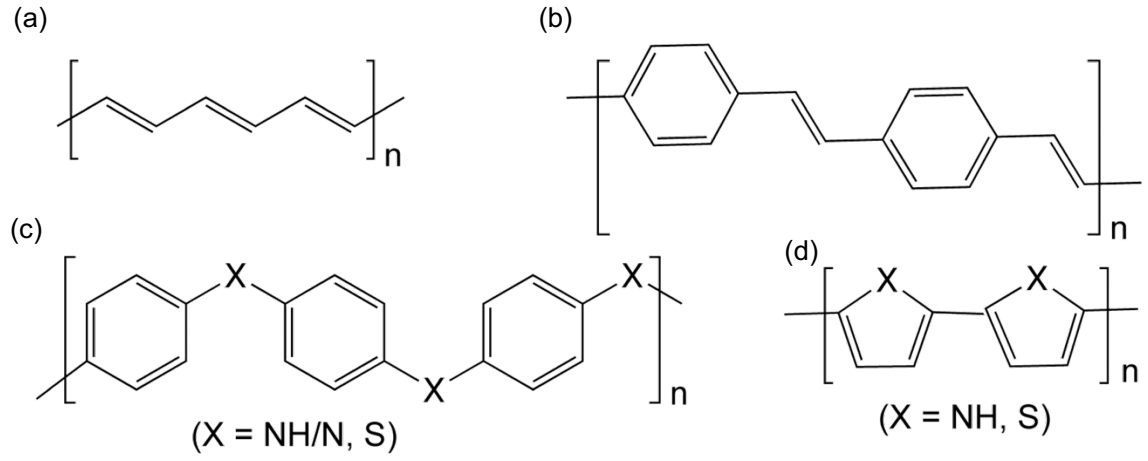

Figure 1.12 Chemical structures of several conductive polymers (a) polyacetylene, (b) poly(phenylene vinylene), (c) polyaniline (X= NH/N) or polyphenylene sulfide (X=S), (d) polypyrrole (X= NH) or polythiophene (X=S)

Among the many conductive polymers, polypyrrole is especially common in many applications due to its simple synthesis and high electrical conductivity.[150] Polypyrrole deposition on membranes can occur through electro-polymerization or solution polymerization. Bobacka and coworkers prepared PPy-modified polyvinylidene fluoride (PVDF) membranes by applying constant current (1mA/cm^2) at a PVDF-coated Pt electrode immersed in PPy.[151] Liu and coworkers created polypyrrole-modified polyester membranes through solution polymerization, and the coatings decreased fouling.[152] In addition, electrosynthesis can provide stand-alone polypyrrole membranes. Wallace and co-coworkers reported electrosynthesis of a polypyrrole

membrane using a constant current at a stainless steel or glassy carbon electrode. Ten min of electropolymerization gave a 5 μm thick film, and they stripped the polypyrrole from the supporting substrate to obtain a stand-alone membrane.[153-155]

Polyaniline is another very common conductive polymer. The polyaniline structure can switch between its reduced (leucoemeraldine), half-oxidized (emeraldine) and fully oxidized (pernigraniline) states in aqueous solutions with an average of one electron extracted per two monomer units.[156] Only the emeraldine state is highly conductive. Hillier and coworkers reported electrochemical polymerization of aniline onto gold-coated porous alumina.[156] Delogoz prepared polyaniline-based asymmetric membranes by the phase inversion method from a casting solution containing N-methyl pyrrolidone.[157] Jungbauer and coworkers reported gas separations with an unsupported polyaniline membrane cast from polyaniline powder.[158]

PEDOT:PSS is a polymer complex consisting of positively charged, conjugated PEDOT and negatively charged saturated PSS (Figure 1.13). PEDOT:PSS is a successful commercial conducting polymer sold under the trade name of Baytron® by Bayer AG and subsequently by H.C.Starck, and under the name of Clevios® by Heraeus. Spin casting, spray deposition, inkjet printing, screen printing and layer-by-layer assembly can all yield thin PEDOT:PSS films.[159-160] The thin films exhibit a wide range of conductivities from 10^{-2} to 10^{3} S cm^{-1} depending on the thickness, coating method, additives and post-treatment. Mixing PEDOT:PSS with solvents such as dimethyl sulfoxide (DMSO), ethylene glycol (EG), and dimethylformamide (DMF) can increase the conductivity more than 1 order of magnitude.[161-162] The low molecular weight solvent induces the reorientation of PEDOT/PSS chains to lower resistance.[163] Kim and coworkers proposed that polar solvents with a high dielectric constant screen interactions between the positively charged PEDOT and negatively charge PSS, thereby reducing the

electrical coupling between the counter ions and the charge carrier to increase conductivity.[164] In addition to commercial PEDOT:PSS solutions, formation of PEDOT films can take place through electrochemical polymerization, vapor phase polymerization, and oxidative polymerization.[165-167]

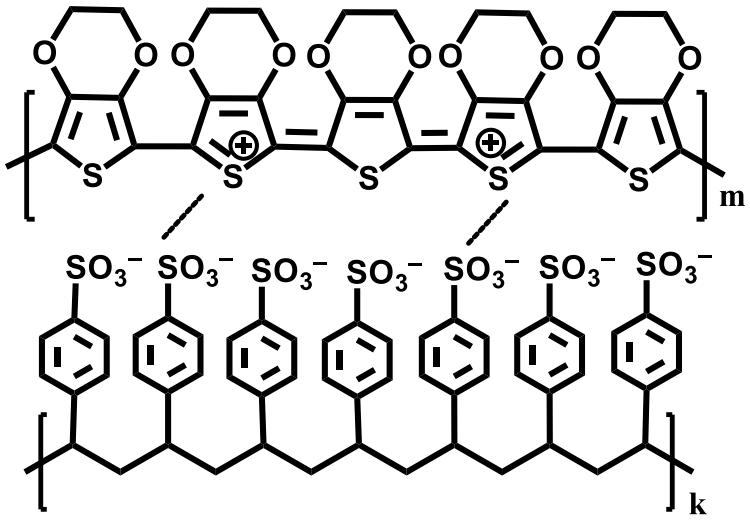

Figure 1.13 Chemical structure of a PEDOT:PSS complex

1.3.1.2 Gold coated membranes

In 1995, Martin and coworkers reported gold-based electrically conductive membranes. They employed electroless deposition to coat the pores of membranes with gold.[143] The electroless metal deposition employs a chemical reducing agent to plate the metal from solution onto a surface. The first advantage of the electroless method is that it does not require an electronically conductive substrate. As a second asset, the coating covers both the interior of pores and the membrane surface. Thirdly, the method applies to various membranes such as track-etched polycarbonate, porous alumina and polymeric nanopores.[168-169] Sputter coating and

evaporation can also coat commercial membranes with gold.[156, 170] However, such methods do not yield controlled deposition in pores.

1.3.1.3 Carbon materials

Carbon materials including carbon nanotubes (CNTs), graphene, and doped diamond can potentially create electrically conductive membranes. Wiesner and coworkers fabricated CNT-coated membranes by pressure filtering a thin layer of poly (vinyl alcohol) cross linked with carboxylated multiwalled CNTs. The membranes showed a conductivity of 3600 S m^{-1}.[171] Other groups developed freestanding CNT membranes for possible water treatment and desalination. These include isoporous CNT membranes in which CNTs align as cylindrical pores across an impermeable matrix and bucky-paper CNT membranes in which CNTs arrange randomly.[172] Chemical vapor deposition (CVD) of graphene followed by focused ion beam (FIB) drilling of nanopores (<10 nm to 1 μm) yields permeable graphene films.[173] Recently, Gao and Nebel grew boron-doped diamond on quartz filters through CVD to give membranes with self-cleaning properties.[174]

1.3.2 Applications of conductive membranes

Conductive membranes can potentially control ion transport, separate proteins, and combat fouling. Several groups investigated the ion permselectivity of conductive polymer membranes under various potentials. In its oxidized and reduced states, polypyrrole membranes are highly permeable to anions or cations, respectively.[175] Morita found that the ion permeability dependence on applied potential varies with both ion radius and valence. The permeabilities of anions with lower ionic radii and higher valences are especially dependent on the applied

potential.[176] Hillier and coworkers reported the electrochemical modulation of ion transport on PAN-modified alumina membranes, based on PAN oxidation states.[177]

Although the applied potential affects ion transport through conductive polymer membranes, the permeability changes often rely on an electrochemical reaction within the polymer. Martin's group investigated the ion permeability of gold nanotubule membranes, which can show cation, anion or no selectivity depending on the applied potential. The Au nanotubules have pore radii of ~ 2.5 nm, which is smaller than the double layer thickness at low ionic strength, so the strong electric field rejects ions with same charge as the sign of the applied potential.[143] The potential has more significant effects in low-concentration solutions where double-layer thicknesses are low.[178]

In addition to ion transport, Nguyen et al. investigated protein transport through alumina membranes coated on both sides with Pt. The selectivity is 96:1:12 for chicken egg white : bovine serum albumin: myoglobin at a transmembrane potential of -1.5V.[179-180] Several groups employed conductive membrane to combat fouling. Applied electrical potentials with CNT/polyamide composite membranes prevent biofilm formation even with high bacteria and organic material loadings.[181] Zhang and Vecitis operated a CNT-polyvinylidene fluoride mesh as a cathode to create negatively charged surfaces and reduce organic fouling.[182]

1.4 Dissertation outline

This dissertation investigates ion separations with modified cation-exchange membranes, conductive membranes and nanofiltration membranes in electrodialysis, diffusion dialysis and nanofiltration. Chapter 2 studies adsorption of PEM coatings on inexpensive Fujifilm cation-exchange membranes. The coating achieves the same high monovalent/multivalent cation

selectivities previously seen with modified Nafion. The Fujifilm membranes consist of an aromatic polyimide matrix surrounding a fibrous support, and thus should be much less expensive than the fluoropolymer Nafion. The relatively smooth surface of the Fujifilm membranes is also attractive for potentially forming continuous polyelectrolyte films. Specifically, I coated the Fujifilm Type1 cation-exchange membranes with two types of polyelectrolyte films, $(PAH/PSS)_n$ and $(PDADMAC/PSS)_n$, and subsequently examined selective electrodialysis through these membranes. Additionally, current density-voltage curves give insight into limiting currents and water splitting at the PEM-cation-exchange membrane interface.

In chapter 3, we aim to achieve enhanced current efficiencies with PEM-coated membranes. PDADMAC/PSS films swell strongly in water, and high swelling may lead to a high monovalent ion permeance, and therefore high current efficiency. Thus, this research examines ED through Nafion membranes coated with PDADMAC/PSS films. We investigate the effects of feed-solution ion concentration and number of PEM bilayers on ion flux, selectivity and transference numbers of coated membranes. Importantly, Nafion membranes coated with $(PDADMAC/PSS)_5PDADMAC$ show high selectivities with a current efficiency of ~0.75.

Chapter 4 demonstrates the development of electrically conductive membranes coated with conductive polymers and gold using LbL assembly, electroless deposition and electropolymerization. The coated membranes show high electrical conductivity, but unfortunately the ion-transport selectivity does not reversibly change when varying the applied electrical potential.

Finally, Chapter 5 investigate the effect of surface charge on salt rejection in nanofiltration. The K_2SO_4 passage increase 3-fold after coating bare NF 270 with a polycation,

whereas the passage of $MgCl_2$ decreases 3-fold as the surface turns positive. Thus, surface charge greatly affects ion permeability. A solution-diffusion-electro-migration model provides a possible explanation for how the charged surface creates regions of nonelectroneutrality where the excluded ion controls the resistance to salt transport.

REFERENCES

REFERENCES

1. Bruening, M. L.; Dotzauer, D. M.; Jain, P.; Ouyang, L.; Baker, G. L., Creation of functional membranes using polyelectrolyte multilayers and polymer brushes. *Langmuir* **2008,** *24*, 7663-7673.

2. Cadotte, J.; Forester, R.; Kim, M.; Petersen, R.; Stocker, T., Nanofiltration membranes broaden the use of membrane separation technology. *Desalination* **1988,** *70*, 77-88.

3. Tanaka, Y.; Ehara, R.; Itoi, S.; Goto, T., Ion-exchange membrane electrodialytic salt production using brine discharged from a reverse osmosis seawater desalination plant. *Journal of Membrane Science* **2003,** *222*, 71-86.

4. Kim, D. H., A review of desalting process techniques and economic analysis of the recovery of salts from retentates. *Desalination* **2011,** *270*, 1-8.

5. Wang, Z. X.; Luo, Y. B.; Yu, P., Recovery of organic acids from waste salt solutions derived from the manufacture of cyclohexanone by electrodialysis. *Journal of Membrane Science* **2006,** *280*, 134-137.

6. Willard, H. H., Separation by precipitation from homogeneous solution. *Analytical Chemistry* **1950,** *22*, 1372-1374.

7. Fu, F. L.; Wang, Q., Removal of heavy metal ions from wastewaters: A review. *Journal of Environmental Management* **2011,** *92*, 407-418.

8. Jungbauer, A.; Hahn, R., Ion-exchange chromatography. *Guide to Protein Purification, Second Edition* **2009,** *463*, 349-371.

9. Rare earth elements: A review of produciton, processing, recycling, and associated environmental issues, united states environmental protection agency, **2012**.

10. Shenvi, S. S.; Isloor, A. M.; Ismail, A. F., A review on ro membrane technology: Developments and challenges. *Desalination* **2015,** *368*, 10-26.

11. Elimelech, M.; Phillip, W. A., The future of seawater desalination: Energy, technology, and the environment. *Science* **2011,** *333*, 712-717.

12. Hilal, N.; Al-Zoubi, H.; Darwish, N. A.; Mohammad, A. W.; Abu Arabi, M., A comprehensive review of nanofiltration membranes: Treatment, pretreatment, modelling, and atomic force microscopy. *Desalination* **2004,** *170*, 281-308.

13. McCutcheon, J. R.; McGinnis, R. L.; Elimelech, M., Desalination by ammonia-carbon dioxide forward osmosis: Influence of draw and feed solution concentrations on process performance. *Journal of Membrane Science* **2006,** *278*, 114-123.

14. Lutchmiah, K.; Verliefde, A. R. D.; Roest, K.; Rietveld, L. C.; Cornelissen, E. R., Forward osmosis for application in wastewater treatment: A review. *Water Research* **2014,** *58*, 179-197.

15. Coday, B. D.; Xu, P.; Beaudry, E. G.; Herron, J.; Lampi, K.; Hancock, N. T.; Cath, T. Y., The sweet spot of forward osmosis: Treatment of produced water, drilling wastewater, and other complex and difficult liquid streams. *Desalination* **2014,** *333*, 23-35.

16. Fallanza, M.; Ortiz, A.; Gorri, D.; Ortiz, I., Polymer-ionic liquid composite membranes for propane/propylene separation by facilitated transport. *Journal of Membrane Science* **2013,** *444*, 164-172.

17. Sheng, C. J.; Wijeratne, S.; Cheng, C.; Baker, G. L.; Bruening, M. L., Facilitated ion transport through polyelectrolyte multilayer films containing metal-binding ligands. *Journal of Membrane Science* **2014,** *459*, 169-176.

18. Strathmann, H., Electrodialysis, a mature technology with a multitude of new applications. *Desalination* **2010,** *264*, 268-288.

19. Stancheva, K. A., Applications of dialysis. *Oxidation Communications* **2008,** *31*, 758-775.

20. Luo, J. Y.; Wu, C. M.; Xu, T. W.; Wu, Y. H., Diffusion dialysis-concept, principle and applications. *Journal of Membrane Science* **2011,** *366*, 1-16.

21. Xu, T. W.; Yang, W. H., Tuning the diffusion dialysis performance by surface cross-linking of ppo anion exchange membranes - simultaneous recovery of sulfuric acid and nickel from electrolysis spent liquor of relatively low acid concentration. *Journal of Hazardous Materials* **2004,** *109*, 157-164.

22. Kiyono, R.; Koops, G. H.; Wessling, M.; Strathmann, H., Mixed matrix microporous hollow fibers with ion-exchange functionality. *Journal of Membrane Science* **2004,** *231*, 109-115.

23. Wallace, R. M., Concentration and separation of ions by donnan membrane equilibrium. *Industrial & Engineering Chemistry Process Design and Development* **1967,** *6*, 423-431.

24. Cheng, C.; Yaroshchuk, A.; Bruening, M. L., Fundamentals of selective ion transport through multilayer polyelectrolyte membranes. *Langmuir* **2013,** *29*, 1885-1892.

25. Mohammad, A. W.; Teow, Y. H.; Ang, W. L.; Chung, Y. T.; Oatley-Radcliffe, D. L.; Hilal, N., Nanofiltration membranes review: Recent advances and future prospects. *Desalination* **2015,** *356*, 226-254.

26. Yaroshchuk, A.; Zhu, Y.; Bondarenko, M.; Bruening, M. L., Deviations from electroneutrality in membrane barrier layers: A possible mechanism underlying high salt rejections. *Langmuir* **2016,** *32*, 2644-2658.

27. Csefalvay, E.; Pauer, V.; Mizsey, P., Recovery of copper from process waters by nanofiltration and reverse osmosis. *Desalination* **2009,** *240*, 132-142.

28. Yaroshchuk, A.; Martinez-Llado, X.; Llenas, L.; Rovira, M.; de Pablo, J., Solution-diffusion-film model for the description of pressure-driven trans-membrane transfer of electrolyte mixtures: One dominant salt and trace ions. *Journal of Membrane Science* **2011,** *368*, 192-201.

29. Yaroshchuk, A.; Martinez-Llado, X.; Llenas, L.; Rovira, M.; de Pablo, J.; Flores, J.; Rubio, P., Mechanisms of transfer of ionic solutes through composite polymer nano-filtration membranes in view of their high sulfate/chloride selectivities. *Desalination and Water Treatment* **2009,** *6*, 48-53.

30. Van der Bruggen, B.; Vandecasteele, C., Removal of pollutants from surface water and groundwater by nanofiltration: Overview of possible applications in the drinking water industry. *Environmental Pollution* **2003,** *122*, 435-445.

31. Kosutic, K.; Kunst, B., Removal of organics from aqueous solutions by commercial ro and nf membranes of characterized porosities. *Desalination* **2002,** *142*, 47-56.

32. Chellam, S.; Taylor, J. S., Simplified analysis of contaminant rejection during ground- and surface water nanofiltration under the information collection rule. *Water Research* **2001,** *35*, 2460-2474.

33. Schaep, J.; Van der Bruggen, B.; Vandecasteele, C.; Wilms, D., Influence of ion size and charge in nanofiltration. *Separation and Purification Technology* **1998,** *14*, 155-162.

34. Schaep, J.; Vandecasteele, C.; Mohammad, A. W.; Bowen, W. R., Modelling the retention of ionic components for different nanofiltration membranes. *Separation and Purification Technology* **2001,** *22-3*, 169-179.

35. Li, X.; Cao, Y. M.; Yu, H. J.; Kang, G. D.; Jie, X. M.; Liu, Z. N.; Yuan, Q., A novel composite nanofiltration membrane prepared with phgh and tmc by interfacial polymerization. *Journal of Membrane Science* **2014,** *466*, 82-91.

36. Yang, Z. F.; Tarabara, V. V.; Bruening, M. L., Adsorption of anionic or cationic surfactants in polyanionic brushes and its effect on brush swelling and fouling resistance during emulsion filtration. *Langmuir* **2015,** *31*, 11790-11799.

37. Malaisamy, R.; Bruening, M. L., High-flux nanofiltration membranes prepared by adsorption of multilayer polyelectrolyte membranes on polymeric supports. *Langmuir* **2005,** *21*, 10587-10592.

38. Stanton, B. W.; Harris, J. J.; Miller, M. D.; Bruening, M. L., Ultrathin, multilayered polyelectrolyte films as nanofiltration membranes. *Langmuir* **2003,** *19*, 7038-7042.

39. Zhu, W. P.; Sun, S. P.; Gao, J.; Fu, F. J.; Chung, T. S., Dual-layer polybenzimidazole/polyethersulfone (PBI/PES) nanofiltration (NF) hollow fiber membranes for heavy metals removal from wastewater. *Journal of Membrane Science* **2014,** *456*, 117-127.

40. Chang, F. F.; Liu, W. J.; Wang, X. M., Comparison of polyamide nanofiltration and low-pressure reverse osmosis membranes on as(III) rejection under various operational conditions. *Desalination* **2014,** *334*, 10-16.

41. Yu, Y.; Zhao, C. W.; Wang, Y. G.; Fan, W. H.; Luan, Z. K., Effects of ion concentration and natural organic matter on arsenic(v) removal by nanofiltration under different transmembrane pressures. *Journal of Environmental Sciences* **2013,** *25*, 302-307.

42. Berg, P.; Hagmeyer, G.; Gimbel, R., Removal of pesticides and other micropollutants by nanofiltration. *Desalination* **1997,** *113*, 205-208.

43. Koyuncu, I., Reactive dye removal in dye/salt mixtures by nanofiltration membranes containing vinylsulphone dyes: Effects of feed concentration and cross flow velocity. *Desalination* **2002,** *143*, 243-253.

44. Homayoonfal, M.; Akbari, A.; Mehrnia, M. R., Preparation of polysulfone nanofiltration membranes by UV-assisted grafting polymerization for water softening. *Desalination* **2010,** *263*, 217-225.

45. Nanda, D.; Tung, K. L.; Li, Y. L.; Lin, N. J.; Chuang, C. J., Effect of pH on membrane morphology, fouling potential, and filtration performance of nanofiltration membrane for water softening. *Journal of Membrane Science* **2010,** *349*, 411-420.

46. Rahimpour, A.; Jahanshahi, M.; Mortazavian, N.; Madaeni, S. S.; Mansourpanah, Y., Preparation and characterization of asymmetric polyethersulfone and thin-film composite polyamide nanofiltration membranes for water softening. *Applied Surface Science* **2010,** *256*, 1657-1663.

47. Wen, X.; Ma, P.; Chaoliang, Z.; He, Q.; Deng, X., Preliminary study on recovering lithium chloride from lithium-containing waters by nanofiltration. *Separation and Purification Technology* **2006,** *49*, 230-236.

48. Szekely, G.; Bandarra, J.; Heggie, W.; Sellergren, B.; Ferreira, F. C., Organic solvent nanofiltration: A platform for removal of genotoxins from active pharmaceutical ingredients. *Journal of Membrane Science* **2011,** *381*, 21-33.

49. Martinez, M. B.; Van der Bruggen, B.; Negrin, Z. R.; Alconero, P. L., Separation of a high-value pharmaceutical compound from waste ethanol by nanofiltration. *Journal of Industrial and Engineering Chemistry* **2012,** *18*, 1635-1641.

50. Szekely, G.; Bandarra, J.; Heggie, W.; Sellergren, B.; Ferreira, F. C., A hybrid approach to reach stringent low genotoxic impurity contents in active pharmaceutical ingredients: Combining molecularly imprinted polymers and organic solvent nanofiltration for removal of 1,3-diisopropylurea. *Separation and Purification Technology* **2012,** *86*, 79-87.

51. Meyer, K. H.; Straus, W., The permeability of membranes VI the passage of the electrical current across selective membranes. *Helvetica Chimica Acta* **1940,** *23*, 795-800.

52. Xu, T. W., Ion exchange membranes: State of their development and perspective. *Journal of Membrane Science* **2005,** *263*, 1-29.

53. Katz, W. E., Electrodialysis reversal (EDR) process. *Desalination* **1979,** *28*, 31-40.

54. Trivedi, G. S.; Shah, B. G.; Adhikary, S. K.; Indusekhar, V. K.; Rangarajan, R., Studies on bipolar membranes 2. Conversion of sodium acetate to acetic acid and sodium hydroxide. *Reactive & Functional Polymers* **1997,** *32*, 209-215.

55. Koter, S.; Warszawski, A., Electromembrane processes in environment protection. *Polish Journal of Environmental Studies* **2000,** *9*, 45-56.

56. Li, H.; Mustacchi, R.; Knowles, C. J.; Skibar, W.; Sunderland, G.; Dalrymple, I.; Jackman, S. A., An electrokinetic bioreactor: Using direct electric current for enhanced lactic acid fermentation and product recovery. *Tetrahedron* **2004,** *60*, 655-661.

57. Lee, E. G.; Moon, S. H.; Chang, Y. K.; Yoo, I. K.; Chang, H. N., Lactic acid recovery using two-stage electrodialysis and its modelling. *Journal of Membrane Science* **1998,** *145*, 53-66.

58. Cauwenberg, V.; Peels, J.; Resbeut, S.; Pourcelly, G., Application of electrodialysis within fine chemistry. *Separation and Purification Technology* **2001,** *22-3*, 115-121.

59. Greiter, M.; Novalin, S.; Wendland, M.; Kulbe, K. D.; Fischer, J., Desalination of whey by electrodialysis and ion exchange resins: Analysis of both processes with regard to sustainability by calculating their cumulative energy demand. *Journal of Membrane Science* **2002,** *210*, 91-102.

60. Banasiak, L. J.; Kruttschnitt, T. W.; Schafer, A. I., Desalination using electrodialysis as a function of voltage and salt concentration. *Desalination* **2007,** *205*, 38-46.

61. Hideo, K.; Tsuzura, K.; Shimuzu, H., Ion-exchange membranes. *K.Dorfner (Ed.), Ion Exchangers, Walter de Gruyter, Berlin* **1991**.

62. Choi, P.; Jalani, N. H.; Datta, R., Thermodynamics and proton transport in Nafion I. Membrane swelling, sorption, and ion-exchange equilibrium. *Journal of the Electrochemical Society* **2005,** *152*, E84-E89.

63. Nandan, D.; Mohan, H.; Iyer, R. M., Methanol and water-uptake, densities, equivalental volumes and thicknesses of several univalent and divalent ionic perfluorosulfonate exchange membranes (Nafion-117) and their methanol water fractionation behavior at 298K. *Journal of Membrane Science* **1992,** *71*, 69-80.

64. Molau, G. E., Heterogeneous ion-exchange membranes. *Journal of Membrane Science* **1981,** *8*, 309-330.

65. Choi, J. H.; Kim, S. H.; Moon, S. H., Heterogeneity of ion-exchange membranes: The effects of membrane heterogeneity on transport properties. *Journal of Colloid and Interface Science* **2001,** *241*, 120-126.

66. Nagarale, R. K.; Gohil, G. S.; Shahi, V. K., Recent developments on ion-exchange membranes and electro-membrane processes. *Advances in Colloid and Interface Science* **2006,** *119*, 97-130.

67. Gregor, H. P.; Bruins, P. F.; Kramer, R. M., Chloride-sulfate equilibria and transport processes in benzidine-formaldehyde and other anion-permeable membranes. *Journal of Applied Polymer Science* **1966,** *10*, 807-811.

68. Kariduraganavar, M. Y.; Nagarale, R. K.; Kittur, A. A.; Kulkarni, S. S., Ion-exchange membranes: Preparative methods for electrodialysis and fuel cell applications. *Desalination* **2006,** *197*, 225-246.

69. Mauritz, K. A.; Moore, R. B., State of understanding of Nafion. *Chemical Reviews* **2004,** *104*, 4535-4585.

70. Savadogo, O., Emerging membranes for electrochemical systems - part II. High temperature composite membranes for polymer electrolyte fuel cell (PEFC) applications. *Journal of Power Sources* **2004,** *127*, 135-161.

71. He, G. W.; Li, Z.; Zhao, J.; Wang, S. F.; Wu, H.; Guiver, M. D.; Jiang, Z. Y., Nanostructured ion-exchange membranes for fuel cells: Recent advances and perspectives. *Advanced Materials* **2015,** *27*, 5280-5295.

72. Yee, R. S. L.; Rozendal, R. A.; Zhang, K.; Ladewig, B. P., Cost effective cation exchange membranes: A review. *Chemical Engineering Research & Design* **2012,** *90*, 950-959.

73. Smitha, B.; Sridhar, S.; Khan, A. A., Solid polymer electrolyte membranes for fuel cell applications - a review. *Journal of Membrane Science* **2005,** *259*, 10-26.

74. Fan, Q.; Hussain, H., High temperature composite proton exchange membranes. *International Patent WO 2004/073085* A2, August 26. **2004**.

75. Dlugolecki, P.; Anet, B.; Metz, S. J.; Nijmeijer, K.; Wessling, M., Transport limitations in ion exchange membranes at low salt concentrations. *Journal of Membrane Science* **2010,** *346*, 163-171.

76. Tanaka, Y., Mass transport and energy consumption in ion-exchange membrane electrodialysis of seawater. *Journal of Membrane Science* **2003,** *215*, 265-279.

77. Verbrugge, M. W.; Hill, R. F., Ion and solvent transport in ion-exchange membranes .2. A radiotracer study of the sulfuric-acid, Nafion-117 system. *Journal of the Electrochemical Society* **1990,** *137*, 893-899.

78. Rubinstein, I.; Staude, E.; Kedem, O., Role of the membrane-surface in concentration polarization at ion-exchange membrane. *Desalination* **1988,** *69*, 101-114.

79. Ibanez, R.; Stamatialis, D. F.; Wessling, M., Role of membrane surface in concentration polarization at cation exchange membranes. *Journal of Membrane Science* **2004,** *239*, 119-128.

80. Baker, R. W., Membrane technology and applications, 2nd ed: J. Wiley: Chichester; New York. **2004**.

81. Silva, V.; Poiesz, E.; van der Heijden, P., Industrial wastewater desalination using electrodialysis: Evaluation and plant design. *Journal of Applied Electrochemistry* **2013,** *43*, 1057-1067.

82. Lee, J. B.; Park, K. K.; Eum, H. M.; Lee, C. W., Desalination of a thermal power plant wastewater by membrane capacitive deionization. *Desalination* **2006,** *196*, 125-134.

83. Fidaleo, M.; Moresi, M., Electrodialysis applications in the food industry. *Advances in Food and Nutrition Research, Vol 51* **2006,** *51*, 265-360.

84. Andreeva, D. V.; Skorb, E. V.; Shchukin, D. G., Layer-by-layer polyelectrolyte/inhibitor nanostructures for metal corrosion protection. *Acs Applied Materials & Interfaces* **2010,** *2*, 1954-1962.

85. Frau, A. F.; Pernites, R. B.; Advincula, R. C., A conjugated polymer network approach to anticorrosion coatings: Poly(vinylcarbazole) electrodeposition. *Industrial & Engineering Chemistry Research* **2010,** *49*, 9789-9797.

86. Li, P. H.; Wu, G. S.; Xu, R. Z.; Wang, W. H.; Wu, S. L.; Yeung, K. W. K.; Chu, P. K., In vitro corrosion inhibition on biomedical shape memory alloy by plasma-polymerized allylamine film. *Materials Letters* **2012,** *89*, 51-54.

87. Nuraje, N.; Asmatulu, R.; Cohen, R. E.; Rubner, M. F., Durable antifog films from layer-by-layer molecularly blended hydrophilic polysaccharides. *Langmuir* **2011,** *27*, 782-791.

88. Zhang, L. B.; Li, Y.; Sun, J. Q.; Shen, J. C., Mechanically stable antireflection and antifogging coatings fabricated by the layer-by-layer deposition process and postcalcination. *Langmuir* **2008,** *24*, 10851-10857.

89. Introzzi, L.; Fuentes-Alventosa, J. M.; Cozzolino, C. A.; Trabattoni, S.; Tavazzi, S.; Bianchi, C. L.; Schiraldi, A.; Piergiovanni, L.; Farris, S., "Wetting enhancer" pullulan coating for antifog packaging applications. *Acs Applied Materials & Interfaces* **2012,** *4*, 3692-3700.

90. Lee, H.; Alcaraz, M. L.; Rubner, M. F.; Cohen, R. E., Zwitter-wettability and antifogging coatings with frost-resisting capabilities. *Acs Nano* **2013,** *7*, 2172-2185.

91. Banerjee, I.; Pangule, R. C.; Kane, R. S., Antifouling coatings: Recent developments in the design of surfaces that prevent fouling by proteins, bacteria, and marine organisms. *Advanced Materials* **2011,** *23*, 690-718.

92. Tsai, Y. C.; Li, S. C.; Chen, J. M., Cast thin film biosensor design based on a Nafion backbone, a multiwalled carbon nanotube conduit, and a glucose oxidase function. *Langmuir* **2005,** *21*, 3653-3658.

93. Muguruma, H.; Hiratsuka, A.; Karube, I., Thin-film glucose biosensor based on plasma-polymerized film: Simple design for mass production. *Analytical Chemistry* **2000,** *72*, 2671-2675.

94. Myler, S.; Eaton, S.; Higson, S. P. J., Poly(o-phenylenediamine) ultra-thin polymer-film composite membranes for enzyme electrodes. *Analytica Chimica Acta* **1997,** *357*, 55-61.

95. Koehler, J. A.; Ulbricht, M.; Belfort, G., Intermolecular forces between proteins and polymer films with relevance to filtration. *Langmuir* **1997,** *13*, 4162-4171.

96. Bhattacharjee, S.; Dong, J. L.; Ma, Y. D.; Hovde, S.; Geiger, J. H.; Baker, G. L.; Bruening, M. L., Formation of high-capacity protein-adsorbing membranes through simple adsorption of poly(acrylic acid)-containing films at low ph. *Langmuir* **2012,** *28*, 6885-6892.

97. Decher, G., Fuzzy nanoassemblies: Toward layered polymeric multicomposites. *Science* **1997,** *277*, 1232-1237.

98. Schlenoff, J. B.; Dubas, S. T., Mechanism of polyelectrolyte multilayer growth: Charge overcompensation and distribution. *Macromolecules* **2001,** *34*, 592-598.

99. Schlenoff, J. B.; Ly, H.; Li, M., Charge and mass balance in polyelectrolyte multilayers. *Journal of the American Chemical Society* **1998,** *120*, 7626-7634.

100. Joanny, J. F., Polyelectrolyte adsorption and charge inversion. *European Physical Journal B* **1999,** *9*, 117-122.

101. Bucur, C. B.; Sui, Z.; Schlenoff, J. B., Ideal mixing in polyelectrolyte complexes and multilayers: Entropy driven assembly. *Journal of the American Chemical Society* **2006,** *128*, 13690-13691.

102. Fu, Y.; Bai, S. L.; Cui, S. X.; Qiu, D. L.; Wang, Z. Q.; Zhang, X., Hydrogen-bonding-directed layer-by-layer multilayer assembly: Reconformation yielding microporous films. *Macromolecules* **2002,** *35*, 9451-9458.

103. Sukhishvili, S. A.; Granick, S., Layered, erasable polymer multilayers formed by hydrogen-bonded sequential self-assembly. *Macromolecules* **2002,** *35*, 301-310.

104. Richert, L.; Boulmedais, F.; Lavalle, P.; Mutterer, J.; Ferreux, E.; Decher, G.; Schaaf, P.; Voegel, J. C.; Picart, C., Improvement of stability and cell adhesion properties of polyelectrolyte multilayer films by chemical cross-linking. *Biomacromolecules* **2004,** *5*, 284-294.

105. Zhang, X.; Chen, H.; Zhang, H. Y., Layer-by-layer assembly: From conventional to unconventional methods. *Chemical Communications* **2007**, 1395-1405.

106. Bergbreiter, D. E.; Liao, K. S., Covalent layer-by-layer assembly-an effective, forgiving way to construct functional robust ultrathin films and nanocomposites. *Soft Matter* **2009,** *5*, 23-28.

107. Quinn, J. F.; Johnston, A. P. R.; Such, G. K.; Zelikin, A. N.; Caruso, F., Next generation, sequentially assembled ultrathin films: Beyond electrostatics. *Chemical Society Reviews* **2007,** *36*, 707-718.

108. Richardson, J. J.; Bjornmalm, M.; Caruso, F., Technology-driven layer-by-layer assembly of nanofilms. *Science* **2015,** *348*.

109. Dubas, S. T.; Schlenoff, J. B., Factors controlling the growth of polyelectrolyte multilayers. *Macromolecules* **1999,** *32*, 8153-8160.

110. Decher, G.; Hong, J. D.; Schmitt, J., Buildup of ultrathin multilayer films by a self-assembly process .3. Consecutively alternating adsorption of anionic and cationic polyelectrolytes on charged surfaces. *Thin Solid Films* **1992,** *210*, 831-835.

111. Lee, D.; Rubner, M. F.; Cohen, R. E., All-nanoparticle thin-film coatings. *Nano Letters* **2006,** *6*, 2305-2312.

112. Cho, J.; Char, K.; Hong, J. D.; Lee, K. B., Fabrication of highly ordered multilayer films using a spin self-assembly method. *Advanced Materials* **2001,** *13*, 1076-1078.

113. Chiarelli, P. A.; Johal, M. S.; Casson, J. L.; Roberts, J. B.; Robinson, J. M.; Wang, H. L., Controlled fabrication of polyelectrolyte multilayer thin films using spin-assembly. *Advanced Materials* **2001,** *13*, 1167-1171.

114. Schaaf, P.; Voegel, J. C.; Jierry, L.; Boulmedais, F., Spray-assisted polyelectrolyte multilayer buildup: From step-by-step to single-step polyelectrolyte film constructions. *Advanced Materials* **2012,** *24*, 1001-1016.

115. Dierendonck, M.; De Koker, S.; De Rycke, R.; De Geest, B. G., Just spray it - LbL assembly enters a new age. *Soft Matter* **2014,** *10*, 804-807.

116. Hong, X.; Li, J.; Wang, M. J.; Xu, J. J.; Guo, W.; Li, J. H.; Bai, Y. B.; Li, T. J., Fabrication of magnetic luminescent nanocomposites by a layer-by-layer self-assembly approach. *Chemistry of Materials* **2004,** *16*, 4022-4027.

117. Madaboosi, N.; Uhlig, K.; Jager, M. S.; Mohwald, H.; Duschl, C.; Volodkin, D. V., Microfluidics as a tool to understand the build-up mechanism of exponential-like growing films. *Macromolecular Rapid Communications* **2012,** *33*, 1775-1779.

118. Wang, Y. F.; Liu, Y.; Cheng, Y.; Kim, E.; Rubloff, G. W.; Bentley, W. E.; Payne, G. F., Coupling electrodeposition with layer-by-layer assembly to address proteins within microfluidic channels. *Advanced Materials* **2011,** *23*, 5817-5821.

119. Peiffre, D. G.; Corley, T. J.; Halpern, G. M.; Brinker, B. A., Utilization of polymeric materials in laser fusion target fabrication. *Polymer* **1981,** *22*, 450-460.

120. Fery, A.; Scholer, B.; Cassagneau, T.; Caruso, F., Nanoporous thin films formed by salt-induced structural changes in multilayers of poly(acrylic acid) and poly(allylamine). *Langmuir* **2001,** *17*, 3779-3783.

121. Krasemann, L.; Toutianoush, A.; Tieke, B., Self-assembled polyelectrolyte multilayer membranes with highly improved pervaporation separation of ethanol/water mixtures. *Journal of Membrane Science* **2001,** *181*, 221-228.

122. Picart, C.; Lavalle, P.; Hubert, P.; Cuisinier, F. J. G.; Decher, G.; Schaaf, P.; Voegel, J. C., Buildup mechanism for poly(l-lysine)/hyaluronic acid films onto a solid surface. *Langmuir* **2001,** *17*, 7414-7424.

123. Caruso, F.; Niikura, K.; Furlong, D. N.; Okahata, Y., 1. Ultrathin multilayer polyelectrolyte films on gold: Construction and thickness determination. *Langmuir* **1997,** *13*, 3422-3426.

124. Kujawa, P.; Moraille, P.; Sanchez, J.; Badia, A.; Winnik, F. M., Effect of molecular weight on the exponential growth and morphology of hyaluronan/chitosan multilayers: A surface plasmon resonance spectroscopy and atomic force microscopy investigation. *Journal of the American Chemical Society* **2005,** *127*, 9224-9234.

125. McAloney, R. A.; Sinyor, M.; Dudnik, V.; Goh, M. C., Atomic force microscopy studies of salt effects on polyelectrolyte multilayer film morphology. *Langmuir* **2001,** *17*, 6655-6663.

126. Choi, I.; Suntivich, R.; Plamper, F. A.; Synatschke, C. V.; Muller, A. H. E.; Tsukruk, V. V., Ph-controlled exponential and linear growing modes of layer-by-layer assemblies of star polyelectrolytes. *Journal of the American Chemical Society* **2011,** *133*, 9592-9606.

127. Blomberg, E.; Poptoshev, E.; Caruso, F., Surface interactions during polyelectrolyte multilayer build-up. 2. The effect of ionic strength on the structure of preformed multilayers. *Langmuir* **2006,** *22*, 4153-4157.

128. Dodoo, S.; Steitz, R.; Laschewsky, A.; von Klitzing, R., Effect of ionic strength and type of ions on the structure of water swollen polyelectrolyte multilayers. *Physical Chemistry Chemical Physics* **2011,** *13*, 10318-10325.

129. McAloney, R. A.; Goh, M. C., In situ investigations of polyelectrolyte film formation by second harmonic generation. *Journal of Physical Chemistry B* **1999,** *103*, 10729-10732.

130. Dressick, W. J.; Wahl, K. J.; Bassim, N. D.; Stroud, R. M.; Petrovykh, D. Y., Divalent-anion salt effects in polyelectrolyte multilayer depositions. *Langmuir* **2012,** *28*, 15831-15843.

131. Salomaki, M.; Tervasmaki, P.; Areva, S.; Kankare, J., The hofmeister anion effect and the growth of polyelectrolyte multilayers. *Langmuir* **2004,** *20*, 3679-3683.

132. Yoo, D.; Shiratori, S. S.; Rubner, M. F., Controlling bilayer composition and surface wettability of sequentially adsorbed multilayers of weak polyelectrolytes. *Macromolecules* **1998,** *31*, 4309-4318.

133. Lebedeva, O. V.; Kim, B. S.; Vasilev, K.; Vinogradova, O. I., Salt softening of polyelectrolyte multilayer microcapsules. *Journal of Colloid and Interface Science* **2005,** *284*, 455-462.

134. Farhat, T. R.; Schlenoff, J. B., Doping-controlled ion diffusion in polyelectrolyte multilayers: Mass transport in reluctant exchangers. *Journal of the American Chemical Society* **2003,** *125*, 4627-4636.

135. Volodkin, D.; von Klitzing, R., Competing mechanisms in polyelectrolyte multilayer formation and swelling: Polycation-polyanion pairing vs. Polyelectrolyte-ion pairing. *Current Opinion in Colloid & Interface Science* **2014,** *19*, 25-31.

136. Steitz, R.; Leiner, V.; Siebrecht, R.; von Klitzing, R., Influence of the ionic strength on the structure of polyelectrolyte films at the solid/liquid interface. *Colloids and Surfaces a-Physicochemical and Engineering Aspects* **2000,** *163*, 63-70.

137. Dubas, S. T.; Schlenoff, J. B., Swelling and smoothing of polyelectrolyte multilayers by salt. *Langmuir* **2001,** *17*, 7725-7727.

138. Miller, M. D.; Bruening, M. L., Correlation of the swelling and permeability of polyelectrolyte multilayer films. *Chemistry of Materials* **2005,** *17*, 5375-5381.

139. Carriere, D.; Krastev, R.; Schonhoff, M., Oscillations in solvent fraction of polyelectrolyte multilayers driven by the charge of the terminating layer. *Langmuir* **2004,** *20*, 11465-11472.

140. Jaber, J. A.; Schlenoff, J. B., Counterions and water in polyelectrolyte multilayers: A tale of two polycations. *Langmuir* **2007,** *23*, 896-901.

141. Stair, J. L.; Harris, J. J.; Bruening, M. L., Enhancement of the ion-transport selectivity of layered polyelectrolyte membranes through cross-linking and hybridization. *Chemistry of Materials* **2001,** *13*, 2641-2648.

142. Loh, I. H.; Moody, R. A.; Huang, J. C., Electrically conductive membranes - synthesis and applications. *Journal of Membrane Science* **1990,** *50*, 31-49.

143. Nishizawa, M.; Menon, V. P.; Martin, C. R., Metal nanotubule membranes with electrochemically switchable ion-transport selectivity. *Science* **1995,** *268*, 700-702.

144. Salehi, E.; Madaeni, S. S., Influence of conductive surface on adsorption behavior of ultrafiltration membrane. *Applied Surface Science* **2010,** *256*, 3010-3017.

145. Rashid, M. H. O.; Pham, S. Q. T.; Sweetman, L. J.; Alcock, L. J.; Wise, A.; Nghiem, L. D.; Triani, G.; Panhuis, M. I. H.; Ralph, S. F., Synthesis, properties, water and solute permeability of MWNT buckypapers. *Journal of Membrane Science* **2014,** *456*, 175-184.

146. Rahaman, M. S.; Vecitis, C. D.; Elimelech, M., Electrochemical carbon-nanotube filter performance toward virus removal and inactivation in the presence of natural organic matter. *Environmental Science & Technology* **2012,** *46*, 1556-1564.

147. Liu, L. F.; Liu, J. D.; Gao, B.; Yang, F. L.; Chellam, S., Fouling reductions in a membrane bioreactor using an intermittent electric field and cathodic membrane modified by vapor phase polymerized pyrrole. *Journal of Membrane Science* **2012,** *394*, 202-208.

148. Ateh, D. D.; Navsaria, H. A.; Vadgama, P., Polypyrrole-based conducting polymers and interactions with biological tissues. *Journal of the Royal Society Interface* **2006,** *3*, 741-752.

149. Wallace, G.; Spinks, G., Conducting polymers - bridging the bionic interface. *Soft Matter* **2007,** *3*, 665-671.

150. Wang, L. X.; Li, X. G.; Yang, Y. L., Preparation, properties and applications of polypyrroles. *Reactive & Functional Polymers* **2001,** *47*, 125-139.

151. Akieh, M. N.; Ralph, S. F.; Bobacka, J.; Ivaska, A., Transport of metal ions across an electrically switchable cation exchange membrane based on polypyrrole doped with a sulfonated calix[6]arene. *Journal of Membrane Science* **2010,** *354*, 162-170.

152. Liu, L. F.; Liu, J. D.; Bo, G.; Yang, F. L.; Crittenden, J.; Chen, Y. C., Conductive and hydrophilic polypyrrole modified membrane cathodes and fouling reduction in mbr. *Journal of Membrane Science* **2013,** *429*, 252-258.

153. Zhao, H.; Price, W. E.; Teasdale, P. R.; Wallace, G. G., Transport across stand-alone conducting polypyrrole membranes containing dodecyl-sulfate counterions. *Reactive Polymers* **1994,** *23*, 213-220.

154. Zhao, H.; Price, W. E.; Wallace, G. G., Effect of the counterion employed during synthesis on the properties of polypyrrole membranes. *Journal of Membrane Science* **1994,** *87*, 47-56.

155. Zhao, H.; Price, W. E.; Too, C. O.; Wallace, G. G.; Zhou, D., Parameters influencing transport across conducting electroactive polymer membranes. *Journal of Membrane Science* **1996,** *119*, 199-212.

156. Pile, D. L.; Hillier, A. C., Electrochemically modulated transport through a conducting polymer membrane. *Journal of Membrane Science* **2002,** *208*, 119-131.

157. Deligoz, H., Preparation of self-standing polyaniline-based membranes: Doping effect on the selective ion separation and reverse osmosis properties. *Journal of Applied Polymer Science* **2007,** *105*, 2640-2645.

158. Illing, G.; Hellgardt, K.; Wakeman, R. J.; Jungbauer, A., Preparation and characterisation of polyaniline based membranes for gas separation. *Journal of Membrane Science* **2001,** *184*, 69-78.

159. Smith, R. R.; Smith, A. P.; Stricker, J. T.; Taylor, B. E.; Durstock, M. F., Layer-by-layer assembly of poly(3,4-ethylenedioxythiophene): Poly(3,4-ethylenedioxythiophene): Poly(styrenesulfonate). *Macromolecules* **2006,** *39*, 6071-6074.

160. Jalili, R.; Razal, J. M.; Wallace, G. G., Wet-spinning of PEDOT: PSS/functionalized-SWNTs composite: A facile route toward production of strong and highly conducting multifunctional fibers. *Scientific Reports* **2013,** *3*, 2438.

161. Gong, C.; Yang, H. B.; Song, Q. L.; Lu, Z. S.; Li, C. M., Mechanism for dimethylformamide-treatment of poly(3,4-ethylenedioxythiophene): Poly(styrene sulfonate) layer to enhance short circuit current of polymer solar cells. *Solar Energy Materials and Solar Cells* **2012,** *100*, 115-119.

162. Yamashita, M.; Otani, C.; Shimizu, M.; Okuzaki, H., Effect of solvent on carrier transport in poly(3,4-ethylenedioxythiophene)/poly(4-styrenesulfonate) studied by terahertz and infrared-ultraviolet spectroscopy. *Applied Physics Letters* **2011,** *99*, 143307.

163. Crispin, X.; Marciniak, S.; Osikowicz, W.; Zotti, G.; Van der Gon, A. W. D.; Louwet, F.; Fahlman, M.; Groenendaal, L.; De Schryver, F.; Salaneck, W. R., Conductivity, morphology, interfacial chemistry, and stability of poly(3,4-ethylene dioxythiophene)-poly(styrene sulfonate): A photoelectron spectroscopy study. *Journal of Polymer Science Part B-Polymer Physics* **2003,** *41*, 2561-2583.

164. Kim, J. Y.; Jung, J. H.; Lee, D. E.; Joo, J., Enhancement of electrical conductivity of poly(3,4-ethylenedioxythiophene)/poly(4-styrenesulfonate) by a change of solvents. *Synthetic Metals* **2002,** *126*, 311-316.

165. Poverenov, E.; Li, M.; Bitler, A.; Bendikov, M., Major effect of electropolymerization solvent on morphology and electrochromic properties of pedot films. *Chemistry of Materials* **2010,** *22*, 4019-4025.

166. Brooke, R.; Evans, D.; Dienel, M.; Hojati-Talemi, P.; Murphy, P.; Fabretto, M., Inkjet printing and vapor phase polymerization: Patterned conductive pedot for electronic applications. *Journal of Materials Chemistry C* **2013,** *1*, 3353-3358.

167. Ha, Y. H.; Nikolov, N.; Pollack, S. K.; Mastrangelo, J.; Martin, B. D.; Shashidhar, R., Towards a transparent, highly conductive poly(3,4-ethylenedioxythiophene). *Advanced Functional Materials* **2004,** *14*, 615-622.

168. Kohli, P.; Wharton, J. E.; Braide, O.; Martin, C. R., Template synthesis of gold nanotubes in an anodic alumina membrane. *Journal of Nanoscience and Nanotechnology* **2004,** *4*, 605-610.

169. Menon, V. P.; Martin, C. R., Fabrication and evaluation of nanoelectrode ensembles. *Analytical Chemistry* **1995,** *67*, 1920-1928.

170. Xiao, R.; Il Cho, S.; Liu, R.; Lee, S. B., Controlled electrochemical synthesis of conductive polymer nanotube structures. *Journal of the American Chemical Society* **2007,** *129*, 4483-4489.

171. de Lannoy, C. F.; Jassby, D.; Davis, D. D.; Wiesner, M. R., A highly electrically conductive polymer-multiwalled carbon nanotube nanocomposite membrane. *Journal of Membrane Science* **2012,** *415*, 718-724.

172. Sears, K.; Dumee, L.; Schutz, J.; She, M.; Huynh, C.; Hawkins, S.; Duke, M.; Gray, S., Recent developments in carbon nanotube membranes for water purification and gas separation. *Materials* **2010,** *3*, 127-149.

173. Celebi, K.; Buchheim, J.; Wyss, R. M.; Droudian, A.; Gasser, P.; Shorubalko, I.; Kye, J. I.; Lee, C.; Park, H. G., Ultimate permeation across atomically thin porous graphene. *Science* **2014,** *344*, 289-292.

174. Gao, F.; Nebel, C. E., Electrically conductive diamond membrane for electrochemical separation processes. *ACS Applied Materials & Interfaces* **2016,** *8*, 18640-18646.

175. Juttner, K.; Ehrenbeck, C., Electrochemical measurements of the ion conductivity, permselectivity and transference numbers of polypyrrole and polypyrrole derivatives. *Journal of Solid State Electrochemistry* **1998,** *2*, 60-66.

176. Morita, M., Effects of applied potentials on permselectivity of ions through polypyrrole/porous-polypropylene composite membrane. *Journal of Applied Polymer Science* **1998,** *70*, 647-653.

177. Pile, D. L.; Zhang, Y.; Hillier, A. C., Electrochemically modulated permeability of poly(aniline) and composite poly(aniline)-poly(styrenesulfonate) membranes. *Langmuir* **2006,** *22*, 5925-5931.

178. Kang, M. S.; Martin, C. R., Investigations of potential-dependent fluxes of ionic permeates in gold nanotubule membranes prepared via the template method. *Langmuir* **2001,** *17*, 2753-2759.

179. Nguyen, B. T. T.; Ting, E. Z. C.; Toh, C. S., Development of a biomimetic nanoporous membrane for the selective transport of charged proteins. *Bioinspiration & Biomimetics* **2008,** *3*, 1-6.

180. Cheow, P. S.; Zhi, E.; Ting, C.; Tan, M. Q.; Toh, C. S., Transport and separation of proteins across platinum-coated nanoporous alumina membranes. *Electrochimica Acta* **2008,** *53*, 4669-4673.

181. Bard, A. J.; Faulkner, L. R., Electrochemical methods: Fundamentals and applications; John Wiley & Sons: New York. **2000**.

182. Zhang, Q. Y.; Vecitis, C. D., Conductive cnt-pvdf membrane for capacitive organic fouling reduction. *Journal of Membrane Science* **2014,** *459*, 143-156.

Chapter 2 Highly Selective Separations of Divalent and Monovalent Cations in Electrodialysis Through Fujifilm Cation-Exchange Membranes Coated with Polyelectrolyte Multilayers

2.1 Introduction

Electrodialysis (ED) is a membrane-based separation technology for applications including pre-concentration of salt solutions,[1] production of salts from seawater,[2-3] brackish water desalination,[4] demineralization of food products,[5] and recovery of organic acids from waste salt solutions.[6] In contrast to pressure-driven separations such as microfiltration, nanofiltration and reverse osmosis, in ED an electric field drives transmembrane ion flux. From specific compartments, cations migrate through cation-exchange membranes toward a cathode and anions migrate through anion-exchange membranes toward an anode. Thus, ion-exchange membranes that allow selective passage of anions or cations are vital to efficient ED.

Commercial ion-exchange membranes have high permselectivities for cations over anions or vice versa, but they exhibit low selectivities among anions or cations. Nevertheless, high selectivities among cations or anions are important for separations such as acid recycling from industrial wastewater containing metallic salts[7] and hard water softening.[8] Accordingly, several studies investigated methods to improve the monovalent/divalent or

monovalent/multivalent ion selectivities of ion-exchange membranes. Based on differences among hydrated ionic radii, denser cation-exchange may show size-based selectivity for monovalent over divalent ions. However, increasing the amount of cross-linking agent during the formation of ion-exchange membranes increased the Na^+/Ca^{2+} selectivity only slightly.[9] Ge and co-workers fabricated a nanofiltration membrane with a dense top layer to achieve a Na^+/Mg^{2+} ED selectivity of 7.[10] Sata and co-workers showed that cation-exchange membranes change from Ca^{2+} selective to Na^+ selective after impregnation with chelating agents,[11] and electrodeposition of the positively charged polyethylene imine (PEI) on Nafion yielded membranes with a Na^+/Cr^{3+} selectivity of 10-20.[12] Nevertheless, these selectivities are still relatively low.

A few recent studies reported modification of ion-exchange membranes through layer-by-layer adsorption of polyelectrolyte multilayers (PEMs). This method yields ultrathin selective films on the membrane, and variation of polyelectrolytes and their adsorption conditions can tailor film selectivity by controlling films properties such as thickness, pore size and charge density.[13-14] Modification of Neosepta CMX cation-exchange membranes with PEI/polystyrenesulfonate (PSS) multilayers increased Na^+/Ca^{2+} selectivity from 0.64 to 1.5,[15] and deposition of PSS/protonated poly(allylamine) (PAH) films on Neosepta AMX anion-exchange membranes changed the Cl^-/SO_4^{2-} selectivity from 0.8 to 2.5.[16] Again, the selectivities in these studies are relatively modest.

Remarkably, formation of PAH/PSS films on Nafion 115 cation-exchange membranes generates monovalent/divalent and monovalent/multivalent cation ED selectivities >1000.[17] The high selectivities likely reflect the formation of a defect-free PEM on the smooth Nafion surface. However, the high cost of Nafion may preclude its use in many ED applications.[5] Additionally,

the current efficiency in ED separations through PEM-modified Nafion membranes was ~0.5, implying that unwanted ions such as protons carry 50% of the current.[17-18]

This research aims to coat a relatively inexpensive ion-exchange membrane with a PEM and achieve the same high selectivities seen with modified Nafion. Specifically, we coat Fujifilm Type1 cation-exchange membranes with PAH/PSS films and subsequently examine selective electrodialysis through these membranes. The Fujifilm membranes consist of an aromatic polyamide matrix surrounding a fibrous support, and thus should be less expensive than the fluoropolymer Nafion. The relatively smooth surface of the Fujifilm membranes is also attractive for potentially forming continuous polyelectrolyte films. In addition to ED studies, current density-voltage curves give insight into limiting currents and water splitting at the PEM-cation-exchange membrane interface.

2.2 Experimental section

2.2.1 Materials

Poly (sodium 4-styrenefulfonate) (Mw = 70 000 Da) and poly(allylamine hydrochloride) (Mw = 17 500 Da) were obtained from Sigma-Aldrich. Potassium nitrate, magnesium nitrate, and sodium chloride were purchased from Columbus Chemical, and all salts were used as received. Deionized water (Milli-Q Reference Ultra-pure Water Purification System, 18MΩ) was used to prepare all solutions. The pH of polyelectrolyte solutions was adjusted with 0.1M HCl or 0.1M NaOH. Nafion 115 membranes were acquired from Ion power (New Castle, DE, thickness 127 nm), and Fujifilm type 1 cation exchange membranes were a gift from Fujifilm.

2.2.2 Film formation and characterization

Fujifilm membranes were cut into 25-mm disks with a metal punch and immersed in room-temperature 0.1 M NaCl for 24 h before modification. Polyelectrolyte films were deposited on both sides of the cation-exchange membranes through layer-by-layer assembly. After pretreatment, membranes were immersed in 0.02 M PAH in 1 M NaCl (pH 2.3) for 5 min, rinsed for ~1 min with deionized water from a squirt bottle to remove weakly adsorbed polyelectrolytes, immersed in 0.02 M PSS in 0.5 M NaCl (pH 2.3) for 5 min, and again rinsed with deionized water. (Polymer concentrations are those of the repeat unit, and during the modification, membranes were handled with tweezers only near their edge.) This adsorption process was repeated until the desired number of layers was deposited. Images of bare and modified membranes were obtained with a JEOL 7500F scanning electron microscope with a cold field–emission emitter. All samples were dried in vacuum overnight and sputter-coated with 4 nm of platinum prior to imaging. Single-side coated membranes were modified in a home-made O-ring holder which exposed only one side of the membrane to the deposition solution.

2.2.3 Electrodialysis

Electrodialysis was performed as described previously.[19] A membrane was placed between two homemade glass cells (sealed with an O-ring) that exposed a membrane area of 3.14 cm^2. The source-phase cell (anode side) was filled with 90 mL of salt solution and the receiving-phase cell (cathode side) contained 90 mL of 0.01 M HNO_3. Both cells were stirred vigorously to reduce concentration polarization, and Pt wire electrodes served as the anode and cathode. To generate a constant current, a resistor (499 Ω) was connected between the working and reference terminals of a CH Instruments (model 604) potentiostat. The reference terminal

was also connected to the platinum anode in the source phase, and the counter electrode terminal was attached to the Pt cathode in the receiving phase. In most experiments, a 1 V potential was applied across the resistor to generate a constant 2.0 mA current (0.63 mA cm^{-2}), such that cations migrated toward the receiving phase. During 120 min of ED, 1-mL aliquots were withdrawn periodically from the receiving phase for determination of the concentrations of target cations, and corresponding aliquots were collected from the source phase to maintain equal volumes. The cation concentrations were determined using inductively couple plasma-optical emission spectroscopy (Varian 710-ES) with calibration curves. The calibration standards were prepared by dilution of commercial ICP-OES standard solutions (GFS chemicals) with Milli-Q water. The feed solutions were occasionally analyzed to ensure the source-phase concentration.

The total amounts of target ions that permeated through the membrane were plotted as a function of time, and ion fluxes were determined by dividing the slope in such a plot by the exposed membrane area. When the source phase contains the same concentrations of the two cations, the K^+/Mg^{2+} selectivities are simply the ratios of ion fluxes. The transference number of a given ion, the fraction of current carried by that cation, was calculated from equation 1, where J_i is the flux of ion i, z_i is the ion charge, F is the Faraday constant, and I is the total current density.

$$t_i = \frac{J_i \times z_i \times F}{I} \quad (1)$$

Note that this equation assumes that all transport results from the applied current. If significant transport occurs due to Donnan diffusion, equation (1) will overestimate the transference number.

2.2.4 Transmembrane potential measurements

Transmembrane potential experiments were carried out with bare Fujifilm membranes to determine the transference numbers of cations and anions in the cation-exchange membranes. The experiments were performed in a homemade two-compartment cell similar to that for electrodialysis. Ag/AgCl reference electrodes (3M KCl, CH Instruments) were sealed in homemade Haber-Luggin capillaries and inserted into the source and receiving sides of the cell. Each capillary was brought to within ~4 mm of the membrane surface to minimize the ohmic voltage drop through the solution between the reference electrode and the membrane. The receiving phase always contained 0.001M KNO_3, and the source phase concentration of KNO_3 ranged from 0.001 to 0.02 M. Both cells were stirred vigorously to reduce the concentration polarization. The electrical potential differences between the two electrodes were measured with an electrical multimeter (TEKPower TP2844R). Before experiments, the two capillaries were both placed in the receiving solution to determine the small potential difference between reference electrodes, and this value was subtracted from the multimeter reading. As described previously, the junction potentials in the capillaries were also subtracted from multi-meter readings to obtain the membrane potential.[14]

2.2.5 Current-voltage curves

The current-voltage curves were conducted in the same apparatus used to measure the transmembrane potential. Platinum electrodes were inserted into the source and receiving cells to apply current. At current densities ranging from 0 to 3 mA/cm^2, the transmembrane potential was determined from the electrical potential difference between reference electrodes. In these

experiments, both cells contained 0.01 M KNO_3 and 0.1 M $Mg(NO_3)_2$ and were stirred vigorously.

2.3 Results and discussion

Remarkably, ED through $(PAH/PSS)_5PAH$-coated Nafion membranes gives monovalent/divalent cation selectivities >1000.[17] Despite the selectivity of these membranes, the high cost of Nafion may preclude their use in many applications. This chapter investigates whether adsorption of $(PAH/PSS)_5PAH$ films on more practical Fujifilm cation-exchange membranes leads to the same selectivities seen with coated Nafion.

The extreme selectivities of coated Nafion imply that the PEM completely covers the smooth membrane surface. However, other cation-exchange membranes did not show high K^+/Mg^{2+} selectivities after coating with PEMs, presumably due to defects or rough membrane surfaces.[15, 17] Thus, this section first examines the surface morphology of bare and PEM-modified Fujifilm membranes, and then investigates whether ED through coated membranes yields the high monovalent/divalent cation selectivities observed with $(PAH/PSS)_nPAH$ films on Nafion. We also examine how monovalent/divalent cation selectivities and the monovalent cation transference number depend on the numbers of bilayer in the PEM, the source-phase salt concentrations, and for single-side-modified membranes whether the modified surface faces the anode or cathode. Finally, we explore limiting currents and water splitting using current density-voltage curves.

2.3.1 Characterization of Fujifilm cation-exchange membranes

Transmembrane electrical potential measurements with single salts give an estimate of the cation/anion selectivity of a membrane. For a membrane that separates two solutions with

different salt activities, equation (2.1) describes the equilibrium potential drop, E, where t_+ and t_- are the cation and anion transference numbers, z_+ and z_- are the cation and anion charges,

$$E = \left(\frac{t_+}{z_+} + \frac{t_-}{z_-}\right)\frac{RT}{F} ln\left(\frac{a_1}{a_2}\right) \qquad 2.1$$

and a_1 and a_2 are salt activities in the source and receiving phases, respectively.[20] For ideal cation-exchange membranes, t_- is zero, and t_+ is unity, so these membranes should give a slope of 59 mV in plots of E vs $ln\left(\frac{a_1}{a_2}\right)$. Figure 2.1 plots E vs $ln\left(\frac{a_1}{a_2}\right)$ for Fujifilm membranes flanked by different KNO_3 solutions. The slope of the linear fit to the data is 57.9 mV, indicating that the Fujifilm membranes are nearly impermeable to anions ($t_- = 0.01 - 0.02$).

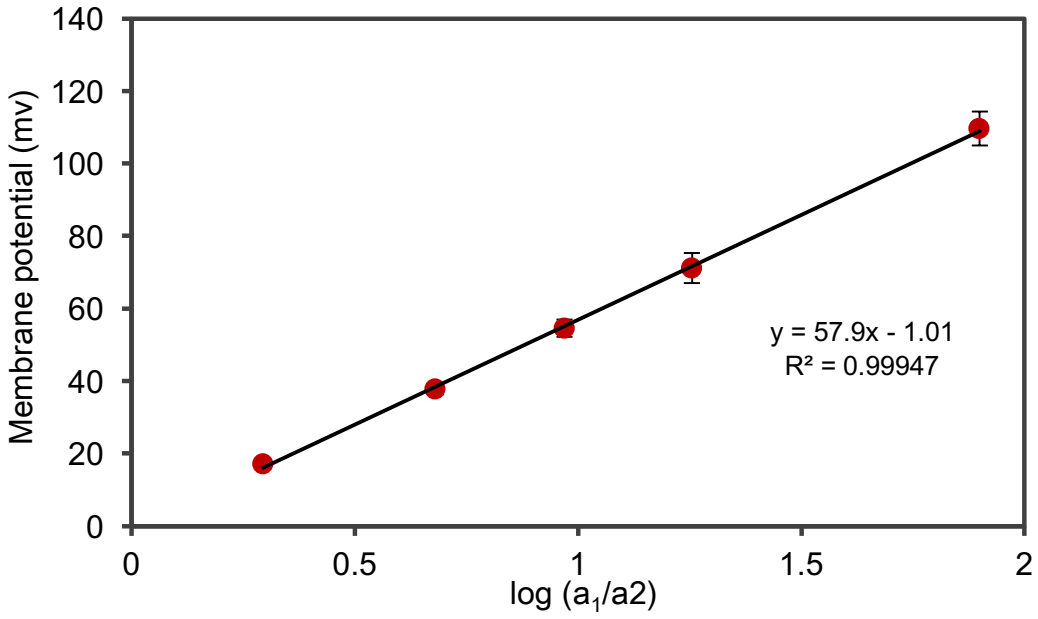

Figure 2.1 Electrical potential drops (receiving-source phase) across a Fujifilm membrane as a function of the ratio of KNO_3 activities in the source (a_1) and receiving (a_2) solutions. The error bars represent the standard deviations from three Fujifilm membranes.

Complete coverage of a membrane with a film containing only a few polyelectrolyte layers will likely require a membrane surface that is smooth at the nm, or at least 10's of nm, scale. Figures 2.2(A) and (B) show the front and back sides, respectively, of Fujifilm membranes, which consist of fibers coated with aromatic polyamides. Although the underlying fibers and a few holes at the micron scale are visible, the majority of the membrane appears smooth at this magnification. Both sides of these membranes show similar features. The round and elongated holes may form in part due to drying of the membrane. Thus, we immersed a membrane in 0.1 M NaCl for at least 17 h to completely swell the polymer before coating with a PEM. Figure 2.2 C and similar images suggest that the sizes of the voids decrease after immersion in 0.1 M NaCl, despite again drying the membrane prior to imaging. The image of the $(PAH/PSS)_5PAH$-coated membrane in Figure 2.2D suggests full PEM coverage, as no underlying voids are visible, even in larger images (10 μm x 10 μm) of the membrane. The particles on the surface may correspond to insoluble polycation/polyanion complexes that form in the presence of excess polyelectrolytes.

The surface roughness of the Fujifilm membrane is ~ 0.4 nm from AFM, which is much smaller than the 2.7 nm roughness of CMI-7000 cation-exchange membranes. Our previous attempts to coat CMI-7000 membranes with $(PAH/PSS)_5PAH$ did not give highly selective membranes.[17] The smooth Fujifilm surface may allow more complete PEM coverage to enhance selectivity.

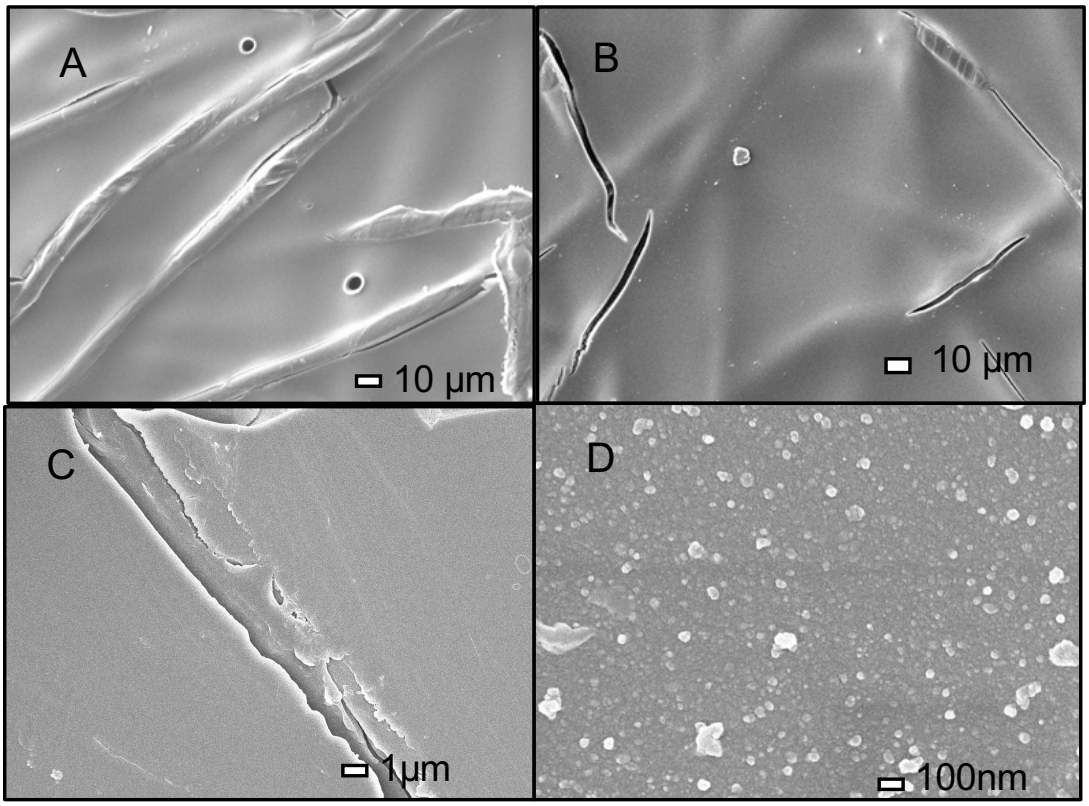

Figure 2.2 SEM images of the (A) top and (B) bottom surfaces of Fujifilm membranes. Images C and D show the tops of membranes after (C) immersion in 0.1 M NaCl and (D) coating with a $(PAH/PSS)_5PAH$ film.

2.3.2 Electrodialysis with bare and modified Fujifilm cation-exchange membranes

As with Nafion membranes, coating of Fujifilm membranes with $(PAH/PSS)_5PAH$ films leads to a remarkable increase in ED selectivity for monovalent over divalent ions. Figure 2.3 shows the amounts of K^+ or Mg^{2+} in the receiving phase as a function of time during 2 h of electroldialysis from a source phase initially containing 0.01 M KNO_3 and 0.01 M $Mg(NO_3)_2$ to a receiving phase containing 0.01 M HNO_3. Due to the constant current density (0.63 mA cm^{-2}), the amounts of K^+ and Mg^{2+} in the receiving phase increase approximately linearly with time.

The average K^+ and Mg^{2+} fluxes, which are proportional to the slopes in plots such as those in Figure 2.3, were 2.83 ± 0.01 and 2.91±0.21 nmole $s^{-1}cm^{-2}$, respectively, for three bare membranes, and the average K^+/Mg^{2+}selectivity was only 0.98 ± 0.05. Thus, although these membranes are selective for cations over anions (see Figure 2.1), they are not selective among cations. In contrast, after coating both sides of the Fujifilm membranes with $(PAH/PSS)_5PAH$ films, the Mg^{2+} flux decreases to 2 pmol cm^{-2} s^{-1}, and the average K^+ flux increases to 3.64 ± 0.34 nmol cm^{-2} s^{-1}, giving rise to a K^+/Mg^{2+} selectivity > 1000. The high selectivity implies that the PEM covers essentially all of the Fujifilm membrane, despite some μm-size surface voids in the dry underlying substrate (see Figure 2.2). The PEM may cover the interior of these voids, which also likely decrease in size when the membrane swells in water.

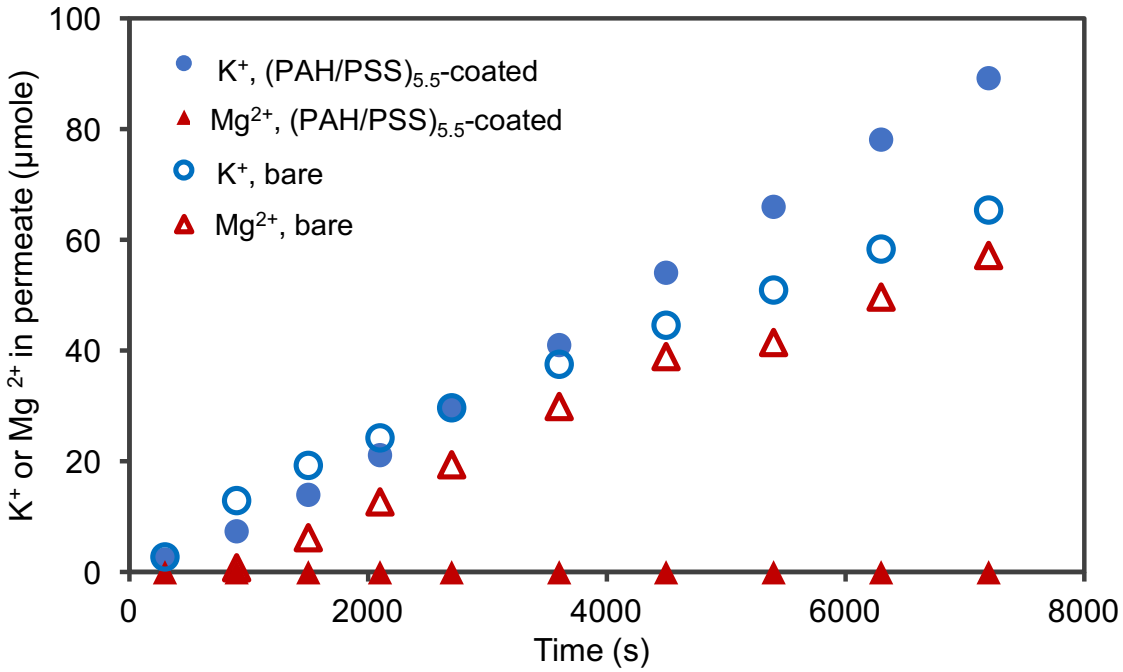

Figure 2.3 Moles of K^+ (circles) and Mg^{2+} (squares) in the receiving phase as a function of time during ED with initial solutions containing 0.01 M KNO_3 and 0.01 M $Mg(NO_3)_2$ in the source phase and 0.01 M HNO_3 in the receiving phase. ED used either a bare Fujifilm membrane (open symbols) or a Fujifilm membrane coated with $(PAH/PSS)_5PAH$ on both sides (filled symbols). The current density was 0.63 mA cm^{-2}.

Although coating both sides of the Fujifilm membrane yields exceptional selectivities, membranes coated on only one face could present less ion-transport resistance and increase the limiting current to enhance current efficiency. Thus, we examined the ion fluxes and selectivities of single-side-modified Fujifilm membranes. Figure 2.4 shows the results from ED with single-side-coated Fujifilm membranes where the $(PAH/PSS)_5PAH$-film faced either the anode or cathode. When the coating faced the anode, the K^+ and Mg^{2+} fluxes were 3.46 ± 0.03 nmole cm^{-2} s^{-1} and 0.013 ± 0.006 nmole cm^{-2} s^{-1}, respectively, and the K^+/Mg^{2+} selectivities of three membranes ranged from 200 to 700. However, when the coating faced the cathode, the K^+

flux was 2.30 ± 0.55 nmole cm^{-2} s^{-1}, the Mg^{2+} flux was 1.02 ± 0.45 nmole cm^{-2} s^{-1}, and the selectivities of three membranes ranged from only 1.4 to 5.75. Thus, the PEM on the anode side is essential for high selectivity. When the polyelectrolyte faces the cathode, concentration polarization inside the cation exchange membrane may decrease the selectivity. In this case, the more rejected ion (Mg^{2+}) should accumulate at the interface between the ion-exchange membrane and the PEM to increase Mg^{2+} flux and decrease K^{+}/Mg^{2+} selectivity. When the coating faces the anode, Mg^{2+} will accumulate at the interface between the feed solution and the PEM. However, stirring in the source phase and the relatively high ion diffusion coefficients in the source-phase solution (compared to in the cation-exchange membrane) will limit concentration polarization. It is also possible that rotating the polyelectrolyte film 180° decreases electrostatic exclusion of cations to decrease selectivity.

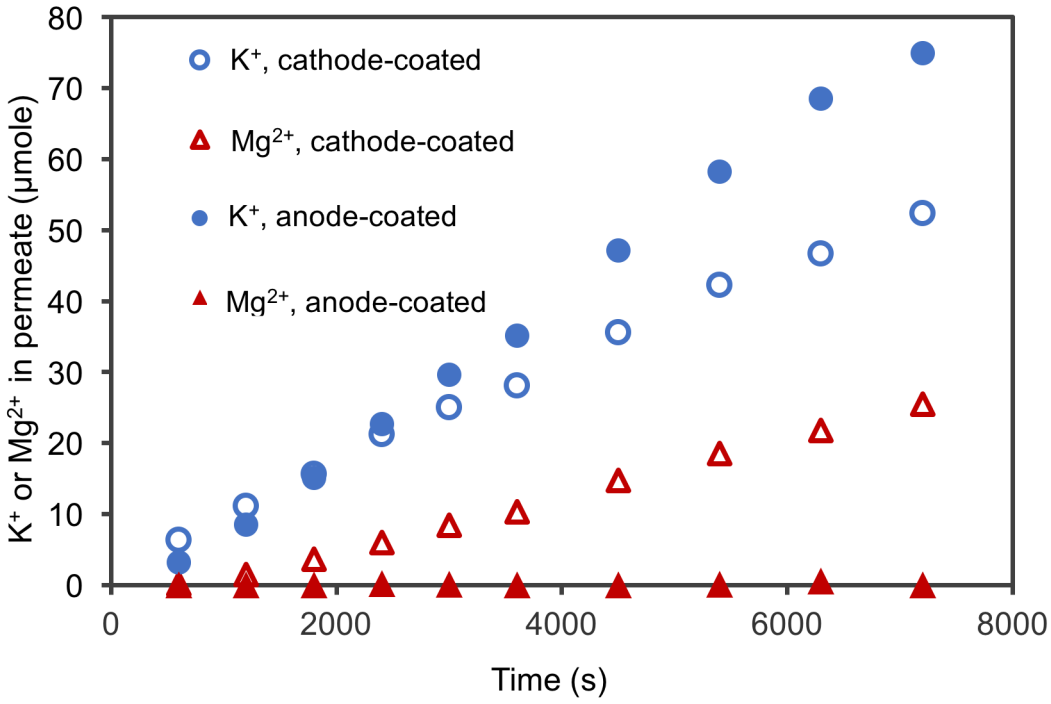

Figure 2.4 Moles of K^+ (circles) and Mg^{2+} (triangles) in the receiving phase as a function time during ED with initial solutions containing 0.01 M KNO_3 and 0.01M $Mg(NO_3)_2$ in the source phase and 0.01 M HNO_3 in the receiving phase. ED used a Fujifilm membrane coated with $(PAH/PSS)_5PAH$ only on the cathode side (open symbols) or anode (filled symbols) side. The current density was 0.63 mA/cm^2.

High current efficiency is important for minimizing the energy consumption in ED separations. The quantitative measure of the current efficiency is the transference number, t_i, which is the fraction of current carried through a membrane by a given ion i. Figure 2.5 presents the transference numbers of K^+ and Mg^{2+} for modified Fujifilm and Nafion membranes. The current efficiency for K^+ is ~0.5 for all selective membranes (anode-side coated Fujifilm, two-side coated Fujifilm and two-side coated Nafion) at the current density of 0.63 mA cm^{-2}. In contrast, the Mg^{2+} transference number is <0.02.

For highly selective membranes, cations other than K^+ and Mg^{2+} carry approximately 50%. of the current through the membrane. (Anion transference numbers should be negligible through these cation-exchange membranes, see Figure 2.1) We suspect that water splitting at the PEM/membrane interface likely produces H^+ ions that carry current through the membrane.[15] At this interface, differences in transference numbers in the membrane and PEM will lead to ion depletion and large potentials gradients that could cause water splitting. However, even with cathode-side-coated membranes that should give rise to ion accumulation rather than depletion, the K^+ and Mg^{2+} transference numbers, 35% and 30%, respectively, do not account for all of the current. Wessling and coworkers showed that PEMs catalyze water splitting, which might account for relatively low current efficiencies.[15]

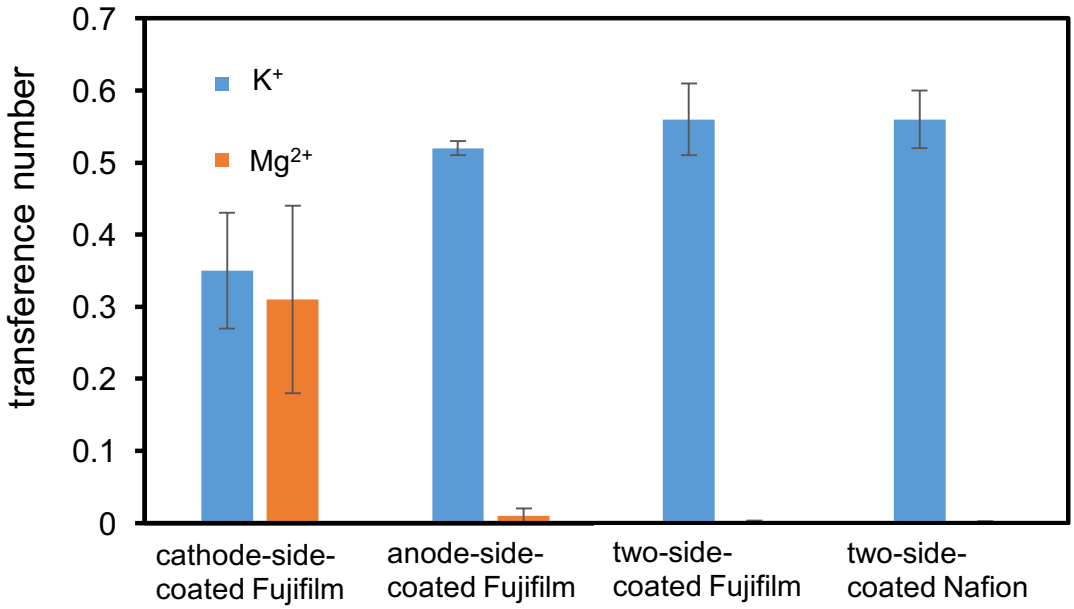

Figure 2.5 K^+ and Mg^{2+} ED transference numbers for cathode-side-coated, anode-side-coated, and two-side-coated Fujifilm membranes and two-side-coated Nafion membranes. The coating was $(PAH/PSS)_5PAH$, and ED employed a solution of 0.01 M KNO_3 and 0.01 M $Mg(NO_3)_2$ in the source phase and 0.01 M HNO_3 in the receiving phase along with a current density of 0.63mA cm^{-2}.

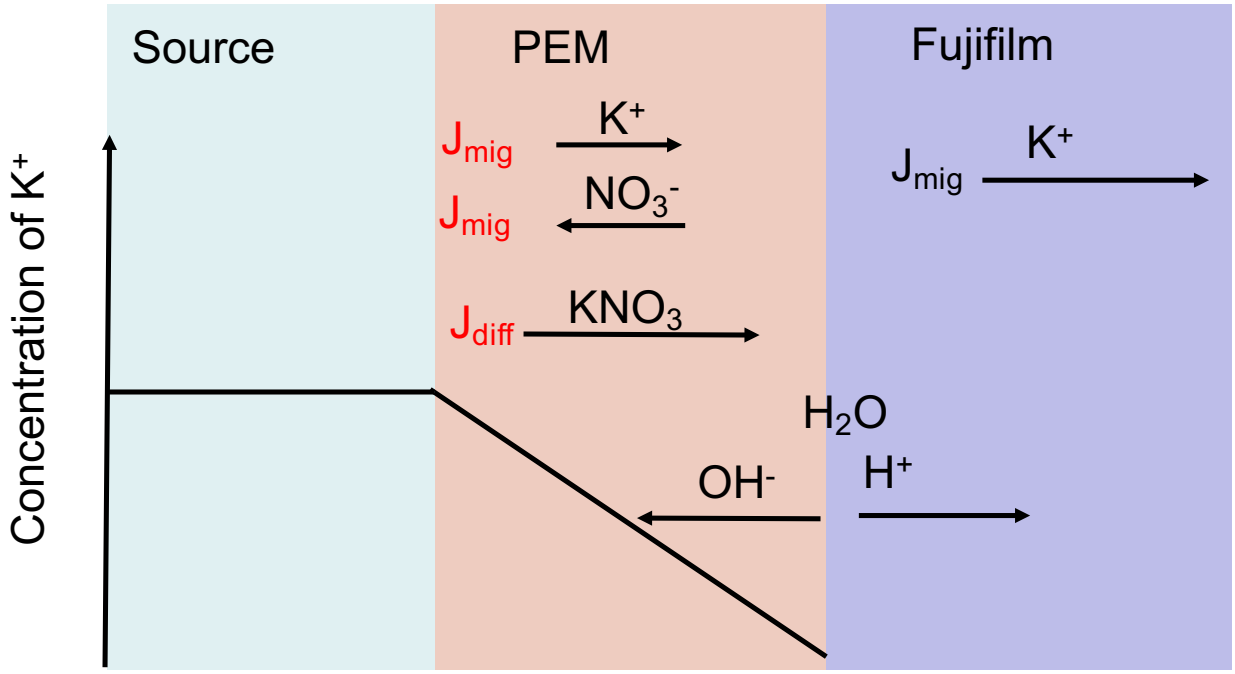

Figure 2.6 Ion transport through $(PAH/PSS)_5PAH$-modified cation-exchange membranes. The migration of NO_3^- and the different K^+ transference numbers in the PEM and Fujifilm membrane generate a depletion zone in the PEM, which leads to water splitting near the PEM/membrane interface.

2.3.3 Current-density-voltage curves for bare and modified Fujifilm membranes

Current density-voltage (I-V) curves provide estimates of the limiting currents through ion-exchange membranes. Typical I-V curves for cation-exchange membranes display three regions. The ohmic region appears at low current densities where the transmembrane potential is proportional to the applied current density. As the current density increases, concentration polarization leads to a diffusion-limited current and, hence, a plateau region in the IV curve. As the current density further increases, multiple phenomena such as water splitting or electro-convection may occur to supply additional ions to the region of concentration polymerization

and give rise to an overlimiting current.[21-22] The intersection of the ohmic region and the 'plateau' gives an approximation for the limiting current density.

Figure 2.7 shows the I-V curves for bare, cathode-coated, anode-coated and two side-coated Fujifilm membranes. I-V curves for anode-coated and two side-coated membranes shows ohmic, 'plateau' and overlimiting regions. Because K^+ primarily carries the current through the ion-exchange membranes and both K^+ and NO_3^- carry current in the PEM, a limiting current results from depletion of K^+ at the membrane/PEM interface. The anode- and two side-coated membranes show similar limiting currents around ~1 mA/cm^2, consistent with the high K^+/Mg^{2+} selectivity of both membranes.

In contrast, bare and cathode-coated Fujifilm membranes, which show low K^+/Mg^{2+} selectivities, exhibit only the ohmic region over this current density range. Given the high Mg^{2+} concentration and the relatively low resistance of these membranes to Mg^{2+} transport, the applied current density never reaches a limiting value. Based on the inverse of the slopes in Figure 2.8, the ohmic resistances of the bare and cathode-side coated Fujifilm membranes are 94 and 112 $\Omega \cdot cm^2$. Thus, the cathode side PEM adds only a small resistance to the membrane system.

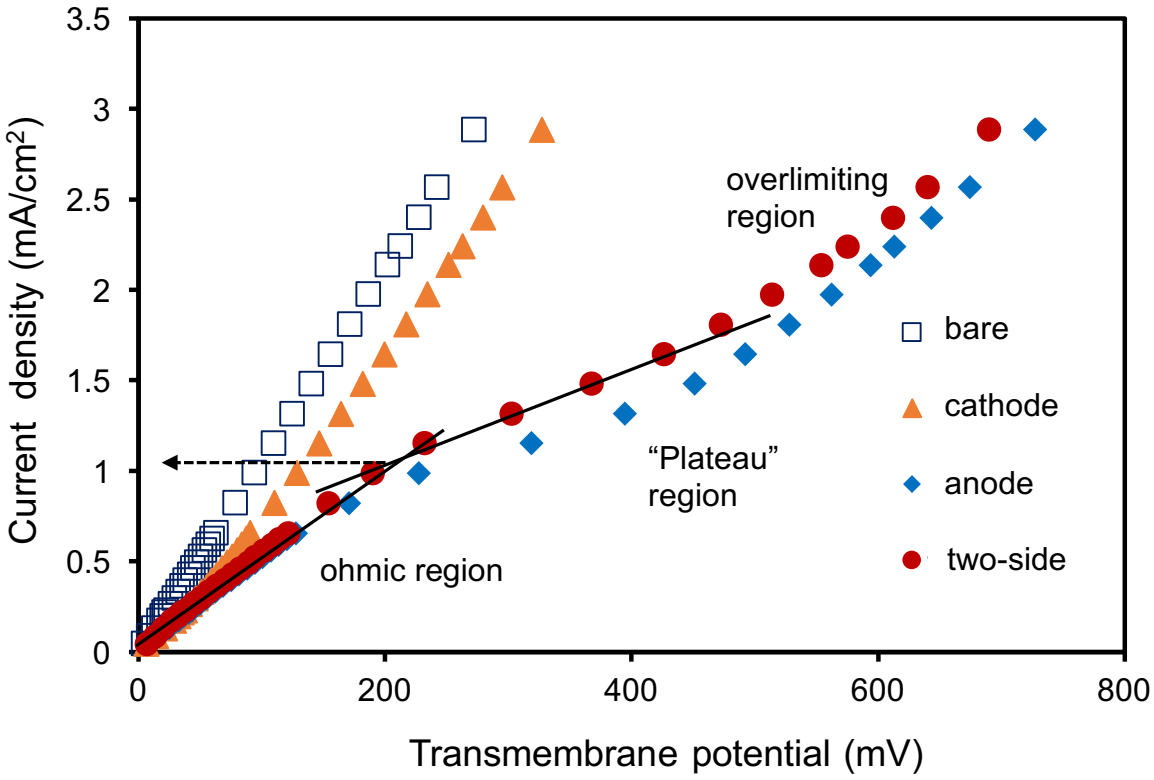

Figure 2.7 Current density as a function of transmembrane potential drop during electrodialysis through bare Fujifilm membranes (squares), and membranes coated with $(PAH/PSS)_5PAH$ films on both sides (circles), on the cathode side (triangles), and on the anode side (diamonds). The experiment employed a two-compartment electrodialysis cell with solutions containing 0.01M KNO_3 and 0.1 M $Mg(NO_3)_2$ on both side of membranes.

2.3 Conclusions

Adsorption of PEMs on relatively inexpensive Fujifilm cation-exchange membranes leads to extremely high K^+/Mg^{2+} cation selectivities >1000 in ED. The high exclusion of Mg^{2+} suggests a complete and dense PEM, presumably because the smooth Fujifilm surface allows formation of a continuous coating. The PEM coated on the anode side is essential for the high selectivity, whereas the cathode-side coating contributes only a small amount to resistance of the membrane system and little selectivity. Nevertheless, the current efficiencies for highly selective membranes are only 50%. Future work should explore methods to increase the current efficiency to enable high-efficiency separations.

APPENDIX

APPENDIX

1. Calculation of K^+ activity

Table A2.1 K^+ activities. γ is the activity coefficient, and a is the ion activity.

Source Conc. (M)	γ K^+	a_1	Receiving Conc. (M)	γ K^+	a_2	a_1/a_2	$\log(a_1/a_2)$
0.1	0.766	0.0766	0.001	0.965	0.000965	79.4	1.90
0.02	0.868	0.0174	0.001	0.965	0.000965	18.0	1.26
0.01	0.901	0.0090	0.001	0.965	0.000965	9.34	0.97
0.005	0.926	0.0046	0.001	0.965	0.000965	4.80	0.68
0.002	0.951	0.0019	0.001	0.965	0.000965	1.97	0.29

* source phase and receiving phase both contain KNO_3
* activity values are adapted from CRC handbook of chemistry and physics.

2. Calculation of junction potentials

The junction potential was calculated using the Henderson equation (A2.1), and the details were described previously.[14]

$$E_j = \phi^{\beta} - \phi^{\alpha} = \frac{\Sigma_i \frac{|Z_j|\mu_j}{Z_i}[C_i(\beta) - C_i(\alpha)]}{\Sigma_i |Z_{i|}\mu_i[C_i(\beta) - C_i(\alpha)]} \frac{RT}{F} \ln \frac{\Sigma_i |Z_i|\mu_i C_i(\alpha)}{\Sigma_i |Z_i|\mu_i C_i(\beta)} \quad \text{(A2.1)}$$

E_j is the junction potential, Z_i is the ion charge, μ_i is the ion mobility, C_i is the ion concentration, and α and β are different solution phases.

Table A2.2 One example of the calculated junction potentials in membrane potential measurements. Ej,s is the junction potential between the source solution and the reference electrode filling solution. Ej,r is the junction potential between the reference electrode filling solution and the receiving phase. Ej = Ej,r – Ej,s.

Source Conc. (M)	Receiving Conc. (M)	Ej,s (mV)	Ej,r (mV)	Ej (mV)
0.1	0.001	-1.35	-3.37	-2.03
0.02	0.001	-1.98	-3.37	-1.39
0.01	0.001	-2.29	-3.37	-1.08
0.005	0.001	-2.61	-3.37	-0.76
0.002	0.001	-3.04	-3.37	-0.33

* source phases and receiving phases both contain KNO_3
* reference electrodes are commercial Ag/AgCl electrodes from CH instrument with filling solution of 1M KCl

3. Calculation of the membrane potential

In actual measurement, the membrane potential ΔE is calculated from equation A2.2

$$\Delta E = \Delta E_{measured} - \Delta E_{control} - E_j \quad \text{A2.2}$$

$\Delta E_{measured}$ is the potential difference between two reference electrodes, and $\Delta E_{control}$ is the potential reading when the same two electrodes were placed in 0.001 M KNO_3 solution.

REFERENCES

REFERENCES

1. Sata, T.; Sata, T.; Yang, W. K., Studies on cation-exchange membranes having permselectivity between cations in electrodialysis. *Journal of Membrane Science* **2002,** *206*, 31-60.

2. Tanaka, Y.; Ehara, R.; Itoi, S.; Goto, T., Ion-exchange membrane electrodialytic salt production using brine discharged from a reverse osmosis seawater desalination plant. *Journal of Membrane Science* **2003,** *222*, 71-86.

3. Kim, D. H., A review of desalting process techniques and economic analysis of the recovery of salts from retentates. *Desalination* **2011,** *270*, 1-8.

4. Seto, T.; Ehara, L.; Komori, R.; Yamaguchi, A.; Miwa, T., Seawater desalination by electrodialysis. *Desalination* **1978,** *25*, 1-7.

5. Strathmann, H., Electrodialysis, a mature technology with a multitude of new applications. *Desalination* **2010,** *264*, 268-288.

6. Wang, Z. X.; Luo, Y. B.; Yu, P., Recovery of organic acids from waste salt solutions derived from the manufacture of cyclohexanone by electrodialysis. *Journal of Membrane Science* **2006,** *280*, 134-137.

7. Vallois, C.; Sistat, P.; Roualdes, S.; Pourcelly, G., Separation of H^+/Cu^{2+} cations by electrodialysis using modified proton conducting membranes. *Journal of Membrane Science* **2003,** *216*, 13-25.

8. Van der Bruggen, B.; Koninckx, A.; Vandecasteele, C., Separation of monovalent and divalent ions from aqueous solution by electrodialysis and nanofiltration. *Water Research* **2004,** *38*, 1347-1353.

9. Sata, T., Ion exchange memebranes : Preparation, characterization, modification and applicaiton ; royal society of chemistry. **2007**, 139.

10. Ge, L.; Wu, B.; Li, Q. H.; Wang, Y. Q.; Yu, D. B.; Wu, L.; Pan, J. F.; Miao, J. B.; Xu, T. W., Electrodialysis with nanofiltration membrane (EDNF) for high-efficiency cations fractionation. *Journal of Membrane Science* **2016,** *498*, 192-200.

11. Sata, T.; Tanimoto, M.; Kawamura, K.; Matsusaki, K., Transport properties of cation exchange membranes in the presence of ether compounds in electrodialysis. *Journal of Colloid and Interface Science* **1999,** *219*, 310-319.

12. Lambert, J.; Avila-Rodriguez, M.; Durand, G.; Rakib, M., Separation of sodium ions from trivalent chromium by electrodialysis using monovalent cation selective membranes. *Journal of Membrane Science* **2006,** *280*, 219-225.

13. Decher, G., Fuzzy nanoassemblies: Toward layered polymeric multicomposites. *Science* **1997,** *277*, 1232-1237.

14. Cheng, C.; Yaroshchuk, A.; Bruening, M. L., Fundamentals of selective ion transport through multilayer polyelectrolyte membranes. *Langmuir* **2013,** *29*, 1885-1892.

15. Abdu, S.; Marti-Caatayud, M. C.; Wong, J. E.; Garcia-Gabaldon, M.; Wessling, M., Layer-by-layer modification of cation exchange membranes controls ion selectivity and water splitting. *ACS Applied Materials & Interfaces* **2014,** *6*, 1843-1854.

16. Mulyati, S.; Takagi, R.; Fujii, A.; Ohmukai, Y.; Matsuyama, H., Simultaneous improvement of the monovalent anion selectivity and antifouling properties of an anion exchange membrane in an electrodialysis process, using polyelectrolyte multilayer deposition. *Journal of Membrane Science* **2013,** *431*, 113-120.

17. White, N.; Misovich, M.; Yaroshchuk, A.; Bruening, M. L., Coating of nafion membranes with polyelectrolyte multilayers to achieve high monovalent/divalent cation electrodialysis selectivities. *ACS Applied Materials & Interfaces* **2015,** *7*, 6620-6628.

18. White, N.; Misovich, M.; Alemayehu, E.; Yaroshchuk, A.; Bruening, M. L., Highly selective separations of multivalent and monovalent cations in electrodialysis through nafion membranes coated with polyelectrolyte multilayers. *Polymer* **2016,** *103*, 478-485.

19. Cheng, C.; White, N.; Shi, H.; Robson, M.; Bruening, M. L., Cation separations in electrodialysis through membranes coated with polyelectrolyte multilayers. *Polymer* **2014,** *55*, 1397-1403.

20. Bard, A. J.; Faulkner, L. R., Electrochemical methods: Fundamentals and applications; John Wiley & Sons: New York. **2000**.

21. Rubinstein, I.; Zaltzman, B., Electro-osmotically induced convection at a permselective membrane. *Physical Review E* **2000,** *62*, 2238-2251.

22. Krol, J. J.; Wessling, M.; Strathmann, H., Concentration polarization with monopolar ion exchange membranes: Current-voltage curves and water dissociation. *Journal of Membrane Science* **1999,** *162*, 145-154.

Chapter 3 Adsorption of Highly Water-Swollen Polyelectrolyte Multilayers on Cation-Exchange Membranes to Achieve High Selectivities among Cations

3.1 Introduction

The data in chapter 2 show that $(PAH/PSS)_5PAH$-modified Fujifilm membranes exhibit remarkably high monovalent/divalent cation selectivities. Coating Nafion 115 cation-exchange membranes with PAH/PSS films also generates monovalent/divalent and monovalent/multivalent cation ED selectivities >1000.[1-2] However, the current efficiencies in ED separations through PEM-modified Nafion and Fujifilm membranes were only ~0.5, implying that unwanted ions such as protons carry 50% of the current.[3]

Enhanced current efficiencies with PEM-coated membranes will likely require an increase in the PEM permeability to the monovalent cation. Poly(diallyldimethylammonium chloride) (PDADMAC) /PSS films swell strongly in water, and high swelling may lead to a high monovalent ion permeance.[4-6] Thus, this chapter examines ED through Fujifilm and Nafion membranes coated with $(PDADMAC/PSS)_5PDADMAC$ films. We investigate the effects of feed solution concentration and the number of PEM bilayers on ion fluxes, selectivities and transference numbers of coated membranes. Importantly, Nafion membranes coated with $(PDADMAC/PSS)_n$ show monovalent/divalent cation selectivities >200 along with a current efficiency of ~0.8.

3.2 Experimental section

3.2.1 Materials

Poly(sodium 4-styrenefulfonate) (Mw = 70 000 Da) and poly(diallyldimethylammonium chloride) (Mw~ 100 000-200 000) were obtained from Sigma-Aldrich. Potassium nitrate, magnesium nitrate, potassium chloride and magnesium chloride were obtained from Columbus Chemical. Co(II) nitrate·$6H_2O$ was purchased from Mallinckrodt. Lithium nitrate and barium nitrate were acquired from Spectrum, and all salts were used as received without further purification. Deionized water (Milli-Q Reference Ultra-pure Water Purification System, 18MΩ cm) was used to prepare all solutions. The pH of polyelectrolyte solutions was adjusted with 0.1 M HCl or 0.1 M NaOH. Nafion 115 membranes were acquired from Ion power (New Castle, DE, thickness 127 nm), and Fujifilm type 1 cation exchange membranes were gifts from Fujifilm.

3.2.2 Film formation and characterization

Nafion and Fujifilm membranes were cut into 25-mm disks with a metal punch, and pretreatment of Nafion membranes followed a literature procedure.[2] The membranes were immersed sequentially in 100 ˚C solutions of 3% H_2O_2, deionized water, 1M H_2SO_4, and deionized water for 30 min each. Between each immersion, Nafion membranes were rinsed with room-temperature deionized water from a washing bottle for 20s. Fujifilm membranes were immersed in room-temperature 0.1 M NaCl for 24 h before modification. Polyelectrolyte films were deposited through layer-by-layer assembly using the same methods described in chapter 2.

Images of bare and modified membranes were obtained with a JEOL 7500F scanning electron microscope with a cold field–emission emitter. All samples were dried in vacuum overnight and sputter-coated with 4 nm of platinum prior to imaging.

3.2.3 Electrodialysis and Donnan dialysis

Electrodialysis was performed as described in chapter 2 using an exposed membrane area of 3.14 cm^2. In some experiments, 0.01 M $Ba(NO_3)_2$ served as the receiving phase instead of HNO_3 to minimize the diffusion of cations from the receiving phase to the source phase. Donnan dialysis was performed same with electrodialysis apparatus without an applied current. The cation concentrations were determined using inductively coupled plasma optical emission spectroscopy (Varian 710-ES) with calibration curves. The standard solutions were prepared through dilution of commercial ICP standard (GFS chemicals).

The transference number of a given ion, the fraction of current carried by that cation, was calculated from equation 3.1, where J_i is the flux of ion i, z_i is the ion charge, F is the Faraday constant, and I is the total current density.

$$t_i = \frac{J_i \times z_i \times F}{I} \quad (3.1)$$

The current density-voltage curves were obtained as described in chapter 2.

3.3 Results and discussion

3.3.1 ED through cation-exchange membranes modified with PDADMAC/PSS films

Although $(PAH/PSS)_5$PAH-coated Fujifilm membranes are highly selective for K^+ over Mg^{2+}, the current efficiency is only 0.5. A highly swollen polyelectrolyte film may have a high monovalent ion permeance, which could lead to a high limiting current and relatively high current efficiencies below the limiting current. Moreover, if such a film can electrostatically exclude divalent ions, it may still induce high ED selectivity between monovalent and divalent cations. Because the water uptake in $(PDADMAC/PSS)_n$PDADMAC films is as much as 4 times greater than in $(PAH/PSS)_n$PAH films,[4, 7] we examined whether Nafion membranes coated

with $(PDADMAC/PSS)_5PDADMAC$ show high K^+/Mg^{2+} selectivities along with current efficiencies that are higher than the 0.5 value for $(PAH/PSS)_nPAH$-coated Nafion.

Figure 3.1 shows receiving phase concentrations during ED through Nafion membranes with and without $(PDADMAC/PSS)_5PDADMAC$ coatings. Clearly the film greatly increases the K^+/Mg^{2+} selectivity, but it also decreases the K^+ flux. In ED with three bare Nafion membranes, on average the K^+ flux was 4.8 ± 1.0 nmole cm^{-2} s^{-1}, the Mg^{2+} flux was 2.5 ± 0.5 nmole cm^{-2} s^{-1}, and the K^+/Mg^{2+} selectivity was 1.9 ± 0.1. The K^+ flux through $(PDADMAC/PSS)_5PDADMAC$-modified Nafion membranes decreased ~30% to 3.4 ± 0.3 nmole cm^{-2} s^{-1}. In contrast, the Mg^{2+} flux through modified membranes was lower than the detection limit (2 pmol cm^{-2} s^{-1}) for all three replicate membranes, which gives K^+/Mg^{2+} selectivities > 1000. Additionally, the Li^+/Co^{2+} ED selectivity is also >1000 through the $(PDADMAC/PSS)_5PDADMAC$-coated Nafion, with a Li^+ flux of 4.7±1.3 nmole cm^{-2} s^{-1} and a Co^{2+} flux under the detection limit. These remarkable selectivities, which are similar to the values for $(PAH/PSS)_5PAH$-coated Nafion membranes, presumably stem from the electrostatic exclusion of Mg^{2+}. We think that size-based selectivity should be small in these swollen PEMs. The K^+/Mg^{2+} selectivity is also >1000 for Nafion modified with $(PDADMAC/PSS)_5PDADMAC$ only on the anode side, but selectivity is just 7 for cathode-side modified Nafion. The low selectivity for the membrane coated on the cathode side may reflect concentration polarization at the membrane/PEM interface near the receiving phase.

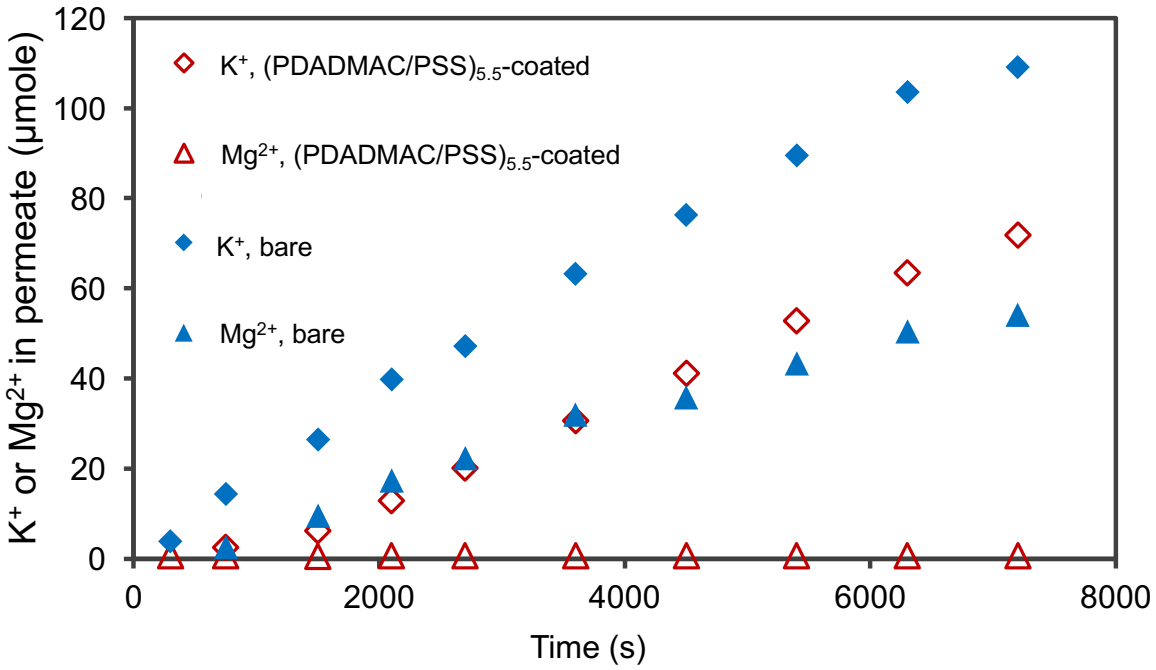

Figure 3.1 Moles of K^+ and Mg^{2+} in the receiving phase as a function of time during ED with initial solutions containing 0.01 M KNO_3 and 0.01 M $Mg(NO_3)_2$ in the source phase and 0.01 M HNO_3 in the receiving phase. Electrodialysis used bare Nafion membranes (blue) and Nafion coated with $(PDADMAC/PSS)_5PDADMAC$ films on both sides (red). The current density was 0.63 mA cm^{-2}.

Interestingly, the K^+ flux through $(PDADMAC/PSS)_5PDADMAC$-coated Nafion membranes is less than that through bare Nafion membranes. The same trend appears with $(PAH/PSS)_5PAH$-modified Nafion membranes. In contrast, the K^+ flux increases ~29% after coating Fujifilm membranes with $(PAH/PSS)_5PAH$ films. This reflects in part the low selectivity of the bare Fujifilm membrane (K^+/Mg^{2+} selectivity of 0.95±0.05) relative to the bare Nafion membranes (K^+/Mg^{2+} selectivity of 1.9±0.1). With the Fujifilm membrane, after coating the K^+

begins to carry some of the current previously carried by Mg^{2+}. Thus, the K^+ flux increases despite some possible water splitting that tends to decrease metal-cation current efficiencies. In the case of Nafion, the higher selectivity before coating means there is less current from Mg^{2+} to replace and water splitting likely results in a net decrease in K^+ flux.

We also investigated the ion fluxes and selectivities of $(PDADMAC/PSS)_5PDADMAC$-modified Fujifilm membranes, but the results differed for two different batches of membranes. For batch 1, the $(PDADMAC/PSS)_5PDADMAC$-modified membranes showed a K^+/Mg^{2+} selectivity of 74±30 with a K^+ flux of 5.51±0.59 nmole cm^{-2} s^{-1} and a Mg^{2+} flux of 0.085±0.037 nmole cm^{-2} s^{-1}. The transference number was 0.84±0.09 for K^+ and 0.026±0.011 for Mg^{2+}. However, for batch 2, the modified membranes showed a K^+/Mg^{2+} selectivity of 4.2±0.7 with a K^+ flux of 4.10±0.78 nmole cm^{-2} s^{-1} and a Mg^{2+} flux of 0.97±0.05 nmole cm^{-2} s^{-1}. The lower selectivity of batch 2 suggests a lower PEM coverage presumably due to some large surface defect that the highly swollen $(PDADMAC/PSS)_5PDADMAC$ film cannot fill. Nevertheless, for both batches of Fujifilm membranes, the PDADMAC/PSS film enhances the K^+/Mg^{2+} selectivity compared to the bare Fujifilm K^+/Mg^{2+} selectivity of ~1. However, with both batches of Fujifilm membranes, adsorption of $(PAH/PSS)_5PAH$ films gives K^+/Mg^{2+} selectivities> 1000, suggesting that the PAH/PSS films better covers the underlying pores.

3.3.2 Characterization of polyelectrolyte multilayer-modified Nafion and Fujifilm membranes

High rejections of multivalent cations imply full PEM coverage of the underlying substrate. Figure 3.2 (A) shows that Nafion membranes have smooth and defect-free surfaces, which should enable full coverage with a PEM. Figure 3.2 (B) and (C) present images of $(PDADMAC/PSS)_5PDADMAC$-modified Nafion and Fujifilm membranes, respectively. Both

images suggest a continuous $(PDADMAC/PSS)_5PDADMAC$ coating, but the film appears porous, at least after drying. Figure 3.2 (D) shows a $(PAH/PSS)_5PAH$-modified Fujifilm membrane. The image suggests that the $(PAH/PSS)_5PAH$ film is less porous than the $(PDADMAC/PSS)_5PDADMSC$ film, thus the $(PAH/PSS)_5PAH$ film may better cover underlying defects. Because of the high exclusion of divalent cations, we think that $(PDADMAC/PSS)_5PDADMAC$ films swells strongly in aqueous solutions to decrease the pore size (or even eliminate pores) in these coatings.

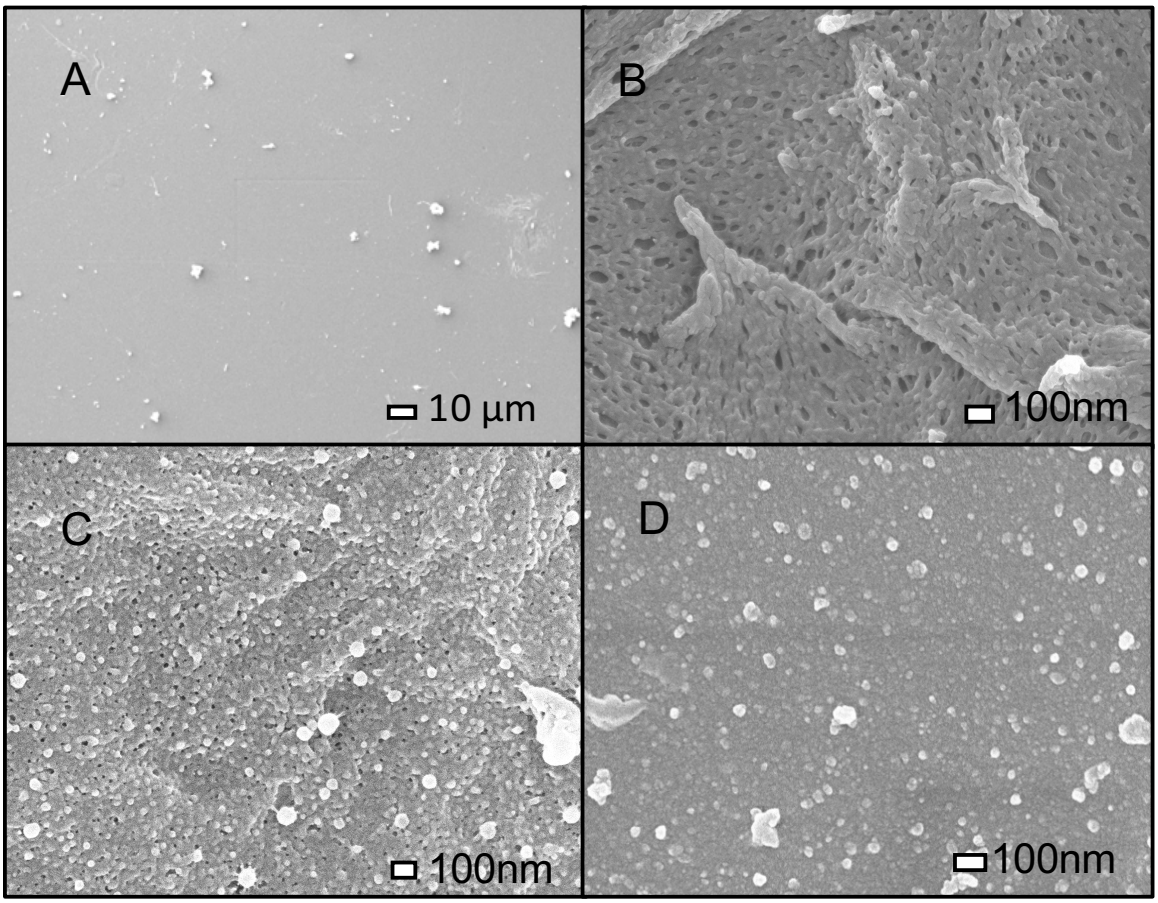

Figure 3.2 SEM images of the surfaces of (A) a bare Nafion membrane, (B) a $(PDADMAC/PSS)_5$PDADMAC-coated Nafion membrane, (C) a $(PDADMAC/PSS)_5$PDADMAC-coated Fujifilm membrane, and (D) a $(PAH/PSS)_5$PAH-coated Fujifilm membrane.

3.3.3 Electrodialysis and Donnan dialysis with HNO_3 or $Ba(NO_3)_2$ in receiving phase

Because $(PDADMAC/PSS)_5$PDADMAC-coated Nafion membranes shows high monovalent/divalent cation selectivities, we determined ion transference number in ED to investigate the current efficiency. Table 3.1 gives the ion flux and transference numbers during ED with a source phase containing 0.01 M $LiNO_3$ and 0.01 M $Co(NO_3)_2$. Based on the Li^+ flux in ED, the Li^+ transference number was 0.72 ± 0.2. However, the Li^+ flux in Donnan dialysis (the

same experiment as the electrodialysis but without an applied potential) is very close to the ED flux (Table 3.1). In the Donnan dialysis experiment, diffusion of cations from the source to the receiving phase couples with the diffusion of H^+ from the receiving to the source phase. Compared to Donnan dialysis, in ED the H^+ flux from the receiving phase to the source phase flux should decrease because of the electric field directed from the source to the receiving phase. Nevertheless, some Donnan diffusion may still occur. As a result, the total cation flux in ED experiments includes both migration flux and Donnan diffusion flux, but only the migration flux reflects the true current efficiency. Therefore, the transference number calculated from the ED flux is most likely an overestimation.

Table 3.1 Li^+ and Co^{2+} fluxes and Li^+/Co^{2+} selectivities during ED and Donnan dialysis through Nafion membranes coated with $(PDADMAC/PSS)_5PDADMAC$ films. The source phase contained 0.01 M $LiNO_3$ and 0.01 M $Co(NO_3)_2$, the receiving phase was 0.01 M HNO_3, and the current density was 0.63 mA/cm^2. The transference numbers for ED are listed in parentheses.

	Li^+ flux (nmol cm^{-2} s^{-1})	Co^{2+} flux (pmol cm^{-2}s^{-1})	selectivity
ED	4.7±1.3(0.72±0.20)	< 2 (0.00060)	>1000
Donnan dialysis	4.5±1.6	< 2	>1000

To better determine the current efficiency we employed 0.01 M $Ba(NO_3)_2$ as the receiving phase instead of 0.01 M HNO_3. The diffusive flux of Ba^{2+} from the receiving phase to the source phase is much smaller than that of H^+ because the polyelectrolyte multilayer excludes Ba^{2+} due to its large hydration sphere and high charge.[8] Table 3.2 gives the Donnan dialysis and ED fluxes of K^+ and Mg^{2+} with $Ba(NO_3)_2$ in the receiving phase. The K^+ flux in Donnan dialysis (1.05±0.11 nmole cm^{-2} s^{-1}) is much smaller than the K^+ flux in ED (5.26±0.38 nmole cm^{-2}s^{-1}).

The K^+ transference number of 0.81±0.06, is significantly larger the transference number of 0.61±0.04 obtained with a $(PAH/PSS)_5PAH$-caoted Nafion membrane using 0.01 M $Ba(NO_3)_2$ as the receiving phase. Notably, during 2 h of ED, the pH of the receiving phase increase from 5.8 to 10.7 due to the formation of OH^- at cathode. The K^+/Mg^{2+} selectivity with $Ba(NO_3)_2$ in the receiving phase decreases compared to that with HNO_3 in the receiving phase, perhaps because some species such as $Mg(OH)^+$ are more permeable than Mg^{2+}. In one experiment, after each aliquot sampled, we added 0.14 mL of 1 M HNO_3 to the receiving phase to neutralize the OH^- formed during 2 h of ED at 0.63 mA cm^{-2}, and the K^+/Mg^{2+} selectivity was >1000 in this case.

Table 3.2 K^+ and Mg^{2+} fluxes and K^+/Mg^{2+} selectivities during ED and Donnan dialysis through Nafion membranes coated with $(PDADMAC/PSS)_5PDADMAC$ films. The source phase contained 0.01 M KNO_3 and 0.01 M $Mg(NO_3)_2$, the receiving phase was 0.01M $Ba(NO_3)_2$, and the current density was 0.63 mA/cm^2. The transference numbers for ED are listed in parentheses.

	K^+ flux (nmol cm^{-2} s^{-1})	Mg^{2+} flux (pmol $cm^{-2}s^{-1}$)	selectivity
Donnan dialysis	1.1±0.1	< 2	>1000
ED	5.3±0.4 (0.81±0.06)	9.6±3.2 (0.00087±0.00049)	593±200

3.3.4 Ion fluxes and selectivities as a function of the number of adsorbed layers

Both the thicknesses and surface coverages of PEMs should increase with the number of deposited bilayers. Thus, we expect membrane selectivities to increase with the number of layers in PEMs on membranes, but the limiting currents and current efficiencies should decrease. Consistent with these expectations, Table 3.3 shows that the K^+ transference number decreases with an increasing number of PDADMAC/PSS layers on Nafion membranes. (The sum of the K^+ and Mg^{2+} transference numbers is >1 for membranes coated with

(PDADMAC/PAA)PDADMAC and bare Nafion, implying significant Donnan diffusion in this case.) Although the K^+/Mg^{2+} selectivities are too high to quantify even for membranes coated with $(PDADMAC/PSS)_3$PDADAMC films, we do see the expected increase in selectivity on going from (PDADMAC/PSS)PDADAMC to $(PDADMAC/PSS)_3$PDADAMC films on Nafion. Similar trends occur in ED with 0.01 M $LiNO_3$ and 0.01 M $Co(NO_3)_2$ in the source phase (Table 3.4). In this case, we see increases in Li^+/Co^{2+} selectivity with an increasing number of PDADMAC/PSS layers. The transference number decreases as expected on going from a $(PDADMAC/PSS)_3$PDADMAC to a $(PDADMAC/PSS)_5$PDADMAC film. For a (PDADMAC/PSS)PDADMAC film, however, the Li^+ transference number is relatively low because of the low selectivity (Co^{2+} carries much of the current). The bare Nafion membranes have a Li^+/Co^{2+} selectivity of 0.66,[1] and after coating with a PDADMAC/PSS/PDADMAC film, the Li^+/Co^{2+} selectivities increase to 2.7. For these relatively thin films, low coverages does not allow high selectivities.

Notably, the trend of Li^+ transference numbers with the number of adsorbed PDADMAC/PSS bilayers is very different than that with PAH/PSS bilayers. White et al. reported that the Li^+ transference numbers decrease with a decreasing number of bilayers on $(PAH/PSS)_n$PAH-modified Nafion membranes, and the Co^{2+} transference numbers were smaller than 0.02 even with only 1.5 bilayers on the Nafion. This may suggest more water splitting with a lower number of PAH/PSS bilayers. Overall, depositing $(PDADMAC/PSS)_3$PDADMAC leads to the highest monovalent cation transference numbers (around 0.8 for K^+ and Li^+) along with high selectivities.

Table 3.3 K^+ and Mg^{2+} fluxes and transference numbers and K^+/Mg^{2+} selectivities during ED through bare Nafion and Nafion membranes coated with $(PDADMAC/PSS)_nPDADMAC$ films. The source phase contained 0.01 M KNO_3 and 0.01 M $Mg(NO_3)_2$, the receiving phase was 0.01M HNO_3, and the current density was 0.63 mA/cm^2.

Film	K^+ flux (nmol cm^{-2} s^{-1})	Mg^{2+} flux (pmol $cm^{-2}s^{-1}$)	K^+ Transference number	Mg^{2+} Transference number	selectivity
(PDADMAC/PSS)PDADMAC	6.9±1.3	1050±115	1.1±0.2	0.32±0.04	6.7±2.0
$(PDADMAC/PSS)_3PDADMAC$	4.9±0.7	< 2	0.74±0.11	< 0.0006	>2000
$(PDADMAC/PSS)_5PDADMAC$	3.4±0.3	< 2	0.52±0.04	< 0.0006	>1000
Bare Nafion	4.8±1.0	2600±510	0.73±0.15	0.78±0.16	1.9±0.1

Table 3.4 Li^+ and Co^{2+} fluxes and transference numbers and Li^+/Co^{2+} selectivities during ED through Nafion membranes coated with $(PDADMAC/PSS)_{1.5}$, $(PDADMAC/PSS)_{3.5}$, or $(PDADMAC/PSS)_{5.5}$ films. The source phase contained 0.01 M $LiNO_3$ and 0.01 M $Co(NO_3)_2$, the receiving phase was 0.01 M HNO_3, and the current density was 0.63 mA/cm^2.

Film	Li^+ flux ($nmol\ cm^{-2}\ s^{-1}$)	Co^{2+} flux ($pmol\ cm^{-2}s^{-1}$)	Li^+ Transference number	Co^{2+} Transference number	selectivity
(PDADMAC/PSS)PDADMAC	3.5±0.6	1500±540	0.54±0.1	0.46±0.17	2.7±1.5
$(PDADMAC/PSS)_3$PDADMAC	5.6±0.9	3, 2, 31	0.85±0.13	0.0098,0.00061,0.00098	>170
$(PDADMAC/PSS)_5$PDADMAC	4.7±1.3	<2	0.72 ± 0.2	0.0006	>1000

3.3.5 The effect of source-phase concentrations

Increases in the source-phase salt concentration should lead to increases in limiting currents and consequently higher monovalent/divalent cation selectivities and monovalent cation transference numbers at a fixed current density. Thus, we performed ED with $(PAH/PSS)_5PAH$-coated Fujifilm membranes and $(PDADMAC/PSS)_5PDADMAC$-coated Nafion membrane using source phases containing 0.01 M, 0.02 M or 0.1 M KNO_3 and $Mg(NO_3)_2$. The receiving phases all contained 0.01 M HNO_3.

Table 3.5 shows the K^+ and Mg^{2+} fluxes and transference numbers and K^+/Mg^{2+} selectivities from ED through $(PAH/PSS)_5PAH$-modified Fujifilm membranes. The K^+ flux increases from 3.43±0.29 nmol $cm^{-2}s^{-1}$ to 12.37±0.75 nmol cm^{-2} s^{-1} when the source-phase concentration increases from 0.01 M to 0.1 M, whereas the Mg^{2+} fluxes are all lower than 2 pmole cm^{-2} s^{-1}, the lowest detectable flux. Thus the selectivity is >1000 at all concentrations. The K^+ transference increases from 0.52±0.04 to essentially 1 when the source phase concentration increases from 0.01 M to 0.02 M. The increases in source-phase concentration should approximately double the limiting current density to a value above the applied current density (0.63mA cm^{-2}), which should lead to minimal water splitting and the nearly 100% K^+ current efficiency. However, higher source phase concentration may also increase Donnan diffusion.

At a source-phase salt concentration of 0.1 M, the calculated K^+ transference reaches the non-physical value of 1.87±0.11. As mentioned above, transference numbers >1 imply that some ion transport occurs through mechanisms other than electromigration, presumably Donnan diffusion where cations exchange between the source and receiving phase. Thus, we conducted Donnan dialysis experiments at the same source and receiving phase concentration as in ED,

only without applied current. With 0.1 M salts in the source phase, the Donnan dialysis K^+ flux is 4.1 nmol cm^{-2} s^{-1} and the Mg^{2+} flux is less than 2 pmole cm^{-2} s^{-1}.

Table 3.5 K^+ and Mg^{2+} fluxes, K^+ transference numbers, and K^+/Mg^{2+} selectivities as a function of source-phase cation concentration during ED through Fujifilm membranes coated with $(PAH/PSS)_5PAH$ films. The receiving phase initially contained 0.01 M HNO_3, and the applied current density was 0.63 mA/cm^2. The Donnan dialysis fluxes are listed in parentheses.

Source phase concentration	K^+ flux (nmol cm^{-2} s^{-1})	K^+ transference number	Mg^{2+} flux (nmol cm^{-2} s^{-1})	selectivity
0.01 M	3.6±0.34 (2.3)	0.56±0.06	<0.002	>1000
0.02 M	6.9±0.44 (3.9)	1.1±0.07	<0.002	>1000
0.1 M	12.4±0.75 (4.1)	1.9±0.11	<0.002	>1000

* Mg^{2+} fluxes in donnan dialysis are all < 0.002 nmol cm^{-2} s^{-1}

Table 3.6 shows K^+ and Mg^{2+} fluxes and the K^+ transference number as a function of source-phase salt concentration during ED through $(PDADMAC/PSS)_5PDADMAC$-modified Nafion membranes. In this case, the K^+/Mg^{2+}selectivity decreases from >1000 to 44 as the feed concentration increase from 0.01 to 0.02 M, primarily because of an increase in the Mg^{2+} flux (the K^+ flux also increases but less so). As the feed concentration increase to 0.1 M, the Mg^{2+} flux remains about the same, and the K^+ flux increases. The K^+/Mg^{2+} selectivity increases to 108, although the standard deviation of this value is high. Increased Mg^{2+} fluxes at higher feed concentrations may result from charge screening that decreases electrostatic exclusion of Mg^{2+}. However, this does not explain why the Mg^{2+} flux remains constant when the source-phase

concentration increases to 0.1 M. PEM swelling also increases with ionic strength,[9] but this again does not explain why Mg^{2+} transport does not increase on going to the 0.01 M feed solution. Perhaps an interplay between Mg^{2+} adsorption, which increases charge, and charge screening leads to the constant Mg^{2+} flux.

Table 3.6 K^+ and Mg^{2+} fluxes, K^+ transference numbers, and K^+/Mg^{2+} selectivities as a function of source-phase cation concentration during ED through Nafion membranes coated with $(PDADMAC/PSS)_5PDADMAC$ films. The receiving phase initially contained 0.01 M HNO_3, and the applied current density was 0.63 mA/cm^2. The Donnan dialysis fluxes are listed in parentheses.

Source phase concentration	K^+ flux (nmol cm^{-2} s^{-1})	K^+ transference number	Mg^{2+} flux (nmol cm^{-2} s^{-1})	selectivity
0.01 M	3.4±0.29 (5.5)	0.52±0.04	<0.002 (0.002)	>1000
0.02 M	7.7±0.04 (7.6)	1.18±0.01	0.18±0.04 (0.096)	44±8
0.1 M	16.1±1.9 (17.7)	2.47±0.30	0.18±0.07 (0.16)	108±69

3.3.6 Current-density-voltage curve

Figure 3.3 presents the current density-voltage curve for $(PDADMAC/PSS)_5PDADMAC$-coated Nafion with source and receiving solutions that both contain 0.01 M KNO_3 and 0.1 M $Mg(NO_3)_2$. The high $Mg(NO_3)_2$ concentration reduces the solution resistance. The linear increase of the membrane potential with current density corresponds to an ohmic region from 0 to >4 mA/cm^2. The large ohmic range suggests a high

limiting current for this system. Based on the fluxes in Table 3.6, most of the current should stem from K^+ flux. The current density-voltage curve performed in 0.01 M KNO_3, 0.01 M $Mg(NO_3)_2$ mixture demonstrates ohmic region from 0 to 0.25 mA/cm^2. Unfortunately, the potentiostat (CH Instruments Model 604) and the high resistance of the solution limited the applied current to 0.25 mA/cm^2.

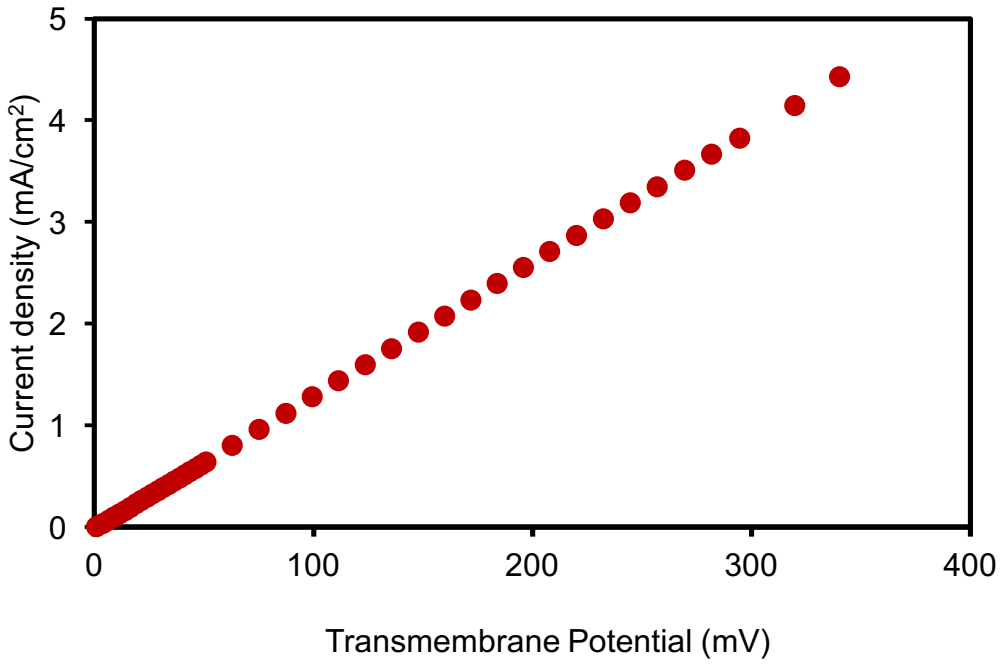

Figure 3.3 Current density as a function of transmembrane potential drop during electrodialysis through $(PDADMAC/PSS)_5$PDADMAC-modified Nafion. The experiment employed a two-compartment electrodialysis cell with solutions containing 0.01 M KNO_3 and 0.1 M $Mg(NO_3)_2$ on both sides of membrane.

3.4 Conclusions

Adsorption of $(PDADMAC/PSS)_n$ films on Nafion membranes leads to monovalent /divalent ED selectivities >1000. Moreover, the monovalent cation transference number is as high as 0.8 with PDADMAC/PSS-coated Nafion. In the contrast, the current efficiency for PAH/PSS-coated Nafion is typically around 0.5~0.6. Among various coatings, $(PDADMAC/PSS)_3PDADMAC$ films give the highest current efficiency in both K^+/Mg^{2+} and Li^+/Co^{2+} separations. The high current efficiency presumably results from the high aqueous swelling of $(PDADMAC/PSS)_n$ films to increase the monovalent cation permeance. Notably, the Donnan dialysis fluxes through $(PDADMAC/PSS)_n$-coated Nafion are high, thus it may possible to utilize Donnan dialysis for to achieve highly selective separations without an applied potential, thus avoiding water splitting. However, $(PDADMAC/PSS)_n$ films are not stable in solutions with high salt concentrations, so future work should aim to increase the film stability.

REFERENCES

REFERENCES

1. White, N.; Misovich, M.; Alemayehu, E.; Yaroshchuk, A.; Bruening, M. L., Highly selective separations of multivalent and monovalent cations in electrodialysis through Nafion membranes coated with polyelectrolyte multilayers. *Polymer* **2016,** *103*, 478-485.

2. White, N.; Misovich, M.; Yaroshchuk, A.; Bruening, M. L., Coating of Nafion membranes with polyelectrolyte multilayers to achieve high monovalent/divalent cation electrodialysis selectivities. *ACS Applied Materials & Interfaces* **2015,** *7*, 6620-6628.

3. Abdu, S.; Marti-Caatayud, M. C.; Wong, J. E.; Garcia-Gabaldon, M.; Wessling, M., Layer-by-Layer modification of cation exchange membranes controls ion selectivity and water splitting. *ACS Applied Materials & Interfaces* **2014,** *6*, 1843-1854.

4. Miller, M. D.; Bruening, M. L., Correlation of the swelling and permeability of polyelectrolyte multilayer films. *Chemistry of Materials* **2005,** *17*, 5375-5381.

5. Lu, O. Y.; Malaisamy, R.; Bruening, M. L., Multilayer polyelectrolyte films as nanofiltration membranes for separating monovalent and divalent cations. *Journal of Membrane Science* **2008,** *310*, 76-84.

6. Adusumilli, M.; Bruening, M. L., Variation of ion-exchange capacity, zeta potential, and ion-transport selectivities with the number of layers in a multilayer polyelectrolyte film. *Langmuir* **2009,** *25*, 7478-7485.

7. Dubas, S. T.; Schlenoff, J. B., Swelling and smoothing of polyelectrolyte multilayers by salt. *Langmuir* **2001,** *17*, 7725-7727.

8. Marcus, Y., A simple empirical-model describing the thermodynamics of hydration of ions of widely varying charges, sizes, and shapes. *Biophysical Chemistry* **1994,** *51*, 111-127.

9. Parveen, N.; Schonhoff, M., Swelling and stability of polyelectrolyte multilayers in ionic liquid solutions. *Macromolecules* **2013,** *46*, 7880-7888.

10. Ladhari, N.; Hemmerle, J.; Haikel, Y.; Voegel, J. C.; Schaaf, P.; Ball, V., Stability of embossed PEI-(PSS-PDADMAC)$_{20}$ multilayer films versus storage time and versus a change in ionic strength. *Applied Surface Science* **2008,** *255*, 1988-1995.

11. Nolte, A. J.; Takane, N.; Hindman, E.; Gaynor, W.; Rubner, M. F.; Cohen, R. E., Thin film thickness gradients and spatial patterning via salt etching of polyelectrolyte multilayers. *Macromolecules* **2007,** *40*, 5479-5486.

12. Kovacevic, D.; van der Burgh, S.; de Keizer, A.; Stuart, M. A. C., Kinetics of formation and dissolution of weak polyelectrolyte multilayers: Role of salt and free polyions. *Langmuir* **2002,** *18*, 5607-5612.

Chapter 4 Fabrication of Membranes with Electrically Conductive Skins for Investigation of Ion Transport as a Function of Applied Potential

4.1 Introduction

Potable water scarcity is a serious global challenge. Membrane-based desalinization and waste-water reclamation, which have a higher energy efficiency than distillation, offer potential solutions to this challenge.[1-3] However, improvements in membrane stability, fouling resistance, selectivity and permeability could increase the impact of membrane separations. Highly charged membrane surfaces, in particular, are attractive for potentially increasing resistance to fouling, enhancing selectivity among ions, and raising fluxes. For example, nanofiltration membranes coated with polyanionic brushes resist fouling by oil emulsions,[4] and other negatively charged membranes resist fouling during treatment of dye wastewater.[5] With regard to selectivity among ions, chapters two and three demonstrate that highly charged polyelectrolyte coatings increase the monovalent/divalent cation selectivities of cation-exchange membranes. Surface charge also enhances salt rejection and ion separations in nanofiltration.[6-7]

Introduction of charge on membrane surfaces typically entails adsorption of polyelectrolytes or covalent derivatization of the substrate with charged moieties. We hypothesized that an applied electrical potential between a conductive membrane surface and an electrode in solution would create extensive surface charge to alter cation and anion partitioning into the membrane, especially for divalent ions. Thus, such an applied potential could provide

high monovalent/divalent cation or anion selectivity, depending on the sign of the applied potential. Compared with chemical surface charge, an externally applied electric field should introduce a much larger double layer potential and have a bigger effect on ion rejection and selectivity.

The mathematical basis of our hypothesis starts from the quasi-equilibrium partitioning of each ion. In the absence of an electrostatic potential, at quasi-equilibrium the chemical potential of ion i in solution, $\mu_{i,solution}$, is equal to that in the membrane, $\mu_{i,membrane}$. Substitution of $\mu_i^0 + RTlnC_i$ for the chemical potential leads to eq (1),

$$\mu_{i,solution}^0 + RTlnC_i^{solution} = \mu_{i,membrane}^0 + RTlnC_i^{membrane} \quad (1)$$

where μ_i^0 is the standard standard state chemical potential (in the solution or the membrane as designated), R is the gas constant, T is temperature, and C_i is the ion concentration (in the solution or the membrane). This equation assumes activity coefficients of 1. Rearrangement of eq (1) leads to the ion partition coefficient, τ_i^0, in eq (2).

$$\tau_i^0 = \frac{C_i^{membrane}}{C_i^{solution}} = \exp\left(\frac{\mu_{i,solution}^0 - \mu_{i,membrane}^0}{RT}\right) \quad (2)$$

When the electrostatic potential, ϕ, differs between the solution and the membrane, the electrochemical potential of ion i in solution, $\bar{\mu}_{i,solution}$, is equal to that in the membrane, $\bar{\mu}_{i,membrane}$. Substitution of expressions for $\bar{\mu}_i$ leads to eq (3)

$$\mu_{i,solution}^0 + RTlnC_i^{solution} + Z_iF\phi^{solution} = \mu_{i,membrane}^0 + RTlnC_i^{membrane} + Z_iF\phi^{membrane} \quad (3)$$

Thus the partition coefficient in the presence of an electrostatic potential difference between the solution and the membrane, $\phi^{solution} - \phi^{membrane}$, is

$$\tau_i = \tau_i^0 \exp\left(\frac{Z_iF}{RT}\left(\phi^{solution} - \phi^{membrane}\right)\right) \quad (4)$$

where τ_i^0 is the partition coefficient without an applied electrostatic potential.

Importantly, the partition coefficient varies exponentially with both the charge of the ion and the potential drop between the solution and the membrane. Thus, even a 50 mV potential drop can lead to a 50-fold change in partition coefficient for a divalent ion. Moreover, a charged surface may create regions of nonelectroneutrality in the membrane, and in these regions the excluded ion controls the resistance to salt transport.[8]

This chapter describes our efforts to achieve highly selective monovalent/divalent cation separations using a potential applied between a conductive membrane surface and an electrode in solution. Such experiments require a membrane with a selective skin that is both conductive and permeable to ions. However, the skins should not contain large pores that lead to decreases in selectivity, so fabrication of such membranes is a major challenge.

We examined fabrication of conducting membrane skins using several methods including layer-by-layer assembly of conductive polymers, sputter coating of a thin metal film, electroless deposition of Au, and electrochemical polymerization from a Au film. Initial characterization included determination of the electrical sheet resistance of the films and imaging using scanning electron microscopy (SEM). Subsequently, we determined ion fluxes and the effects of applied electrical potential on ion transport.

4.2 Experimental section

4.2.1 Materials.

Poly(allylamine hydrochloride) (PAH, Mw=15 000 Da), Poly(sodium 4-styrenesulfonate) (PSS, MW=70,000 Da), Poly(3,4-ethylenedioxythiophene)-poly(styrenesulfonate) (PEDOT:PSS, 1.3 wt% dispersion in H_2O, conductive grade), PEDOT:PSS (3 wt% dispersion in H_2O, high

conductive grade), branched polyethylenimine (B-PEI, Mw=25,000 Da), 3,4-Ethylenedioxythiophene (EDOT) , Dimethyl sulfoxide (DMSO), and hydrogen tetrachloroaurate ($HAuCl_4$) were obtained from Sigma-Aldrich. Potassium chloride, magnesium chloride and hydroxylamine hydrochloride ($NH_2OH{\cdot}HCl$) were obtained from Columbus Chemical. The pH values of all solutions were adjusted by addition of dilute NaOH or HCl. Alumina membranes (Whatman Anodisk filters, 0.02 μm surface pores) served as the substrates for conductive film deposition. Silver conductive epoxy was obtained from MG chemicals. Platinum electrodes and Ag/AgCl electrodes were purchased from CH Instruments.

4.2.2 Layer-by-Layer assembly of conductive membrane coatings

Porous alumina membranes were cleaned in UV-O_3 (Boekel UV-Clean Model 135500) for 15 min to remove organic residues, and then placed in a home-made holder that directly exposes only the filtration side of the membrane to modification solutions. (The holder exposes a membrane surface area of 1.7 $cm^{2.}$) The polycation deposition solutions contained either 0.02M PAH (with respect to the repeating unit) in 1M NaCl or B-PEI (0.3 wt% in H_2O or 1M NaCl). The PEDOT:PSS solutions were used as-received, except 1% wt of DMSO was added in the as-received solutions as dopant in some experiments. The alumina membranes were immersed in the polyanion solution for 5 min, and then in the polycation solution for 5 min, and between exposures to each deposition solution the membranes were rinsed with deionized water for 1min to remove loosely bonded polymer. The process was repeated several times to adsorb the desired number of layers.

Some experiments utilized Au- coated Si wafers or bare glass as the deposition substrate to investigate the film thickness or electrical sheet resistance. The Au wafer was coated with a

primer layer of 3-mercaptopropionic acid (MPA) to introduce charge on the surface before layer-by-layer assembly.[9] The glass was sequentially cleaned in detergent, water, acetone and methanol before modification. With both glass and MPA-modified Au, the layer-by-layer assembly started with the polycation solution due to the negative substrate surface charge.

4.2.3 Au deposition on membrane surfaces

Au was deposited on membranes through electroless deposition according to a literature method.[10-11] Citrate-stabilized gold nanoparticles (NPs) (0.02 mg/mL) with an average diameter of 12 nm were prepared using the citrate reduction method.[12-14] Figure 4.1 demonstrates the coating process. The feed side of an alumina membrane was first coated with a primer $(PSS/PAH)_2$ film (both polyelectrolyte deposition solutions contained 0.02 M polymer repeat units in 1 M NaCl) through layer by layer assembly. The same side of the membrane was then immersed in the colloidal Au nanoparticle solution for 10 min to adsorb seed Au nanoparticles. After rinsing with H_2O for 1min, the membrane was immersed in a 50 mL solution containing 0.4 mM $NH_2OH{\cdot}HCl$ and 0.01 wt% $HAuCl_4$ (enlargement solution). The solution was mixed on an orbital shaker for 20 min, and then the membrane was immersed in 50 mL of fresh enlargement solution for another 20 min. The same process was repeated 10 times using a total of 500 mL of enlargement solution.

Some alumina membranes were coated with Au using a PELCO SC-7 sputter coater with a Au target. The deposition thickness was 50 nm as determined with a FTM2 PELCO film thickness monitor. The thermal evaporation of Au was conducted with an Edwards Auto 306 thermal evaporator equipped with a quartz crystal microbalance (Maxtek P/N 103200-2).

.

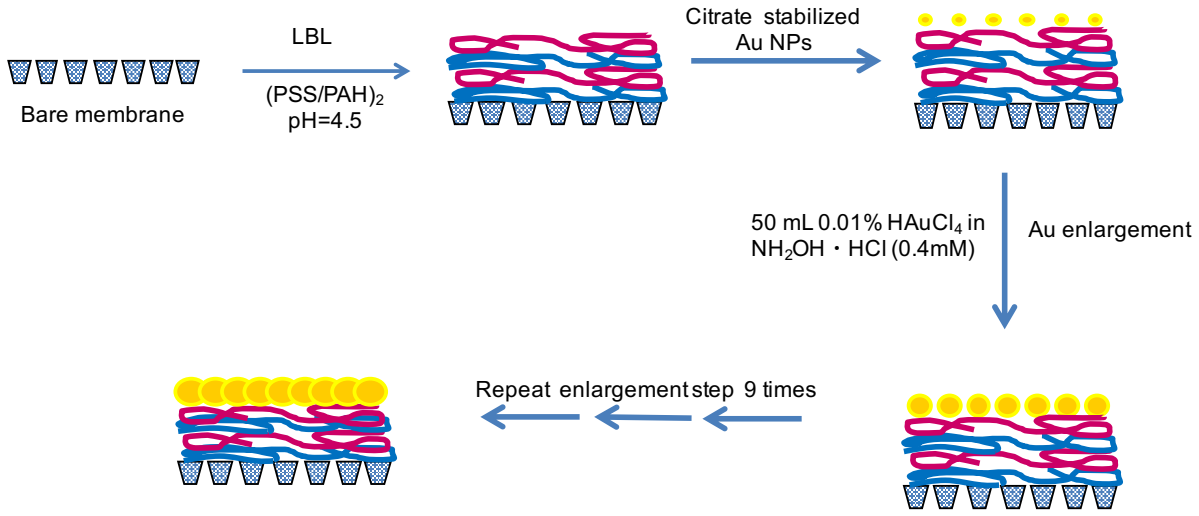

Figure 4.1 Scheme of electroless deposition of gold on a porous alumina membrane.

4.2.4 Electrochemical polymerization

Au-coated membranes were assembled in a home-made two-compartment cell sealed with an o-ring. The coating side faced a source phase containing 0.01 M EDOT and 0.01 M PSS. This solution was sonicated for 15 min to completely dissolve EDOT prior to introduction into the source-phase cell. The receiving cell was empty. A Pt wire and a Ag/AgCl electrode in the source phase served as the counter and reference electrodes, respectively, whereas the membrane acted as the working electrode. The electrochemical polymerization of EDOT was performed using chronoamperometry with a constant potential of 1 V (CHI 604 potentiostat). Different PEDOT films were obtained using a 5 min or 30 min coating time.

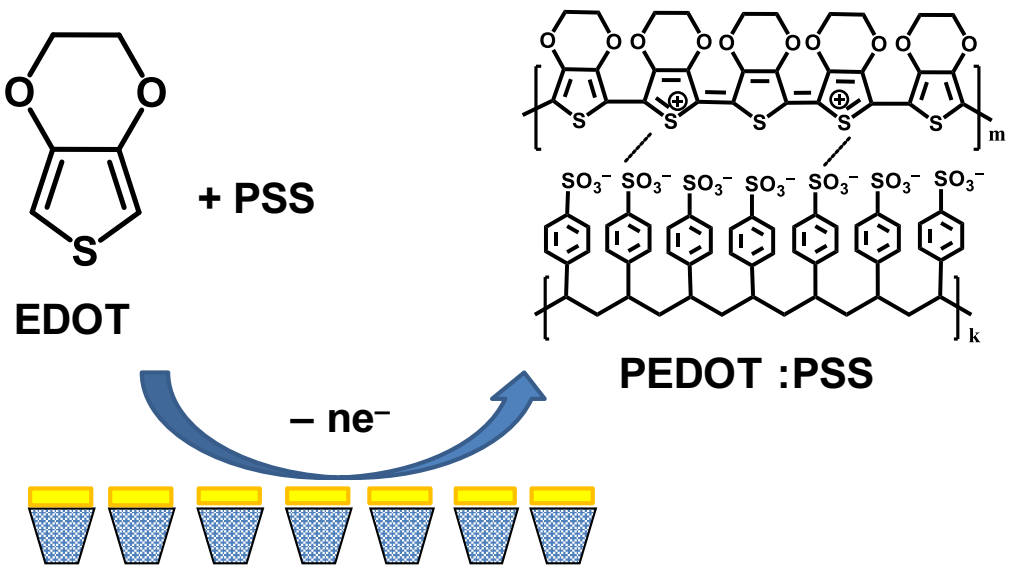

Figure 4.2 Scheme of electrochemical polymerization of EDOT with PSS on Au-coated membranes.

4.2.5 Membrane characterization

The sheet resistances of membrane surfaces were determined using a 4-probe measurement. The probe has spring-loaded tips connected to a Hewlett Packard 3441 multimeter that applies a constant current between two outer probes with the voltage drop was measured between two inner probes (four probes are aligned with equal spacing of 0.1 cm). The sheet resistant was calculated from the equation (5)[15]:

$$R_{sh} = 4.532 \times \frac{V}{I} \qquad (5)$$

where R_{sh} is the sheet resistance (Ω/□), V is the potential drop and I is the applied current in the 4-probe measurement. The imagines of coated membranes were taken with a JEOL 7500F scanning electron microscope (SEM) equipped with a cold field-emission emitter. The thicknesses of polyelectrolyte multilayer films adsorbed on Au-coated Si were determined with a

model M-44, J.A. Woollam ellipsometer using WVASE32 software. The film refractive index was assumed to be 1.5, and the thicknesses was fitting parameters.

4.2.6 Diffusion dialysis with an electrical potential applied between the membrane surface and electrodes in solution

A conductive membrane was connected to a copper wire using silver epoxy at the center of the membrane and was sandwiched between source and receiving cells (see Figure 4.3). The top of copper and silver epoxy was also coated with 5-min epoxy as an insulating layer to avoid corrosion. The conductive side faced the source-phase cell and served as a working electrode. A platinum counter electrode and Ag/AgCl reference electrode were placed in the source phase that contained 90 mL of 0.01 M KCl and 0.01 M $MgCl_2$. The receiving phase contained the same volume of deionized water. During a 1.5-h experiment, a constant potential (CH Instruments model 604 potentiostat) was applied between the membrane and the reference electrode in the source-phase solution. One-mL aliquots were collected periodically from the receiving phase to determine the ion concentration as a function of time, and same amount of solution was withdrawn from the source phase to keep equal volumes. The cation concentration was determined using a Varian 710-ES Inductively Coupled Plasma Optical Emission Spectrophotometer (ICP-OES) with calibration curves.

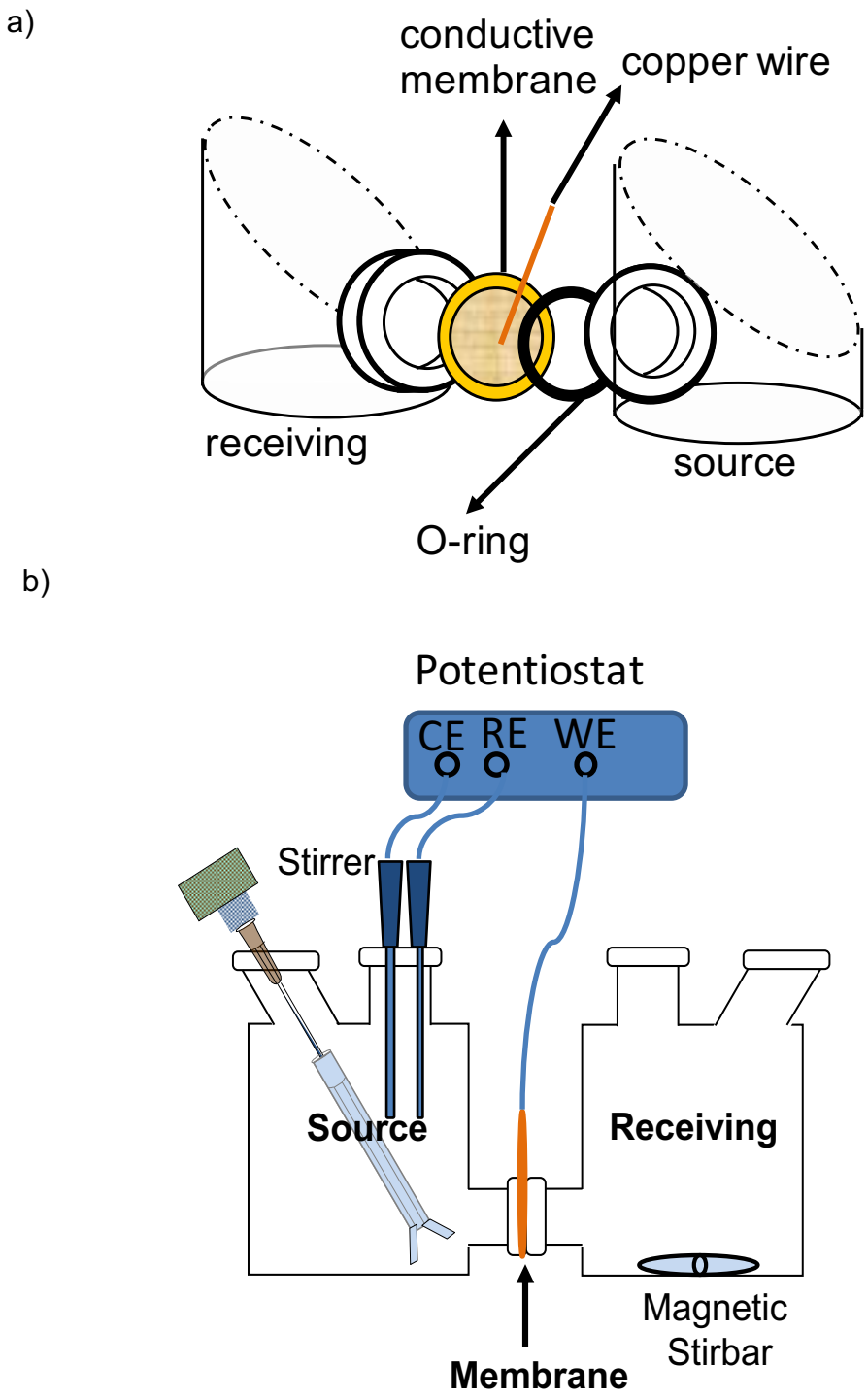

Figure 4.3 Diagram of the membrane cell for diffusion dialysis with an applied potential between the membrane and a reference electrode in the source phase. a) The conductive membrane surface faces the source phase, and electrical connection occurs through a thin copper

Figure 4.3 (cont'd)

wire attached to the conductive surface by silver epoxy. b) The copper wire working electrode (WE), reference electrode (RE) and counter electrode (CE) are connected to a potentiostat to apply a constant potential between the membrane surface and a reference electrode. Both source and receiving phases were stirred vigorously to minimize concentration polarization.

4.2.7 Diffusion dialysis with an applied potential between two carbon meshes that sandwich a membrane

Alumina membranes were coated with $(PSS/PAH)_4$ films, and then sandwiched between two round carbon mesh sheets with diameters just smaller than the membrane to avoid forming a short circuit. The carbon mesh size was 5.3 cm^2. The resistance between the contacts to the two meshes was150 Ω. Each carbon mesh sheet was also contacted with a thin copper wire. The experimental apparatus was the same as in Figure 3 without the Pt and Ag/AgCl electrodes. The $(PAH/PSS)_4$ film faced the source phase, and the carbon mesh on the source-phase side of the membrane served as both the counter and reference electrodes, whereas the carbon mesh facing the receiving phase acted as the working electrode. The source phase contained 0.01M KCl and 0.01M $MgCl_2$, and the receiving phase was initially deionized water. The sampling method and ion analysis were described in section 4.2.6.

4.3 Results and discussion

We deposited conductive films on commercial porous membranes through layer-by-layer assembly, sputtering, electroless deposition or electrochemical polymerization. This section first presents each deposition method along with characterization of coated membranes and the

limitations of each method, and then investigates the effect of applied potential on the ion flux and ion-transport selectivity of different conductive membranes. Finally, I examine the effect of applied transmembrane potential on salt permeability.

4.3.1 Layer-by-layer assembly of conductive polymers

Conjugated polymers such as poly(3,4-ethylenedioxythiophene) (PEDOT) have high conductivities and stabilities that are attractive for formation of conductive films[16] Commercial PEDOT suspensions are homogeneous dispersions of PEDOT: PSS complexes in which PEDOT oligomers attach to the long PSS chains due to electrostatic interactions.[17] The PEDOT:PSS complex acts as a polyanion during layer-by-layer assembly due to the net excess of sulfonic acid.[17]

To initially characterize $(PAH/PEDOT:PSS)_n$ films, we deposited them both on Au-coated silicon wafers to determine their ellipsometric thicknesses and on glass to determine their electrical sheet resistances, R_{sh}. Figure 4.4 shows the values of R_{sh} and ellipsometric thickness as a function of the number of adsorbed PAH/PEDOT:PSS bilayers. After adsorption of the initial bilayer, the film thickness increases approximately linearly with the number of adsorbed bilayers with an average thickness of 100 Å per bilayer. This is similar to the thickness of PSS/PAH films deposited under similar conditions.[18]

The electrical sheet resistance decreases from 6×10^7 Ω/□ for one bilayer to 9×10^5 Ω/□ for 9 bilayers, and a 10-fold decrease in R_{sh} occurs on going from one bilayer to 2 bilayers. After drying the 9-bilayer film in a 70ºC oven for 15 min to remove much of the moisture in the film, the R_{sh} value increases from 9×10^5 to 4×10^6Ω/□. The relatively low conductivity values

suggest that the PSS/PAH complex may dominate the PEDOT:PSS/PAH film, so the limited amount of PEDOT decreases sheet resistance but does not yield a highly conductive film.

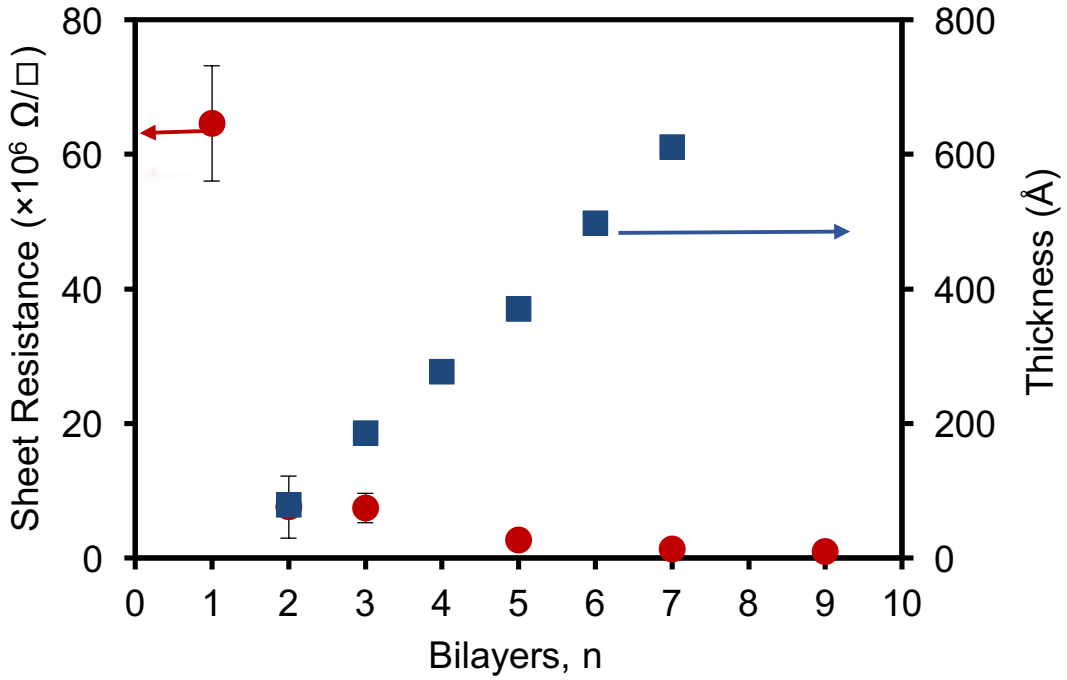

Figure 4.4 The sheet resistances and thicknesses of $(PAH/PEDOT:PSS)_n$ films with different numbers of adsorbed bilayers, n. (Some of the error bars, which represent the standard deviations of determinations on three films , are smaller than the symbols).

In efforts to increase the film conductivity, I (a) varied the polycation in the film and the pH of deposition solutions, (b) attempted to dope PEDOT:PSS with organic solvent and (c) employed a high-conductivity grade of PEDOT:PSS solution. Table 1 summarizes the R_{sh} values for different films. Substituting branched PEI (B-PEI) for PAH in the layer-by-layer assembly did not result in films with low resistance, and deposition of the $(B\text{-}PEI/PEDOT:PSS)_n$ films at low pH gave R_{sh} values that were too high to measure with the apparatus (> 10^8 Ω/□). At pH=3.2 B-PEI carries more positive charge than the partially deprotonated B-PEI at pH=10. The

lower charge density often leads to more adsorption of polyelectrolytes in layer-by-layer deposition,[19] and additional adsorption of the PEDOT:PSS complex likely leads to lower resistances for films deposited at pH=10. Addition of 1 M NaCl to adsorption solutions increased the resistance of $(\text{B-PEI/PEDOT:PSS})_n$ films deposited at pH 10. The extra salt may screen surface charge and lead to less polyelectrolyte deposition.[20-22]

Table 4.1 The sheet resistance, R_{sh} of several PEDOT:PSS-containing films deposited on either glass or porous alumina.

Substrate	Film	$R_{sh}(\times 10^6 \Omega/\square)$
Glass	spin coating on Piranha cleaned glass	0.51±0.01
	$[\text{PAH/PEDOT:PSS}]_{10}$	1.38±0.05
	$[\text{B-PEI(pH=10)/PEDOT:PSS}]_{10}$	0.78±0.03
	$[\text{B-PEI(pH=3.2)/PEDOT:PSS}]_{10}$	Not detectable
	$[\text{B-PEI(pH=10 in 1M NaCl)/PEDOT:PSS}]_{10}$	6.11±0.76
	$[\text{B-PEI(pH=3.2 in 1M NaCl)/PEDOT:PSS}]_{10}$	Not detectable
	[B-PEI(pH=10)/PEDOT:PSS (1% DMSO)]	0.97±0.05
Alumina	$[\text{PEDOT:PSS (1\% DMSO)/ PEI PH=10}]_{10.5}$ on alumina	47.5±3.5
	$[\text{High-Conductivity Grade PEDOT:PSS (1\% DMSO)/ B-PEI(PH=10)}]_{20.5}$ on alumina	35±10

* The pH value of PEDOT:PSS solutions was ~2.7 in all cases.

The conductivity of PEDOT films often increases with DMSO doping because DMSO helps to align the PEDOT.[16, 23-24] Thus, we prepared layer-by-layer films using PEDOT:PSS solutions containing DMSO (1% wt). However, the $[\text{B-PEI/PEDOT:PSS (1\% DMSO)}]_{10}$ film shows an R_{sh} value of of 0.97×10^6 $\Omega/\square$, which is similar to the sheet resistance of undoped films. Thus, regardless of deposition conditions we could not obtain layer-by-layer films with sheet resistances significantly less that $1\times10^6\Omega/\square$.

I also deposited films on porous alumina substrates (20 nm surface pores) because the ultimate purpose of these studies is to fabricate a conductive membrane skin. The R_{sh} values for films on alumina are ~50 times higher than for films grown on glass (Table 4.1). Even with a high-conductivity grade PEDOT:PSS solution, layer-by-layer deposition on alumina still yields a sheet resistance of $35\times10^{6}\Omega/\square$. These high sheet resistances will give a significant potential drop from the center of the membrane to its edge. Thus, I decided that layer-by-layer assembly is not sufficient to fabricate a highly conductive membrane surface.

4.3.2 Deposition of Au to form conductive membrane surfaces

Because layer-by-layer films have high sheet resistances that will lead to a significant potential drop from the center to the edge of the membrane, I began examining metal deposition methods to create conducting membrane skins. These methods including sputter coating, electroless deposition and thermal evaporation to deposit gold on porous membranes. Figure 4.5 shows SEM imagines of bare and coated alumina membranes. The electroless deposition gives a coated but porous surface. The sputtered surface is also porous but contains large gold clusters, and the gold surface from thermal evaporation is very uniform but less porous. All membranes are highly conductive (sheet resistances <100 $\Omega/\square$).

I examined the adhesion of the coatings using a peel test where a piece of Scotch^{TM} tape is attached to a coated membrane surface and then removed. Qualitatively, surfaces that show the most gold on the peeled tape have the lowest adhesion. The sputter coated surface showed the most adhesion, with minimum gold removal from the surface. In contrast, thermal evaporation gave the worst adhesion even with a Titanium primer layer.

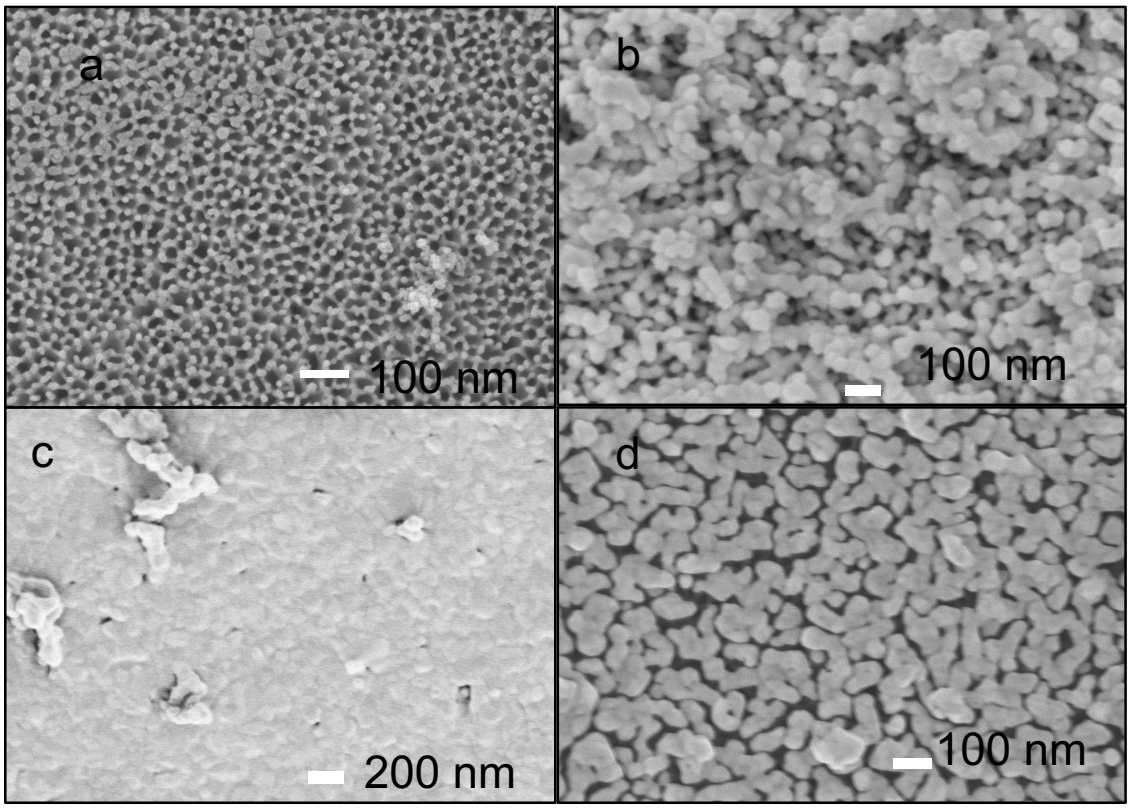

Figure 4.5 SEM imagines of porous alumina (a) before and (b,c,d) after coating with Au using (b) sputtering (50 nm film) (c) thermal evaporation (100 Nm) and (d) electroless deposition (10 deposition cycles after seeding the surface with Au nanoparticles).

4.3.3 Electrochemical polymerization of EDOT to fabricate conductive membrane coatings

Although the Au-coated membranes are highly conductive, the pore size in sputtered and electrolessly deposited coatings is still large compared to the typical double layer thicknesses in solution (around 1-10 nm for salt concentrations from 0.001 to 0.1 M).[25] A positive electric field can significantly decrease the partitioning of cations only if the pore size is smaller than or comparable to the double layer thickness. Otherwise the applied electric field will be negligible in much of the pore and have minimal effect. To decrease the pore size, I employed some Au coated membranes as working electrodes for electrochemical polymerization of EDOT. The

polymerization occurred at a constant potential of 1 V vs Ag/AgCl in a solution containing 0.01M EDOT and 0.01M PSS. Figure 4.6 shows SEM imagines of electrochemically polymerized PEDOT on porous alumina initially coated with electroless Au deposition. Five minutes of electropolymerization leads to a thin layer of polymer on the Au substrate, whereas a thick polymer layer (with some pores) covers the substrate after 30 min of coating.

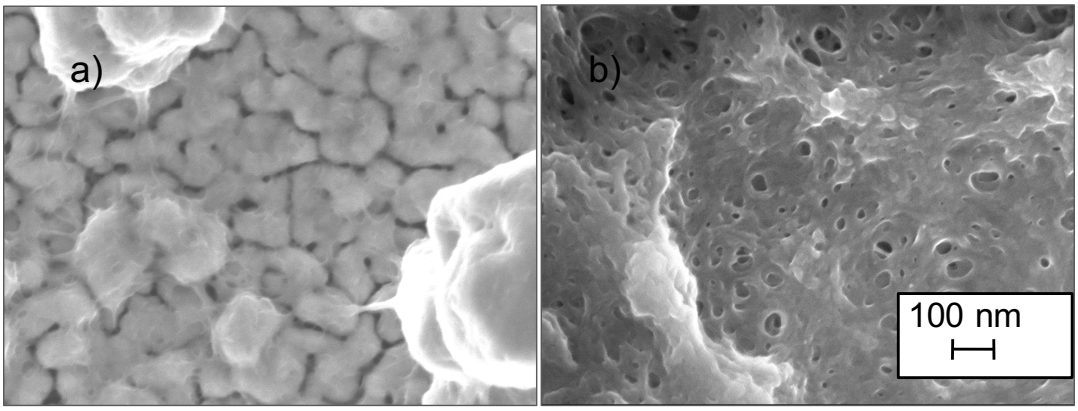

Figure 4.6 SEM imagines of PEDOT films formed during electrochemical polymerization from alumina membranes initially coated with Au through electroless deposition. EDOT electropolymerization occurred for (a) 5 min and (b) 30 min. The scale bar is common to both images.

4.3.4 Ion permeability and selectivity of conductive membranes

Table 4.2 summarizes the ion fluxes and K^+/Mg^{2+} selectivities during diffusion dialysis through conductive membranes. Bare (nonconductive) alumina membranes show high KCl and $MgCl_2$ fluxes but a K^+/Mg^{2+} selectivity of only 1.5. These values indicate unhindered diffusion through membrane pores. The $(PEDOT:PSS/PAH)_{7.5}$-modified alumina membranes show a K^+/Mg^{2+} selectivity of 90, presumably because the film contains PSS/PAH bilayers that highly

reject Mg^{2+}.[26] The sputter-coated membranes allow smaller K^+ and Mg^{2+} fluxes than bare alumina, but the K^+/Mg^{2+} selectivity of 2.6 is similar to that for bare alumina. Polymerization of EDOT:PSS for 5 min from Au-coated membranes gives a selectivity <3. Because polymerization of EDOT:PSS for 30 min from electrolessly deposited Au membranes leads to very low salt permeabilities, I conducted diffusion dialysis using a source-phase solution containing 0.1MKCl and 0.1M $MgCl_2$. Despite the low permeability, the K^+/Mg^{2+} selectivity is only 4.6. In summary, the highly conductive coating PEDOT:PSS coating decreases ion fluxes greatly but increases K^+/Mg^+ selectivity only 3-fold compared to bare alumina.

Table 4.2 K^+ and Mg^{2+} fluxes and K^+/Mg^{2+} selectivities during diffusion dialysis through bare and coated alumina membranes. Dialysis occurred from source-phase solutions initially containing 0.01MKCl and 0.01M $MgCl_2$ to a deionized water receiving phase.

Membrane Coating	KCl Flux (nmole $cm^{-2}s^{-1}$)	$MgCl_2$ Flux (nmole $cm^{-2}s^{-1}$)	Selectivity (K^+/Mg^{2+})
Bare	6.4±0.6	4.4±0.04	1.5±0.2
$(PEDOT:PSS/PAH)_{7.5}$*	3.8	0.043	90
Sputter coated Au	4.6 ±0.6	2.1±0.3	2.6± 0.8
5min of EDOT:PSS polymerization from electrolessly deposited Au	4.4±1.2	1.5±1.0	3.5±1.8
30 min of EDOT:PSS polymerization from electrolessly deposited Au **	3.1±0.7	0.7±0.3	4.6±1.2

*Data is the average of two membranes
**In this case only, the source-phase solution initially contained 0.1M KCl and 0.1M $MgCl_2$.

I investigated the effect of applied potential on ion permeability using an alumina membrane coated with a $(PEDOT:PSS/PAH)_{7.5}$ film. Although these films are modestly conductive, they fully cover the underlying alumina substrate. I initially performed diffusion

dialysis with and without a -0.5 V potential applied between the membrane and a Ag/AgCl reference electrode in the source phase. At this applied potential, the current density between the membrane and a Pt counter electrode in the source phase was ~5.6 μA/cm^2 of membrane. Figure 4.7 plots the amounts of K^+ and Mg^{2+} in the receiving phase as a function of time. (Each experimental condition used a fresh source phase and receiving phase.) Unfortunately, the applied potential does not affect the K^+ and Mg^{2+} fluxes. An experiment with a +0.8 V potential between the membrane and the reference electrode gives a similar result. Thus, the fluxes do not change with potential. This might stem from the high sheet resistance (~$50\times10^6\Omega/\square$) of the $(PEDOT:PSS/PAH)_{7.5}$ film, so much of the potential drop may occur across, rather than perpendicular to, the membrane surface.

With the highly conductive Au-coated membranes (formed with either sputtering or electroless deposition), again the K^+ and Mg^{2+} fluxes are independent of the applied potential. As mentioned above, the pore sizes in the Au coatings are larger than the electrical double layer, which likely leads to the insensitivity of ion transport to potential.

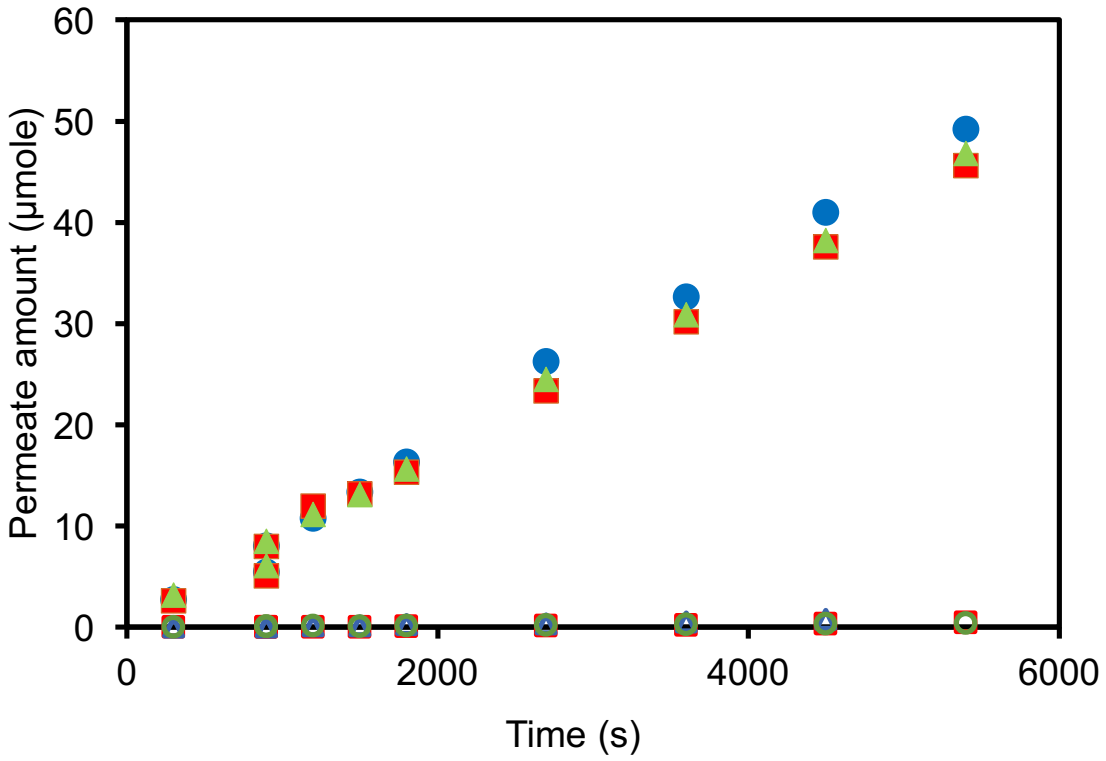

Figure 4.7 Amounts of K^+ (filled data points) or Mg^{2+} (open data points, along the x-axis) in the receiving phase as a function of time during diffusion dialysis with no applied penitential (blue circles), -0.5V (red squares) and and after removal of the applied potential (green triangles). Diffusion dialysis occurred through a $(PEDOT:PSS/PAH)_{7.5}$-modified alumina membrane from a 0.01M KCl, 0.01M $MgCl_2$ source phase to a deionized water receiving phase.

The electrochemically polymerized PEDOT-coated membranes with high conductivity and small pore size are perhaps the most promising to observe the effect of applied electrical potential on ion permeation. With 5 min of EDOT polymerization from electrolessly deposited Au, however, the fluxes are the same at positive applied potentials of 0.1, 0.5 and 0.8 V versus the Ag/AgCl reference electrode. In this case, the K^+ and Mg^{2+} fluxes are 4.2 nmol cm^{-2} s^{-1} and 1.8 nmole cm^{-2} s^{-1}, respectively. Membranes coated with a 30-min EDOT polymerization also

show no sensitivity to applied positive potentials despite a relatively low permeability. In the contrast, with a -0.8 V applied potential, the KCl flux significantly decreased from 3.7 nmole cm^{-2} s^{-1} to 0.7 nmole cm^{-2} s^{-1} and $MgCl_2$ flux declined from 1.0 nmole cm^{-2} s^{-1} to 0.0029 nmole cm^{-2} s^{-1} (Because of the low permeability of the membrane, these experiments employed a source phase containing 0.1MKCl, 0.1M $MgCl_2$.) However, after removal of the potential, the fluxes did not change, which suggests that the potential permanently changes the coating either through reduction or some fouling mechanism such as $Mg(OH)_2$ fouling.

To rule out $Mg(OH)_2$ fouling, I performed dialysis with only 0.1M KCl in the source phase. The KCl flux decreased from 9.2 nmole cm^{-2} s^{-1} (no potential) to 3.4 nmole cm^{-2} s^{-1} (-0.8V), and then increased to 7.2 nmole cm^{-2} s^{-1} after removal of the applied potential. This result suggests that the flux change is due to the applied potential. However, further experiments are needed to confirm this result. The decrease of flux presumably occurs due to the reduced state of PEDOT and doping with cations.[27-28]

4.3.5 Membrane capacitor for ion rejection

Because potentials applied with a conductive membrane surface had negligible effect on salt permeability, we explored whether a potential applied across a membrane between conductive carbon mesh sheets (Figure 4.8) would alter ion transport. The direction of the applied electric field should slow cation diffusion, so we hypothesized that it might decrease K^+ and, especially, Mg^{2+} flux.[29]

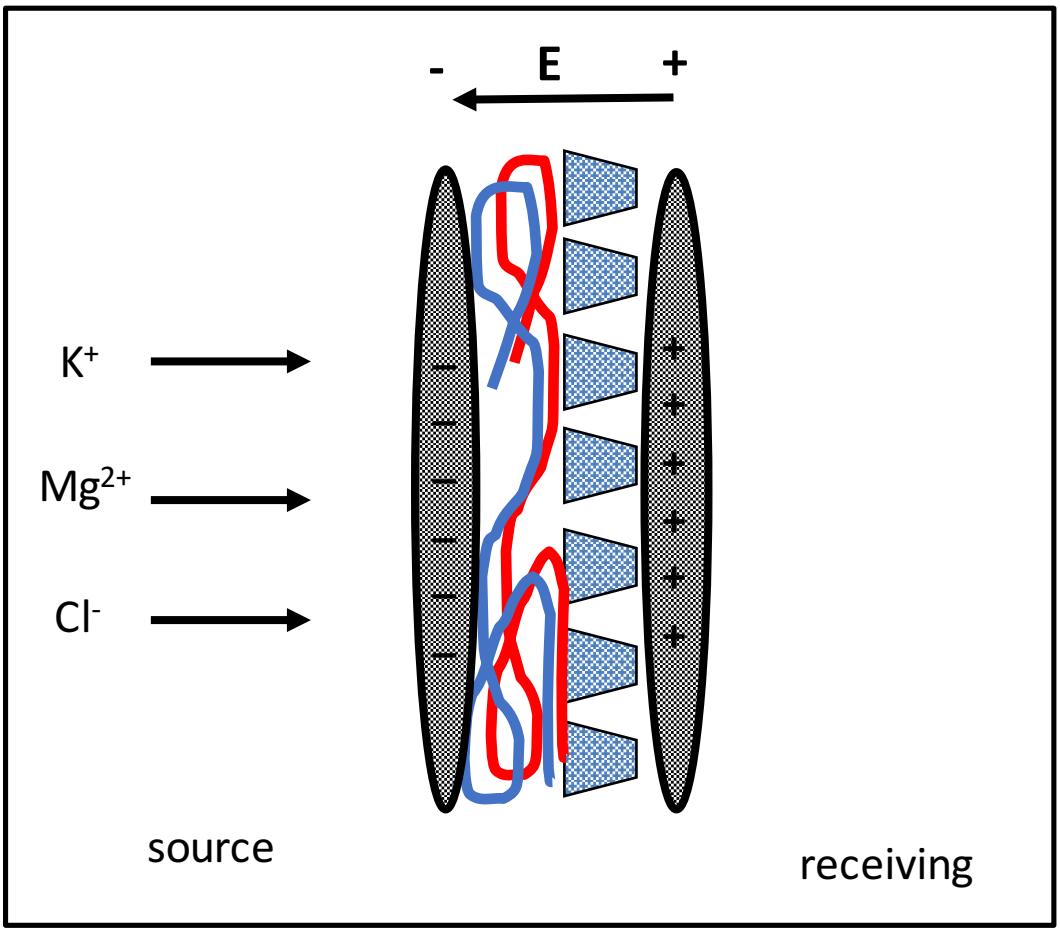

Figure 4.8 Schematic diagram of diffusion dialysis through a $(PSS/PAH)_4$-coated alumina membrane sandwiched between two carbon mesh electrodes.

Figure 4.9 plots the receiving-phase concentration during diffusion dialysis through a $(PSS/PAH)_4$-coated alumina membrane sandwiched between two carbon mesh electrodes (Figure 4.8 illustrates the sandwich structure). The plot initially shows a linear region, which indicates a K^+ flux of 1.2 nmole cm^{-2} s^{-1}. The Mg^{2+} flux is below the detection limit of the analysis (<2 pmole cm^{-2} s^{-1}). Upon application of a 2 V potential, the K^+ flux decreases to ~0.8 nmole cm^{-2} s^{-1}, and flux declines further to 0.1 nmole cm^{-2} s^{-1} with a 4V potential between the carbon meshes. The pH of the source-phase solution decrease from 6.46 at the beginning of the experiment to

5.99 at the end. In contrast, the pH of the receiving phase decreases from 7.11 initially to 7.03 after dialysis with a 2 V transmembrane potential, and finally to 3.51 after dialysis with a 4 V potential. The decrease in the KCl flux likely stems from electromigration of K^+ in a direction opposite to its diffusion. However, current generation at the electrode requires formation of protons at the anode and hydroxide or some other reduced species at the anode. The proton generation is apparent from the decrease in pH in the receiving phase. However, the reaction that may occur at the cathode is not obvious. Perhaps $Mg(OH)_2$ precipitation limits the rise in pH in the source phase.

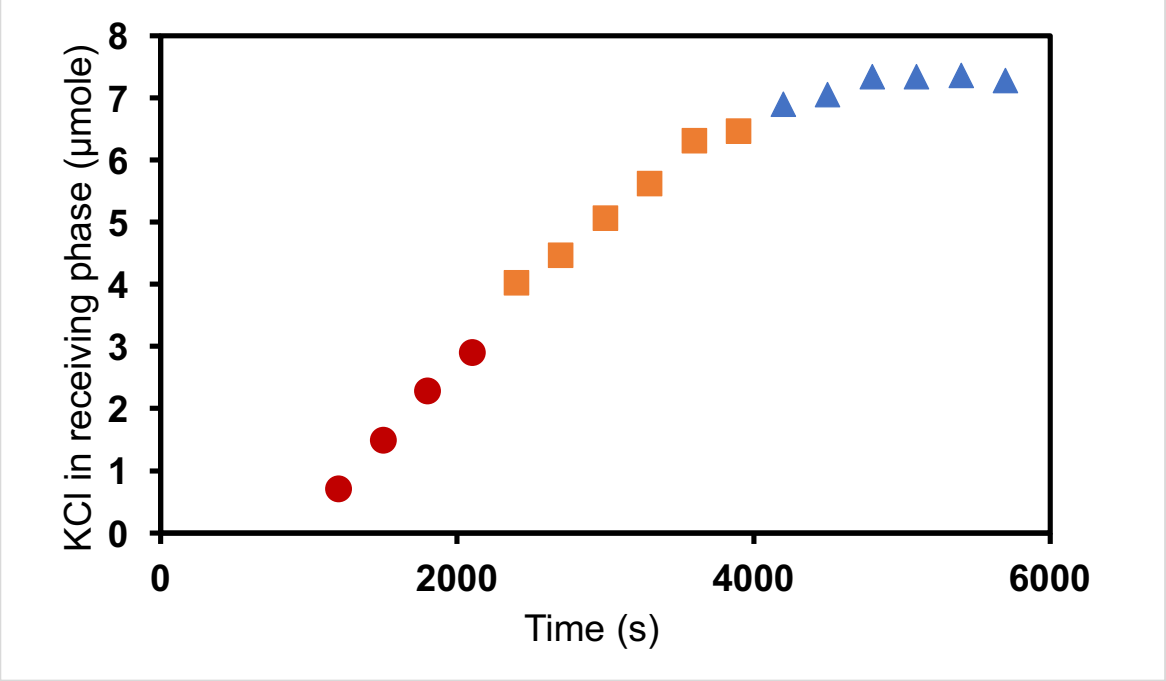

Figure 4.9 Amount of KCl in the receiving phase as the function of time with no potential (red circle), +2V (orange square) and +4V (blue triangle) during a continuous experiment that monitored K+ transport through the carbon mesh-sandwiched $(PAH/PSS)_4$ coated alumina membrane. The source phase contains 0.01M KCl, 0.01M $MgCl_2$ and the receiving phase was initially deionized water.

4.4 Conclusions

This chapter explored several methods for forming electrically conductive coatings on porous membranes. Layer-by-layer assembly with conducting polymers did not yield films with high conductivities, and such coated membranes will show high potential drops from the edge to the center of the membrane (see the appendix). The Au and electrochemically polymerized conducting polymer coatings show high conductivity. However, the salt fluxes through such membranes are independent of applied potentials from -1V to 1V with respect to Ag/AgCl for Au-coated membranes. Preliminary studies show that salt fluxes through conducting polymer-coated membranes do decrease at negative potentials, perhaps because of film doping. Additionally, high transmembrane potentials applied using external electrodes can negate cation transport, but likely at the expense of formation of protons and hydroxide ions.

APPENDIX

APPENDIX

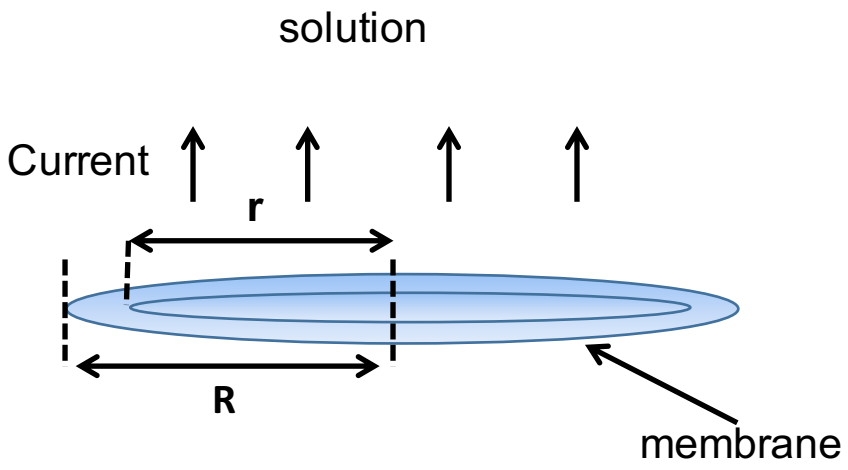

Figure 4.10 Schematic drawing of a conductive membrane with current density perpendicular to the surface. The drawing also shows the membrane radius, *R*, and the radial coordinate, *r*. Current also flows into the membrane and along the surface.

Here, we derive expression for the potential drop from the outer edge of a conductive membrane to the center with the assumption that the current density (in the direction perpendicular to the surface) is uniform across the entire surface. We also assume that all of the current enters via a contact around the membrane. At distances farther from the edge of the membrane, less current flows parallel to the surface due to the shunting of current to the solution.

Eq (a1) defines the total current, i_{total}, where j is the uniform current density and Q is the membrane diameter.

$$i_{total} = j\pi Q^2 \qquad \text{(a1)}$$

Eq (a2) gives the current i flowing radially through a circle whose center is the center of the membrane and whose radius is r.

$$i = j\pi r^2 \quad \text{(a2)}$$

Eq (a3) describes the resistance, *R*, to current flowing through a wire with cross-sectional

$$R = \rho \frac{l}{A} \quad \text{(a3)}$$

area A and length l, where ρ is the wire resistivity. For current flowing into a disk, eq (a4) gives the differential of resistance, dR,

$$dR = \frac{\rho dr}{2\pi rt} \quad \text{(a4)}$$

where t is the disk thickness, so $2\pi rt$ is the cross-sectional area. Thus, equation (a5) gives the Ohm's law differential potential drop, dE.

$$dE = idR = j\pi r^2 \frac{\rho dr}{2\pi rt} = \frac{j\rho}{2t} rdr \quad \text{(a5)}$$

Eq (a6) then gives an expression for the potential drop, ΔE, from the edge to the center of the disk

$$\Delta E = \frac{j\rho}{2t} \int_Q^0 rdr = -\frac{j\rho Q^2}{4t} \quad \text{(a6)}$$

Eq (a7) defines sheet resistance, R_{sh},

$$R_{sh} = \frac{\rho}{t} \quad \text{(a8)}$$

so eq (a6) becomes eq(a9)

$$\Delta E = -\frac{jQ^2 R_{sh}}{4} = -\frac{iR_{sh}}{4\pi} \quad \text{(a9)}$$

if $i = 1\ \mu A, R_{sh} = 10^7\ \Omega/\square, R_{r=R} = 0.8\ V$.

We contact the membrane via a wire that extends the potential from the center of the membrane to the edge. The potential drops across the membrane is 0.8V according to equation a9. The significant potential drop will lead to nonuniform currents.

REFERENCES

REFERENCES

1. Elimelech, M.; Phillip, W. A., The future of seawater desalination: Energy, technology, and the environment. *Science* **2011,** *333*, 712-717.

2. Semiat, R., Energy issues in desalination processes. *Environmental Science & Technology* **2008,** *42*, 8193-8201.

3. Fritzmann, C.; Lowenberg, J.; Wintgens, T.; Melin, T., State-of-the-art of reverse osmosis desalination. *Desalination* **2007,** *216*, 1-76.

4. Yang, Z.; Tarabara, V. V.; Bruening, M. L., Adsorption of anionic or cationic surfactants in polyanionic brushes and its effect on brush swelling and fouling resistance during emulsion filtration. *Langmuir* **2015,** *31*, 11790-9.

5. An, A. K.; Guo, J.; Jeong, S.; Lee, E.-J.; Tabatabai, S. A. A.; Leiknes, T., High flux and antifouling properties of negatively charged membrane for dyeing wastewater treatment by membrane distillation. *Water Research* **2016,** *103*, 362-371.

6. Krasemann, L.; Tieke, B., Selective ion transport across self-assembled alternating multilayers of cationic and anionic polyelectrolytes. *Langmuir* **2000,** *16*, 287-290.

7. Hoffmann, K.; Friedrich, T.; Tieke, B., Layer-by-layer assembled polyelectrolyte blend membranes and their use for ion separation and rejection. *Polymer Engineering and Science* **2011,** *51*, 1497-1506.

8. Yaroshchuk, A.; Zhu, Y.; Bondarenko, M.; Bruening, M. L., Deviations from electroneutrality in membrane barrier layers: A possible mechanism underlying high salt rejections. *Langmuir* **2016,** *32*, 2644-2658.

9. Wijeratne, S.; Bruening, M. L.; Baker, G. L., Layer-by-layer assembly of thick, cu2+-chelating films. *Langmuir* **2013,** *29*, 12720-12729.

10. Supriya, L.; Claus, R. O., Solution-based assembly of conductive gold film on flexible polymer substrates. *Langmuir* **2004,** *20*, 8870-8876.

11. Brown, K. R.; Lyon, L. A.; Fox, A. P.; Reiss, B. D.; Natan, M. J., Hydroxylamine seeding of colloidal au nanoparticles. 3. Controlled formation of conductive au films. *Chemistry of Materials* **2000,** *12*, 314-323.

12. Frens, G., Controlled nucleation for regulation of particle-size in monodisperse gold suspensions. *Nature-Physical Science* **1973,** *241*, 20-22.

13. Dotzauer, D. M.; Dai, J. H.; Sun, L.; Bruening, M. L., Catalytic membranes prepared using layer-by-layer adsorption of polyelectrolyte/metal nanoparticle films in porous supports. *Nano Letters* **2006,** *6*, 2268-2272.

14. Grabar, K. C.; Freeman, R. G.; Hommer, M. B.; Natan, M. J., Preparation and characterization of au colloid monolayers. *Analytical Chemistry* **1995,** *67*, 735-743.

15. Smits, F. M., Measurement of sheet resistivities with the 4-point probe. *Bell System Technical Journal* **1958,** *37*, 711-718.

16. Dawidczyk, T. J.; Walton, M. D.; Jang, W. S.; Grunlan, J. C., Layer-by-layer assembly of uv-resistant poly(3,4-ethylenedioxythiophene) thin films. *Langmuir* **2008,** *24*, 8314-8318.

17. Smith, R. R.; Smith, A. P.; Stricker, J. T.; Taylor, B. E.; Durstock, M. F., Layer-by-layer assembly of poly(3,4-ethylenedioxythiophene): Poly(3,4-ethylenedioxythiophene): Poly(styrenesulfonate). *Macromolecules* **2006,** *39*, 6071-6074.

18. El Haitami, A. E.; Martel, D.; Ball, V.; Nguyen, H. C.; Gonthier, E.; Labbé, P.; Voegel, J.-C.; Schaaf, P.; Senger, B.; Boulmedais, F., Effect of the supporting electrolyte anion on the thickness of pss/pah multilayer films and on their permeability to an electroactive probe. *Langmuir* **2009,** *25*, 2282-2289.

19. Shiratori, S. S.; Rubner, M. F., Ph-dependent thickness behavior of sequentially adsorbed layers of weak polyelectrolytes. *Macromolecules* **2000,** *33*, 4213-4219.

20. Blomberg, E.; Poptoshev, E.; Caruso, F., Surface interactions during polyelectrolyte multilayer build-up. 2. The effect of ionic strength on the structure of preformed multilayers. *Langmuir* **2006,** *22*, 4153-4157.

21. Dubas, S. T.; Schlenoff, J. B., Factors controlling the growth of polyelectrolyte multilayers. *Macromolecules* **1999,** *32*, 8153-8160.

22. Guzman, E.; Ritacco, H.; Rubio, J. E. F.; Rubio, R. G.; Ortega, F., Salt-induced changes in the growth of polyelectrolyte layers of poly(diallyl-dimethylammonium chloride) and poly(4-styrene sulfonate of sodium). *Soft Matter* **2009,** *5*, 2130-2142.

23. Crispin, X.; Marciniak, S.; Osikowicz, W.; Zotti, G.; Van der Gon, A. W. D.; Louwet, F.; Fahlman, M.; Groenendaal, L.; De Schryver, F.; Salaneck, W. R., Conductivity, morphology, interfacial chemistry, and stability of poly(3,4-ethylene dioxythiophene)-poly(styrene sulfonate): A photoelectron spectroscopy study. *Journal of Polymer Science Part B-Polymer Physics* **2003,** *41*, 2561-2583.

24. Heeger, A. J.; Kivelson, S.; Schrieffer, J. R.; Su, W. P., Solitons in conducting polymers. *Reviews of Modern Physics* **1988,** *60*, 781-850.

25. Bard, A. J.; Faulkner, L. R., Electrochemical methods: Fundamentals and applications; John Wiley & Sons: New York. **2000**.

26. Cheng, C.; Yaroshchuk, A.; Bruening, M. L., Fundamentals of selective ion transport through multilayer polyelectrolyte membranes. *Langmuir* **2013,** *29*, 1885-1892.

27. Pile, D. L.; Zhang, Y.; Hillier, A. C., Electrochemically modulated permeability of poly(aniline) and composite poly(aniline)-poly(styrenesulfonate) membranes. *Langmuir* **2006,** *22*, 5925-5931.

28. Pile, D. L.; Hillier, A. C., Electrochemically modulated transport through a conducting polymer membrane. *Journal of Membrane Science* **2002,** *208*, 119-131.

29. Schmuhl, R.; Keizer, K.; van den Berg, A.; ten Elshof, J. E.; Blank, D. H. A., Controlling the transport of cations through permselective mesoporous alumina layers by manipulation of electric field and ionic strength. *Journal of Colloid and Interface Science* **2004,** *273*, 331-338.

Chapter 5 Deviations from Electroneutrality in Membrane Barrier Layers: A Possible Mechanism Underlying High Salt Rejections

Portions of this chapter are reproduced from Andriy Yaroshchuk, Yan Zhu, Mykola Bondarenko, and Merlin Bruening *Langmuir* **2016**, 32, 2644-2658.

5.1 Introduction

Reverse osmosis (RO) and nanofiltration (NF) now produce large quantities of potable water in many areas of the world.[1] To achieve high water fluxes, commercial RO and NF membranes consist of ultrathin barrier layers on porous supports.[2] The barrier layer allows selective passage of water (relative to salts or other small molecules), whereas the much thicker, unselective porous support provides mechanical strength. Salt rejection stems from a combination of low ion solubilities and diffusivities (relative to water) in the ultrathin barrier.[3-4] To better understand possible mechanisms of salt rejection, this study examines the formation of significant electrical double layers *inside* the barrier layer. Specifically, we consider space charge regions that appear in the barrier because of either differences in cation and anion solvation energies[5] or fixed charge on the barrier surface.[6-8] This work shows that the low concentration of the more excluded ion will greatly increase salt rejections when ion solubilities in the barrier are low.

Despite barrier-layer thicknesses as low as 20 nm, thin-film composite membranes often exhibit salt rejections that exceed 90%.[9-12] These high rejections with ultrathin layers and moderate volume flows imply ion permeabilities that are many orders of magnitude lower in the barrier layer of the membrane than in bulk electrolyte solutions. Such low permeabilities suggest an essentially non-porous skin layer where a solution-diffusion-electromigration model describes ion transport.[13-15] However, low permeabilities result from the products of small partition and diffusion coefficients, which are difficult to determine separately for thin films.[3-4, 16-19] Nevertheless, both partition and diffusion coefficients are likely low in relatively dense, nonporous polymers.[20]

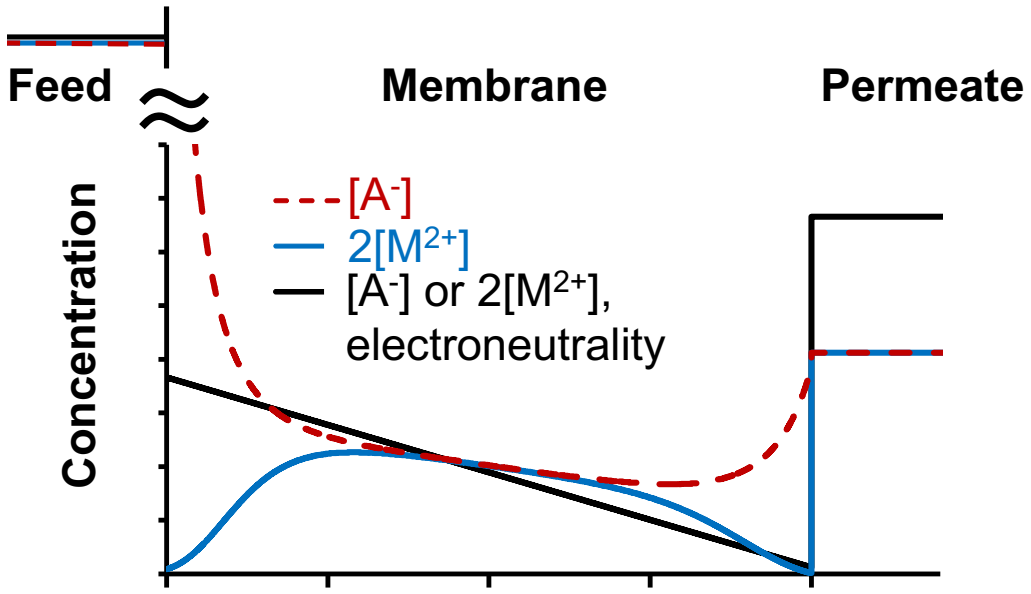

Figure 5.1 Conceptual diagram of ion concentration profiles during NF through a membrane barrier layer that has different intrinsic partition coefficients for the cation and anion of a salt MA_2. The calculations either assume electrical neutrality (black line) or allow for net charge in regions of the barrier layer (red line- anion, blue line- cation). The X-coordinate is the distance inside the 40 nm-thick barrier layer.

Small ion partition coefficients will give rise to low ion concentrations in the barrier layer so electrical screening lengths may become significant compared to the layer thickness. In such cases, immobile charge at the barrier surface[6-8] or unequal solvation energies for cations and anions in the barrier[21-22] will give rise to significant zones where anion and cation concentrations are not equal (Figure 5.1, compare red and blue lines). Moreover, low concentrations of either the cation or anion in these zones will lead to a large resistance to salt transport, R_s. Thus, deviations from local electroneutrality may control ion transport and dictate salt rejection. This chapter presents an initial examination of the effect of deviations from electroneutrality (at the barrier-layer scale) on ion transport. We note that ion-exchange membranes contain fixed charged in their interior and naturally contain unequal concentrations of *mobile* cations and anions. In this work we consider membranes that do not contain fixed charge in their interior.

The traditional application of the solution-diffusion model to RO or NF assumes equilibrium partition coefficients at the barrier-feed and barrier-permeate interfaces, along with transport through the membrane according to Fick's law (no convective transport) with an effective salt diffusion coefficient D_S.[4, 23] With these assumptions, equation 5.1 describes salt flux, j_s, where Γ_S is the salt partition coefficient, or the ratio of the salt concentration in the membrane, c_s^{mem}, to that in the external solution, c_s^{ext}. In equation 5.1 Δc_S is the difference between the feed and permeate salt concentrations and Δx is the thickness of the barrier layer.

$$j_s = \Gamma_S D_S \frac{\Delta c_S}{\Delta x}; \qquad \Gamma_S = \frac{c_s^{mem}}{c_s^{ext}} \tag{5.1}$$

Equation 5.1 implies the concentration profile shown by the black line in Figure 1 if the solubilities of cations and anions are equal throughout the membrane and there is no fixed charge. Implicitly, the linear concentration profile assumes electroneutrality throughout the membrane.

When cations and anions have differing solubilities in the membrane, the region near the membrane surface will contain excess cationic or anionic charge (see Figure 1, red and blue lines). Equation 5.2 describes the ion partition coefficient, Γ_i, the ratio of the ion concentrations in the membrane, C_i^{mem} and in the external feed solution, C_i^{ext}. In this equation, Z_i is the ion charge, F is Faraday's constant, R is the

$$\Gamma_i = \frac{C_i^{mem}}{C_i^{ext}} = \frac{\gamma_i^{ext}}{\gamma_i^{mem}} \exp\left(\frac{-\Delta\mu_{solv}}{RT}\right) \exp\left(-\frac{Z_i F}{RT}\psi_m\right); \quad \Gamma_i^{int} = \exp\left(\frac{-\Delta\mu_{solv}}{RT}\right) \qquad 5.2$$

gas constant, T is temperature, ψ_m is the electrical potential difference at a particular point in the membrane relative to the external bulk solution, and γ_i^{ext} and γ_i^{mem} are the activity coefficients in the external solution and in the membrane barrier, respectively. Equation 5.3 describes the intrinsic ion partition coefficient, Γ_i^{int}, which we define as the partition coefficient due only to ion solvation energies in the solution and the membrane. Excess charge in the membrane will create an electrical potential difference between the

$$\Gamma_i^{int} = \frac{\gamma_i^{ext}}{\gamma_i^{mem}} \exp\left(\frac{-\Delta\mu_{solv}}{RT}\right) \qquad 5.3$$

solution and a given point in the membrane, so equation 5.2, rather than equation 5.3 will describe the local equilibrium ion partition coefficient. If the membrane is sufficiently thick, the quasi-equilibrium electrical potential eventually takes a constant value in the membrane interior, and equilibrium cation and anion partition coefficients are equal in that region.

Some solution-diffusion models account for the effect of electrical potential on ion partitioning using equation (2), but they assume the space-charge region is thin enough that it does not affect salt transport.[24-25] This again leads to a linear concentration profile in the membrane (the black line in Figure 1), and Γ_S is constant and equal to Γ_i in equation (2) but not Γ_i^{int}. Nevertheless, these models neglect the charge distribution that gives rise to ψ_m and the

very high R_s value that will likely stem from the region that supports a charge distribution. For selective cation exclusion from the membrane (Figure 1), regions with near-zero cation concentrations will contribute greatly to R_s.

Additionally, for the solution-diffusion model the assumption of electroneutrality inside the barrier layer predicts that salt transport will not depend on fixed surface charge at the membrane external surface. This consequence of electroneutrality occurs because the value of ψ_m in equation (2) is that required for electroneutrality in the bulk of the membrane, regardless of external surface charge. Thus, the Γ_S value calculated from equation 5.2 and inserted into equation 5.1 will not vary with surface charge. However, experiments show that surface charge can greatly alter salt transport.[26-30]

We should note that many studies employ pore-based models to describe ion transport in NF.[31-33] These models show a dependence of rejection on pore surface-charge density,[34] but they usually assume a uniform charge in membrane pores and do not account for deviations from electroneutrality in the membrane.[26, 29, 35] Changes in the charge density on the pore surface as a function of salt concentration can affect rejection through either Donnan or dielectric exclusion.[31,33] However, a recent study shows that in some cases pore-based models greatly overpredict diffusion coefficients, possibly because the membranes do not contain connected pores.[14] Thus, we prefer a solution-diffusion model over models that consider hindered transport in pores.

This study investigates the salt rejection through negatively charged bare NF270 and polycation-modified NF270 in nanofiltration. The positive surface charge increases the R_s of $MgCl_2$, but decreases the R_s of K_2SO_4. The surface charge may create regions of

nonelectroneutrality in the membrane, and the excluded ion in this region controls the resistance to salt transport.

5.2 Experimental section

NF270 membranes were a gift from Dow Chemical and used as received. Membrane modification included rinsing the membrane in water and a 10-min immersion of the active side of the membrane in a 0.02 M solution of protonated poly(allylamine) (PAH) (Aldrich, M_w=15,000, the concentration is with respect to the repeating unit) containing 1 M NaCl. The pH of the PAH solution was adjusted to 2.3 with HCl. During modification, a holder ensures that the PAH solution contacts only the active surface of the membrane. After PAH adsorption, the membrane was immediately rinsed with deionized water from a squirt bottle for 1 min. Subsequent NF occurred in a home-built apparatus[36] with a transmembrane pressure of 4.3 bar. The cross-flow rate of 0.5 mL/s limits concentration polarization, and the exposed membrane area is 1.7 cm^2. (Although not uniform across this circular cell, the crossflow velocity in the center of the cell is around 0.06 m/s.) After 18 h of filtration, permeate solutions were collected for 20 min, and the feed solution was sampled at the end of each experiment. For the bare NF270 membrane, $MgCl_2$ rejections were similar after only 1 h of filtration. Cation concentrations were determined using inductively coupled plasma optical emission spectroscopy with calibration curves. Both the feed and permeate solutions were analyzed to calculate rejections. Uncertainties represent standard deviations of values calculated for at least 3 different membranes.

(a)

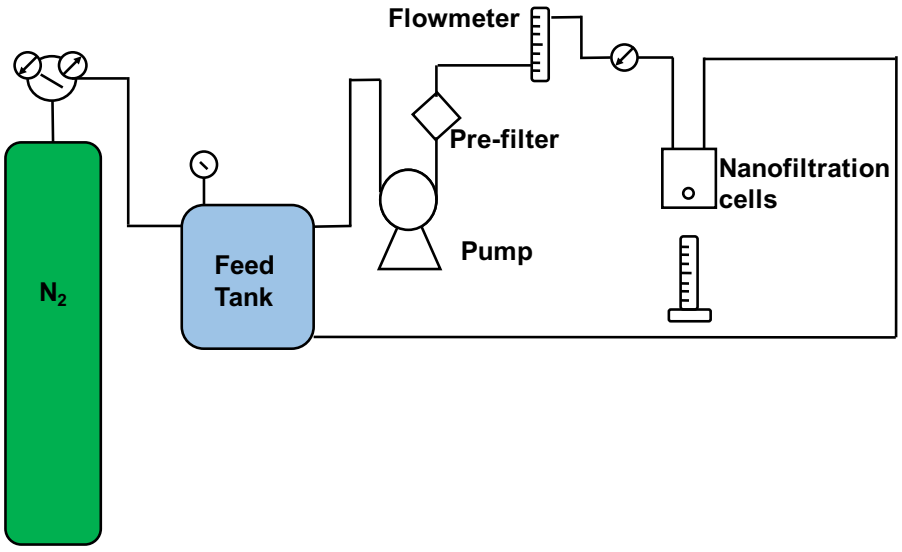

(b)

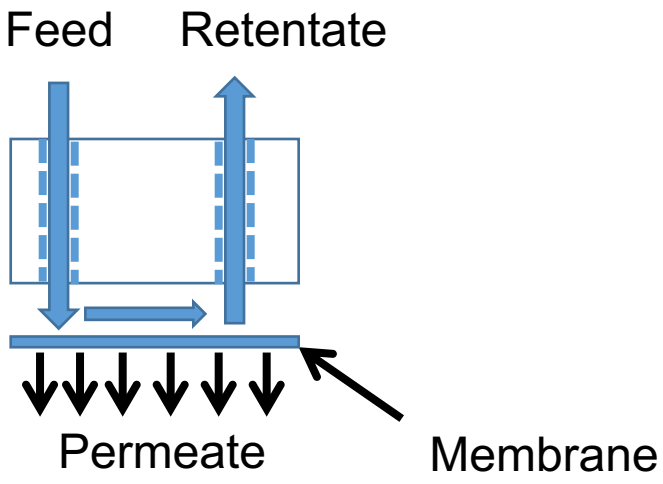

Figure 5.2 Schematic drawing of the nanofiltraiton system (a), and a cross-flow nanofiltration cell (b).

5. 3 Results and discussion

Rejection and surface charge. To experimentally assess the effect of surface charge on salt rejection, we performed NF using NF270 membranes before and after modification by polycation adsorption. Native NF270 membranes have a negative surface charge,[35-37] whereas adsorption of PAH introduces positive charge on the surface. Table 5.1 shows solution volume fluxes and salt rejections for filtration of solutions containing either K_2SO_4 or $MgCl_2$. After adsorption of PAH to change the sign of the surface charge, the K_2SO_4 rejection decreases from 0.985 to 0.949, which corresponds to a 3-fold increase in salt passage. Because J_v decreases about 30% after PAH coating, the changes in rejection correspond to a 2.6-fold decrease in R_s upon going to the positively charged surface, according to equation 5.4. (These changes in R_s neglect small changes in concentration polarization, which should tend to make the rejections higher after coating because of the smaller value of J_v and, hence, less concentration polarization.)

$$Re_s \equiv 1 - \frac{c_{sp}}{c_{sf}} = \frac{R_s J_v}{1+R_s J_v} \qquad 5.4$$

In contrast to K_2SO_4, $MgCl_2$ rejection increases from 0.32 to 0.49 after adsorption of PAH on the NF270 membrane (Table 5.1). Considering the change in volume flow, this represents a 3-fold increase in R_s for $MgCl_2$ after polyelectrolyte adsorption (again assuming minimal change in concentration polarization). These trends are consistent with trends from our model calculations, which account for space-charge layers in ultrathin membranes. Literature values for $MgCl_2$ rejection with untreated NF270 membranes are ~0.7 with 5000 ppm $MgCl_2$.[38] Using the same $MgCl_2$ concentration, we achieved a rejection of 0.43±0.03. The low rejection might stem from concentration polarization in our membrane cell, but the polyelectrolyte layer clearly increases $MgCl_2$ rejection and decreases K_2SO_4 rejection.

Table 5.1 Solution Fluxes, Salt Rejections, and R_s Values for Nanofiltration of 10 mM K_2SO_4 or $MgCl_2$ Through Bare and PAH-Modified NF270 Membranes.

Membrane	Salt	Volume Flux, J_v (μm/s)	Rejection, Re_s	R_s (s/μm) Experimental[a]
NF270	K_2SO_4	14.3±2.4	0.985±0.003	5.2±2.1
NF270/PAH	K_2SO_4	10.1±3.6	0.949±0.003	1.97±0.5
NF270	$MgCl_2$	17.2±0.3	0.32±0.03	0.027±0.004
NF270/PAH	$MgCl_2$	12.6±1.7	0.49±0.07	0.081±0.027

[a]Determined using equation (5.4) assuming no concentration polarization.

As mentioned in the introduction, a solution-diffusion model that assumes electroneutrality throughout the membrane would suggest that surface charge will not affect ion rejection. Simulations that incorporate an immobile volume charge throughout the membrane along with electroneutrality will also not explain this trend because partitioning still will not depend on the surface charge for the case of electroneutrality. Moreover, PAH should not alter the fixed volume charge because it is too large to enter into the barrier layer of an NF270 membrane. NF270 membranes likely contain a negative fixed volume charge that enhances SO_4^{2-} rejection, but the assumption of a fixed volume charge and electroneutrality will not explain the effects of surface charge.

Rejection as a function of salt concentration. Several studies show that $CaCl_2$ rejections initially increase and then decrease with $CaCl_2$ concentration during NF through negatively charged membranes.[26-29] At solution fluxes around 7 μm/s, salt rejections increase from 40-60% to a peak of 80% on going from a $CaCl_2$ concentration of 0.5 mM to 10 or 50 mM. We

calculated MA_2 rejections as a function of fixed surface charge for a range of solution concentrations. For the set of parameters we examined, rejections range from

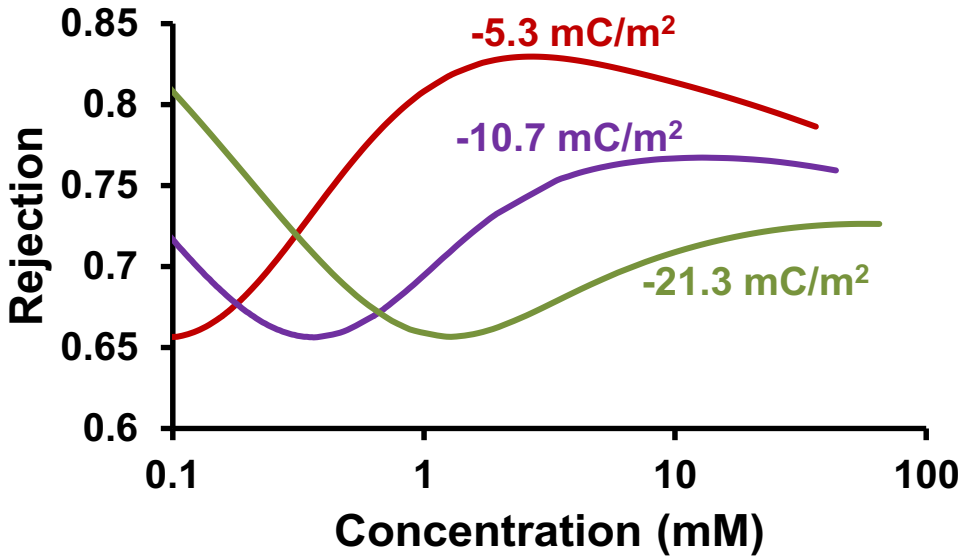

Figure 5.3 Rejection of MA_2 as a function of salt concentration and the magnitude of negative fixed charge on the barrier-layer surface. The simulation assumes a half-layer thickness of 20 nm, intrinsic partition coefficients of 0.14 for A^- and 3.4 x 10^{-4} for M^{2+}, barrier-layer diffusion coefficients of 5 x 10^{-12} m^2/s for M^{2+} and 1 x 10^{-11} m^2/s for A^-, and a volume flow of 6.9 μm/s or 25 L/(m^2h). The numbers with each curve represent the fixed surface-charge density.

a minimum of about 66% to a maximum of 83% (Figure 5.3). We could obtain better agreement with experimental data by varying parameters such as diffusion coefficients, but given the lack of information on membrane properties, our aim is only to show that incorporation of a space-charge zone within a barrier layer yields a maximum in rejection as a function of $CaCl_2$ concentration in the feed. Previous pore-based models account for such trends using nonmonotonic relationships between $CaCl_2$ feed concentration and either volume charge or

dielectric constant in the barrier.[26, 28-29] Deviations from electroneutrality naturally explain this phenomenon without invoking unusual concentration-dependences of membrane properties.

5.4 Conclusions

Space-charge regions may explain how changes in surface charge and salt concentration affect salt rejection. Adsorption of a single polycation layer on a negatively charged NF270 membrane increases $MgCl_2$ rejection but decreases K_2SO_4 rejection. The positive charge due to the polycation will increase the height of the electrostatic "barrier" in the space-charge region during NF of $MgCl_2$ but decrease this "barrier" during NF of K_2SO_4. Local deviations from electroneutrality are also consistent with $CaCl_2$ rejections that increase and then decrease with the $CaCl_2$ feed concentration during NF through a negatively charged membrane.

REFERENCES

REFERENCES

1. Desalination by the Numbers. http://idadesal.org/desalination-101/desalination-by-the-numbers/ (accessed February 8, 2015).

2. Lin, L.; Lopez, R.; Ramon, G. Z.; Coronell, O., Investigating the void structure of the polyamide active layers of thin-film composite membranes. *Journal of Membrane Science* **2016,** *497*, 365-376.

3. Geise, G. M.; Paul, D. R.; Freeman, B. D., Fundamental water and salt transport properties of polymeric materials. *Progress in Polymer Science* **2014,** *39*, 1-42.

4. Wijmans, J. G.; Baker, R. W., The solution-diffusion model - a review. *Journal of Membrane Science* **1995,** *107*, 1-21.

5. Kotelyanskii, M. J.; Wagner, N. J.; Paulaitis, M. E., Atomistic simulation of water and salt transport in the reverse osmosis membrane FT-30. *Journal of Membrane Science* **1998,** *139*, 1-16.

6. Li, X. H.; Zhang, C. J.; Zhang, S. N.; Li, J. X.; He, B. Q.; Cui, Z. Y., Preparation and characterization of positively charged polyamide composite nanofiltration hollow fiber membrane for lithium and magnesium separation. *Desalination* **2015,** *369*, 26-36.

7. Akbari, A.; Solymani, H.; Rostami, S. M. M., Preparation and characterization of a novel positively charged nanofiltration membrane based on polysulfone. *Journal of Applied Polymer Science* **2015,** *132*.

8. Xu, J.; Wang, Z.; Wang, J. X.; Wang, S. C., Positively charged aromatic polyamide reverse osmosis membrane with high anti-fouling property prepared by polyethylenimine grafting. *Desalination* **2015,** *365*, 398-406.

9. Yan, H.; Miao, X. P.; Xu, J.; Pan, G. Y.; Zhang, Y.; Shi, Y. T.; Guo, M.; Liu, Y. Q., The porous structure of the fully-aromatic polyamide film in reverse osmosis membranes. *Journal of Membrane Science* **2015,** *475*, 504-510.

10. Hermans, S.; Bernstein, R.; Volodin, A.; Vankelecom, I. F. J., Study of synthesis parameters and active layer morphology of interfacially polymerized polyamide-polysulfone membranes. *Reactive & Functional Polymers* **2015,** *86*, 199-208.

11. La, Y. H.; Diep, J.; Al-Rasheed, R.; Miller, D.; Krupp, L.; Geise, G. M.; Vora, A.; Davis, B.; Nassar, M.; Freeman, B. D.; McNeil, M.; Dubois, G., Enhanced desalination performance of polyamide bi-layer membranes prepared by sequential interfacial polymerization. *Journal of Membrane Science* **2013,** *437*, 33-39.

12. Freger, V.; Gilron, J.; Belfer, S., TFC polyamide membranes modified by grafting of hydrophilic polymers: an FT-IR/AFM/TEM study. *Journal of Membrane Science* **2002,** *209*, 283-292.

13. Yaroshchuk, A.; Bruening, M. L.; Licon Bernal, E. E., Solution-Diffusion-Electro-Migration model and its uses for analysis of nanofiltration, pressure-retarded osmosis and forward osmosis in multi-ionic solutions. *Journal of Membrane Science* **2013,** *447*, 463-476.

14. Dražević, E.; Košutić, K.; Kolev, V.; Freger, V., Does hindered transport theory apply to desalination Membranes? *Environmental Science & Technology* **2014,** *48*, 11471-11478.

15. Yaroshchuk, A.; Martinez-Llado, X.; Llenas, L.; Rovira, M.; de Pablo, J., Solution-diffusion-film model for the description of pressure-driven trans-membrane transfer of electrolyte mixtures: One dominant salt and trace ions. *Journal of Membrane Science* **2011,** *368*, 192-201.

16. Paul, D. R., Reformulation of the solution-diffusion theory of reverse osmosis. *Journal of Membrane Science* **2004,** *241*, 371-386.

17. Zhang, X. J.; Cahill, D. G.; Coronell, O.; Marinas, B. J., Absorption of water in the active layer of reverse osmosis membranes. *Journal of Membrane Science* **2009,** *331*, 143-151.

18. Dlamini, D. S.; Levchenko, S.; Bass, M.; Mamba, B. B.; Hoek, E. M. V.; Thwala, J. M.; Freger, V., Solute hindrance in non-porous membranes: An ATR-FTIR study. *Desalination* **2015,** *368*, 60-68.

19. Bason, S.; Oren, Y.; Freger, V., Ion transport in the polyamide layer of RO membranes: Composite membranes and free-standing films. *Journal of Membrane Science* **2011,** *367*, 119-126.

20. Lonsdale, H. K.; Merten, U.; Riley, R. L., Transport properties of cellulose acetate osmotic membranes. *Journal of Applied Polymer Science* **1965,** *9*, 1341-&.

21. Yaroshchuk, A. E., Structure of the electric double-layer at an uncharged surface - model of a dielectric step. *Colloid Journal of the Ussr* **1983,** *45*, 236-240.

22. Derjaguin, B. V.; Dukhin, S. S.; Yaroshchuk, A. E., On the role of the electrostatic factor in stabilization of dispersions protected by adsorption layers of polymers. *Journal of Colloid and Interface Science* **1987,** *115*, 234-239.

23. Zaidi, S. M. J.; Fadhillah, F.; Khan, Z.; Ismail, A. F., Salt and water transport in reverse osmosis thin film composite seawater desalination membranes. *Desalination* **2015,** *368*, 202-213.

24. Starov, V. M.; Churaev, N. V., Separation of electrolyte-solutions by reverse-osmosis. *Advances in Colloid and Interface Science* **1993,** *43*, 145-167.

25. Yaroshchuk, A. E., Negative rejection of ions in pressure-driven membrane processes. *Advances in Colloid and Interface Science* **2008,** *139*, 150-173.

26. Hagmeyer, G.; Gimbel, R., Modelling the salt rejection of nanofiltration membranes for ternary ion mixtures and for single salts at different pH values. *Desalination* **1998,** *117*, 247-256.

27. Luo, J.; Wan, Y., Effects of pH and salt on nanofiltration-a critical review. *Journal of Membrane Science* **2013,** *438*, 18-28.

28. Mazzoni, C.; Bandini, S., On nanofiltration Desal-5 DK performances with calcium chloride-water solutions. *Separation and Purification Technology* **2006,** *52*, 232-240.

29. Mazzoni, C.; Bruni, L.; Bandini, S., Nanofiltration: Role of the electrolyte and pH on desal DK performances. *Industrial & Engineering Chemistry Research* **2007,** *46*, 2254-2262.

30. Sata, T.; Sata, T.; Yang, W. K., Studies on cation-exchange membranes having permselectivity between cations in electrodialysis. *Journal of Membrane Science* **2002,** *206*, 31-60.

31. Bowen, W. R.; Mohammad, A. W.; Hilal, N. Characterisation of Nanofiltration Membranes for Predictive Purposes - Use of Salts, Uncharged Solutes and Atomic Force Microscopy. *Journal of Membrane Science* **1997**, *126*, 91-105.

32. Lefebvre, X.; Palmeri, J.; David, P. Nanofiltration Theory: An Analytic Approach for Single Salts. *Journal of Physical Chemistry. B* **2004**, *108*, 16811-16824.

33. Fievet, P.; Sbaï, M.; Szymczyk, A. Analysis of the Pressure-Induced Potential Arising across Selective Multilayer Membranes. *Journal of Membrane Science* **2005**, *264*, 1-12.

34. Szymczyk, A.; Lanteri, Y.; Fievet, P. Modelling the Transport of Asymmetric Electrolytes through Nanofiltration Membranes. *Desalination* **2009**, *245*, 396-407.

35. Liu, C.; Shi, L.; Wang, R., Crosslinked layer-by-layer polyelectrolyte nanofiltration hollow fiber membrane for low-pressure water softening with the presence of SO_4^{2-} in feed water. *Journal of Membrane Science* **2015,** *486*, 169-176.

36. Diop, S. N.; Diallo, M. A.; Diawara, C. K.; Cot, D., Intrinsic properties and performances of NF270 and XLE membranes for water filtration. *Water Science and Technology-Water Supply* **2011,** *11*, 186-193.

37. Choi, J. H.; Fukushi, K.; Yamamoto, K., A study on the removal of organic acids from wastewaters using nanofiltration membranes. *Separation and Purification Technology* **2008,** *59*, 17-25.

38. Hilal, N.; Al-Zoubi, H.; Darwish, N. A.; Mohammad, A. W., Nanofiltration of magnesium chloride, sodium carbonate, and calcium sulphate in salt solutions. *Separation Science and Technology* **2005,** *40*, 3299-3321.

Chapter 6 Conclusions and Future Work

This dissertation examines the enhancement of ion-transport selectivities using charged membrane coatings in ED, Donnan dialysis and nanofiltration. Deposition of PEMs on inexpensive Fujifilm cation-exchange membranes results in continuous films that give rise to remarkable monovalent/divalent cation selectivities >1000, similar to results with much more expensive Nafion membranes. However, the current efficiency for both PEM-coated Fujifilm and Nafion membranes is only 50%. Use of a more water-swollen PEM coating increases the current efficiency to ~80% while retaining high selectivity. High swelling presumably increases the permeance of monovalent cations, whereas the high selectivity likely stems primarily from the positive charge in highly swollen films. Because we think that surface charge is a dominant factor behind monovalent/divalent cation selectivity, we also attempted to apply an electrical potential drop at the surface of conductive membranes to influence ion permeability.

Chapter 1 presents an overview of membrane-based ion separation techniques and discusses the fabrication of membranes, mass-transport mechanisms, and current and future applications of ED. Additionally, I discuss the deposition of functional PEMs and conductive membranes.

Chapter 2 investigates the deposition of PEMs on inexpensive Fujifilm cation-exchange membranes. The Fujifilm membranes consist of an aromatic polyamide matrix surrounding a fibrous support, and thus they should be much less expensive than the fluoropolymer Nafion. The relatively smooth surface of the Fujifilm membranes is also attractive for potentially forming continuous polyelectrolyte films. Coating these membranes with a PEM leads to

remarkably high monovalent/multivalent cation selectivities similar to those previously seen with modified Nafion. The PEM coating on the anode side is essential for the high selectivity, whereas the cathode-side coating contributes only a small amount to resistance to ion transport and little selectivity. Nevertheless, the current efficiencies for highly selective membranes are only 50%.

In chapter 3, I study adsorption of $(PDADMAC/PSS)_nPDADMAC$ films on Nafion membranes to again achieve extremely high monovalent/divalent ED selectivities. The monovalent cation current efficiency is as high as 0.8 in $(PDADMAC/PSS)_nPDADMAC$-coated Nafion, and the coated membranes still show high selectivities . In contrast, the current efficiency for PAH/PSS-coated Nafion is 0.5~0.6. $(PDADMAC/PSS)_3PDADMAC$ coatings give the highest current efficiency in both K^+/Mg^{2+} and Li^+/Co^{2+} separations. The high current efficiency presumably results from the high swelling of $(PDADMAC/PSS)_nPDADMAC$ films in water, which increases the monovalent cation permeance in the film.

Chapter 4 demonstrates the development of electrically conductive membranes prepared through deposition of conductive polymers or gold using LbL assembly, electroless deposition and electropolymerization. The coated membranes show high electrical conductivity, but unfortunately the ion-transport selectivity does not reversibly change when varying the applied electrical potential.

Chapter 5 investigates the effect of surface charge on salt rejection in nanofiltration. The K_2SO_4 passage increase 3-fold after coating bare NF 270 with a polycation, whereas the passage of $MgCl_2$ decreases 3-fold as the surface turns positive. Thus, surface charge greatly affects ion permeability. A solution-diffusion-electro-migration model provides a possible explanation for

how the charged surface creates regions of nonelectroneutrality where the excluded ion controls the resistance to salt transport.[1]

The PEM-coated Nafion and Fujifilm membranes give rise to high selectivities, and highly water-swollen (PDADMAC/PSS)$_n$PDADMAC-coated Nafion membranes demonstrate high current efficiency. However, questions remain about how to improve PEM stabilities and how to process separations with high efficiency through cation-exchange membranes. The electrostatic interaction between polycations and polyanions is insufficient to maintain film stability in highly concentrated salt solutions, and applied electric fields may also delaminate the film.[2-4] Crosslinking of PEMS through covalent bonds may increase the film stability. Poly(acrylic acid) (PAA) and PAH crosslink via simple heating or with addition of 1-ethyl-3-(3-dimethylaminopropyl) carbodiinide (EDC).[5] However, the film still need to contain sufficient charge to provide high ion selectivity.

As mentioned, relatively high current efficiency occurs with highly water-swollen PEMs. Future work should further investigate if the high current efficiency stems from increasing monovalent cation permeance, and better demonstrate whether this greatly increases limiting current in current-voltage measurements. Additionally, we also find that the Donnan dialysis flux is high through (PDADMAC/PSS)$_n$PDADMAC-coated Nafion. Unlike ED, Donnan dialysis does not require an applied electric field for separation, therefore water splitting will not complicate the transport. We could utilize Donnan dialysis to investigate the effect of the number of PEM bilayers on selectivity and the role of adsorption of divalent cations in the film on ion transport. In addition, Donnan dialysis could also prove useful in ion separations such as separating metals from acid.

REFERENCES

REFERENCES

1. Yaroshchuk, A.; Zhu, Y.; Bondarenko, M.; Bruening, M. L., Deviations from electroneutrality in membrane barrier layers: A possible mechanism underlying high salt rejections. *Langmuir* **2016,** *32*, 2644-2658.

2. Nolte, A. J.; Takane, N.; Hindman, E.; Gaynor, W.; Rubner, M. F.; Cohen, R. E., Thin film thickness gradients and spatial patterning via salt etching of polyelectrolyte multilayers. *Macromolecules* **2007,** *40*, 5479-5486.

3. Kovacevic, D.; van der Burgh, S.; de Keizer, A.; Stuart, M. A. C., Kinetics of formation and dissolution of weak polyelectrolyte multilayers: Role of salt and free polyions. *Langmuir* **2002,** *18*, 5607-5612.

4. Ladhari, N.; Hemmerle, J.; Haikel, Y.; Voegel, J. C.; Schaaf, P.; Ball, V., Stability of embossed -PEI(PSS-PDADMAC)$_{20}$ multilayer films versus storage time and versus a change in ionic strength. *Applied Surface Science* **2008,** *255*, 1988-1995.

5. Stair, J. L.; Harris, J. J.; Bruening, M. L., Enhancement of the ion-transport selectivity of layered polyelectrolyte membranes through cross-linking and hybridization. *Chemistry of Materials* **2001,** *13*, 2641-2648.